TECHNISCHE
UNIVERSITÄT
DARMSTADT

Design and Thermo Economic Evaluation of Solar Absorption Cooling Systems

Vom Fachbereich Maschinenbau
an der Technischen Universität Darmstadt
zur
Erlangung des akademischen Grades
Doktor-Ingenieur (Dr.-Ing.)
genehmigte

D I S S E R T A T I O N

M. Sc. ADIL FAWZI HAMAD AL-FALAHI

aus Irak

Berichterstatter: *Prof. Dr.-Ing. Bernd Epple*

Mitberichterstatter: *Priv.-Doz. Dr.-Ing. habil. Falah Alobaid*

            Prof. Dr. Fayad Mohamed Abed

            Prof. Jouni Ritvanen

Tag der Einreichung: *21.06.2022*

Tag der mündlichen Prüfung: *16.05.2023*

Darmstadt 2023

D 17

Genehmigte Dissertation von M.Sc. Adil Fawzi Hamad Al-Falahi

Design and Thermo Economic Evaluation of Solar Absorption Cooling Systems

Darmstadt, Technische Universität Darmstadt

Jahr der Veröffentlichung der Dissertation auf TUprints: 2023

Tag der mündlichen Prüfung: 16.05.2023

Preface

The work of the present doctoral thesis "Design and Thermo Economic Evaluation of Solar Absorption Cooling Systems" started in November 2015 and was carried out at the Institute of Energy Systems and Technology (EST), Department of Mechanical Engineering, Technical University of Darmstadt. The main supervision was done by **Prof. Dr.-Ing. Bernd Epple**[(i)]. *The Dissertation Supervisory Committee consisted furthermore of* **Priv.-Doz. Dr.-Ing. habil. Falah Alobaid**[(i)], **Prof. Dr. Fayadh Mohamed Abed**[(ii)] *and* **Prof. Jouni Ritvanen**[(iii)]**.**

This Ph.D. thesis is organized into two main parts. In the first part, an overview and summary of the work are presented, followed by the second part consisting of the appended papers.

1) Papers included in this thesis

Paper A

Al-Falahi, A.; *Alobaid, F.; Epple, B.: A new design of an integrated solar absorption cooling system driven by an evacuated tube collector: A case study for Baghdad, Iraq. Applied Sciences, 2020, 10(10), 3622;* [*https://doi.org/10.3390/app10103622*](https://doi.org/10.3390/app10103622).

Paper B

Al-Falahi, A.; *Alobaid, F.; Epple, B.: Design and thermo-economic comparisons of large scale solar absorption air conditioning cycles. Case Studies in Thermal Engineering, (22), Volume 22, December 2020, 100763;* [*https://doi.org/10.1016/j.csite.2020.100763.*](https://doi.org/10.1016/j.csite.2020.100763.)

Paper C

Al-Falahi, A.; *Alobaid, F.; Epple, B.: Thermo-Economic Evaluation of Aqua-Ammonia Solar Absorption Air Conditioning System Integrated with Various Collector Types. Entropy 2020, 22(10), 1165;* [*https://doi.org/10.3390/e22101165*](https://doi.org/10.3390/e22101165).

Paper D

Al-Falahi, A.*; Alobaid, F.; Epple, B.: Thermo-Economic Comparisons of Environmentally Friendly Solar Assisted Absorption Air Conditioning Systems. Applied Sciences, 2021, 11(5), 2442; https://doi.org/10.3390/app11052442.*

2) Papers not included in this thesis

Paper E

Al-Falahi, A.; *Alobaid, F.; Epple, B.: Design and Thermo-Economic Comparisons of an Absorption Air Conditioning System Based on Parabolic Trough and Evacuated Tube Solar Collectors. Energies 2020, 13(12), 3198; https://doi.org/10.3390/en13123198.*

Paper F

Soliman, A. M., **Al-Falahi, A.,** *Sharaf Eldean M. A., Elmnifi M., Hassan M., Younis B., Mabrouk A., Fath H. E. S.: A new system design of using solar dish-hydro combined with reverse osmosis for sewage water treatment: case study Al-Marj, Libya. Desalination Water Treatment, 2020, 193, 189-211; https://doi: 10.5004/dwt.2020.25782.*

[i] *Institute of Energy Systems and Technology,Technical University of Darmstadt, Germany.*
[ii] *Department of Mechanical Engineering,Tikrit University,Iraq.*
[iii] *Lappeenranta University of Technology, LUT Energy, Finland.*

Dedication

First, I would like to thank a team of qualified supervisors who took over the responsibility of guiding me through my work on the doctoral degree. At the head of this team is my supervisor **Prof. Dr.-Ing. Bernd Epple***, whose academic experience is greatly appreciated. Thanks go to* **Priv.-Doz. Dr.-Ing. habil. Falah Alobaid** *for spending much of his valuable time guiding me step-by-step with suggestions and comments on my research. Also, I wish to thank* **Prof. Dr. Fayadh Mohamed Abed** *and* **Prof. Jouni Ritvanen** *the reviewers of this Ph.D. thesis, for numerous words of advice and for taking over the co-review of this work.*

I am especially grateful for the feedback and support of **EST** *staff at the* **Technical University of Darmstadt***, who made my time in the institute a memorable and valuable experience. I am thankful to my friend* **Dr.-Ing. Adel Almoslh** *who encouraged and supported me during my work.*

I am grateful acknowledged to the financial support from **Al Anbar University** *and the* **Iraqi Ministry of Higher Education and Scientific Research.** *Their support has allowed me to pursue my academic goals and contribute to the advancement of knowledge in my field and I hope this work be useful to my country* **Iraq***.*

I dedicate this work to the soul of my father, my mother, and my brother, the martyr Taher.

Lastly, I would like to dedicate this Ph.D. thesis to my loving family, my greatest and sincere appreciation goes to my wife, my kids, my brothers, and my sisters for their continued support. I love you all.

Darmstadt, June 2022   *Adil Al-falahi*

Erklärung

Hiermit erkläre ich, dass ich die vorliegende Arbeit, abgesehen von den in ihr ausdrücklich genannten Hilfen, selbständig verfasst habe.

Darmstadt, den 21. Juni 2022

Adil Al-Falahi

Adil Fawzi Hamad Al-Falahi

Summary

A large increase in energy demand for building cooling is expected both in Iraq and internationally in the next decades. In Iraq, like in other hot arid countries, the use of conventional electrically driven chillers for air conditioning (AC) is increasing dramatically, thus leading to high costs, power grid overload, and blackouts. Thermally driven refrigeration processes would be an excellent choice for converting solar heat radiation into cooling energy for indoor thermal comfort. This Ph.D. thesis focuses on the mathematical modeling and simulation of solar thermal-assisted single-effect absorption cooling systems. On the one hand, energy performance, design, and operation of thermally driven refrigeration processes are investigated; on the other hand, optimization and thermos-economic analysis of the different configurations of solar absorption cycles are carried out.

A detailed description of the energic performance analysis of an integrated solar-operated residential-scale cooling system is presented in paper A. The solar fraction and the thermal performance of the solar air-conditioning system are performed for various months in the cooling season under ambient conditions in Baghdad, Iraq. From the parametric analysis of the single-effect water-LiBr absorption cycle, the thermal performance of the system is evaluated and the best system design parameters of the solar-driven cooling system are determined. For this purpose, the TRNSYS-based approach has been adopted. Additionally, in paper A, a technology roadmap for solar thermal cooling in Iraq is developed to reduce the summer peak demand for electricity and to achieve energy savings in terms of primary energy, thus limiting greenhouse gas emissions in the residential air conditioning sector.

In papers B and C, the design of the solar absorption cooling system is modified to include the flashing tank subsystem for steam generation to improve and compare the various configurations of absorption refrigeration cycles by different solar thermal collectors. Two types of solar collectors are considered: parabolic trough collectors (PTC) and evacuated tube collectors (ETC). Two types of single-effect absorption cooling cycles are considered: water-LiBr and ammonia-water. The mathematical models were developed based on the energy balance equations and solved in the Matlab/Simulink environment. The proposed model is operated under the design mode of the modeling technique, which calculates unknown parameters such as areas, dimensions, mass flow rates, energy streams, exergy, cost streams, and the entire process temperatures or any other calculated physical properties. The thermo-economic analysis has been performed for different

configurations of the absorption cooling cycle. The detailed description of a mathematical model of system configurations is presented in the mentioned papers (B and C) and has been compared. Specifically, in paper B, various configurations of a single-effect water-LiBr absorption cycle have been compared based on the coefficient of performance and exergetic efficiency. The comparison is performed based on energy, efficiency, design, cost, and thermo-economics. In paper C, design and thermo-economic analyses are presented to compare two different collector types (parabolic trough and evacuated tube) with ammonia-water (NH_3-H_2O) absorption systems and to select the best operating conditions.

Thermo-economics is the branch of engineering that combines energy analysis and economic principles to provide the system designer or operator with information not available through conventional energy analysis and economic evaluations but crucial to the design and operation of a cost-effective system. Based on the analysis presented in papers B and C, thermo-economic optimization is studied under different operating conditions. The results show that combining a parabolic trough collector with an absorption cycle results in lower design aspects and lower hourly costs. An equation that determines the optimal area and design conditions in thermal systems is formulated. The selection of the module of the collector and the number of collectors in each module are presented. To study whether the implementation of solar thermal cooling in the Iraqi climate is economically feasible. The proposed approach was illustrated through a case study for a sports arena with a 700–800 kW total cooling load, considering the weather data of Baghdad. To achieve the best configuration and accurate thermodynamic models, the mathematical formulation of the different configurations of absorption processes in papers B and C is also thermo-economically analyzed and evaluated in paper D. Here, the analysis is performed to compare two types of absorption cycle water-LiBr and ammonia—water to each other by parabolic trough collectors and evacuated tube collectors under the same operating conditions. Moreover, investment, operating, and maintenance cost analyses are performed for each unit (solar field, flash tank, absorption chiller, and pump units). Here, the interest rate is set at 5% and the lifetime of the plant at 20 years.

Finally, the comparison results reveal that the parabolic trough collector combined with H_2O-LiBr (PTC/H_2O-LiBr) gives lower design aspects and minimum rates of hourly costs (5.2 $/h) than the ETC/$H_2O$-LiBr configuration (5.6 $/h). H_2O-LiBr gives a lower thermo-economic product cost (0.14 $/GJ) compared to NH_3-H_2O (0.16 $/GJ). The absorption refrigeration cycle coefficient of performance ranged between 0.5 and 0.9.

Kurzfassung

In den nächsten Jahrzehnten wird sowohl im Irak als auch international ein starker Anstieg des Energiebedarfs für die Klimatisierung von Gebäuden erwartet. Im Irak, wie auch in anderen heißen trockenen Ländern, nimmt der Einsatz konventioneller, elektrisch betriebener Kältemaschinen für die Klimatisierung (AC) drastisch zu, was zu hohen Kosten, Überlastung des Stromnetzes und Stromausfällen führt. Thermische Kühlprozesse bieten eine perfekte Alternative, um die solare Wärmestrahlung in Kühlenergie umzuwandeln und so den Komfort in Innenräumen zu erhöhen. Diese Doktorarbeit befasst sich mit der mathematischen Modellierung und Simulation von solarthermisch unterstützten Absorptionskältesystemen mit einfachem Effekt. Zum einen werden die Energieleistung, die Auslegung und der Betrieb thermisch angetriebener Kühlprozesse untersucht, zum anderen werden Optimierungen und thermo-ökonomische Analysen der verschiedenen Konfigurationen von Solarabsorptionskreisläufen durchgeführt.

Eine detaillierte Beschreibung der energetischen Leistungsanalyse von integrierten solarbetriebenen Kühlsystemen für Wohngebäude findet sich in Ausarbeitung A. Der Solaranteil und die thermische Leistung des solaren Klimatisierungssystems werden für mehrere Monate in der Kühlsaison unter Umgebungsbedingungen in Bagdad, Irak untersucht. Anhand der parametrischen Analyse des einfach wirkenden Wasser-LiBr-Absorptionskreislaufs wird die thermische Leistung des Systems bewertet und es werden die besten Parameter für die Gestaltung des solarbetriebenen Kühlsystems ermittelt. Hierzu wird der TRNSYS-basierte Ansatz verwendet. Darüber hinaus wird in Ausarbeitung A ein Strategieplan für die solarthermische Kühlung im Irak entwickelt, um Stromspitzen im Sommer zu reduzieren und Energieeinsparungen in Bezug auf die Primärenergie zu erzielen, wodurch die Treibhausgasemissionen im Bereich der Wohnraumklimatisierung verringert werden.

In den Ausarbeitungen B und C wird das Design des solaren Absorptionskühlsystems so verändert, dass es das Flash-Tank-Subsystem für die Dampferzeugung einschließt, um die verschiedenen Konfigurationen von Absorptionskühlkreisläufen mit verschiedenen solarthermischen Kollektoren zu optimieren und zu vergleichen. Es werden zwei Arten von Solarkollektoren betrachtet: Parabolrinnenkollektoren (PTC) und Vakuumröhrenkollektoren (ETC). Dabei werden zwei Arten von Absorptionskühlkreisläufen mit einfacher Wirkung untersucht: Wasser-LiBr und Ammoniak-Wasser.

Die mathematischen Modelle wurden auf der Grundlage der Energiebilanzgleichungen entwickelt und in der Matlab/Simulink-Umgebung berechnet. Das vorgeschlagene Modell wird im Entwurfsmodus der Modellierungstechnik verwendet, bei der unbekannte Parameter wie Flächen, Abmessungen, Massendurchsätze, Energieströme, Exergie, Kostenströme und die gesamten Prozesstemperaturen oder andere errechnete physikalische Eigenschaften berechnet werden. Die thermo-ökonomische Analyse wurde für verschiedene Konfigurationen des Absorptionskühlkreislaufs durchgeführt. Die detaillierte Beschreibung des mathematischen Modells der Systemkonfigurationen ist in den genannten Ausarbeitungen (B und C) enthalten und wurde dort verglichen. In Ausarbeitung B wurden verschiedene Konfigurationen eines einfachwirkenden Wasser-LiBr-Absorptionskreislaufs anhand der Leistungszahl und des exergetischen Wirkungsgrads verglichen. Der Vergleich wird auf der Grundlage der Begriffe Energie, Exergie, Konstruktion, Kosten und Thermoökonomie durchgeführt. In Ausarbeitung C werden konstruktive und thermo-ökonomische Analysen vorgestellt, um zwei verschiedene Kollektortypen (Parabolrinne und Vakuumröhre) mit Ammoniak-Wasser-Absorptionssystemen (NH3-H2O) zu vergleichen und die besten Betriebsbedingungen zu ermitteln.

Die Thermo-Ökonomie ist ein Fachgebiet des Ingenieurwesens, das Exergie-Analysen und ökonomische Prinzipien kombiniert, um dem Systementwickler oder Betreiber Informationen zur Verfügung zu stellen, die durch herkömmliche Energieanalysen und ökonomische Bewertungen nicht verfügbar sind, jedoch für die Planung und den Betrieb eines kosteneffizienten Systems entscheidend sind. Auf der Grundlage der in den Ausarbeitungen B und C vorgestellten Analyse wird die thermo-ökonomische Optimierung unter verschiedenen Betriebsbedingungen untersucht. Die Ergebnisse zeigen, dass der Parabolrinnenkollektor in Kombination mit dem Absorptionszyklus niedrigere Gestaltungsaspekte und minimale Betriebskosten pro Stunde aufweist. Es wird eine Gleichung formuliert, die die optimale Fläche und die Auslegungsbedingungen in thermischen Systemen bestimmt. Die Auswahl der Kollektormodule und die Anzahl der Kollektoren in jedem Modul werden dargestellt. Es wird untersucht, ob der Einsatz von solarthermischer Kühlung im irakischen Klima wirtschaftlich umsetzbar ist. Der vorgestellte Ansatz wurde anhand einer Fallstudie für eine Sportarena mit einer Gesamtkühllast von 700-800 kW unter Berücksichtigung der Wetterdaten von Bagdad dargestellt. Um die beste Konfiguration und genaue thermodynamische Modelle zu erhalten, wird die mathematische Berechnung der verschiedenen Konfigurationen der Absorptionsprozesse in den Ausarbeitungen B und C auch thermoökonomisch analysiert und in der Ausarbeitung D bewertet. Hierbei werden die beiden Absorptionskreisläufe Wasser-LiBr und Ammoniak-Wasser mit Parabolrinnenkollektoren und Vakuumröhrenkollektoren unter den gleichen Betriebsbedingungen miteinander verglichen. Darüber hinaus werden Investitions-, Betriebs- und Wartungskostenanalysen

für jede Einheit (Solarfeld, Flash-Tank, Absorptionskältemaschine und Pumpeneinheiten) durchgeführt. Dabei wird der Zinssatz auf 5% und die Lebensdauer der Anlage auf 20 Jahre festgelegt.

Die Ergebnisse des Vergleichs zeigen, dass der Parabolrinnenkollektor in Kombination mit H2O-LiBr (PTC/H2O-LiBr) weniger gestalterische Merkmale und minimale stündliche Kosten (5,2 $/h) aufweist, gefolgt von der ETC/H2O-LiBr-Konfiguration (5,6 $/h). H2O-LiBr ergibt geringere thermoökonomische Produktkosten (0,14 $/GJ) im Vergleich zu NH3-H2O (0,16 $/GJ). Der Koeffizient des Absorptionskältekreislaufs lag zwischen 0,5 und 0,9.

TABLE OF CONTENTS

Nomenclatures

Latin symbols

A	*Area*	$[\text{m}^2]$
D	*Diameter*	$[\text{m}]$
E	*Exergy stream*	$[\text{Kw}]$
H, h	*High, Enthalpy*	$[\text{m, kJ/kg}]$
L	*Length*	$[\text{m}]$
M	*Mass flow rate*	$[\text{kg/s}]$
P	*Pressure*	$[\text{bar}]$
Q	*Thermal power*	$[\text{Kw}]$
S	*Entropy*	$[\text{kJ /kg.°C}]$
T	*Temperature*	$[\text{°C}]$
U	*Overall heat transfer coefficient*	$[W/\text{m}^2 . \text{°C}]$
V	*Volume*	$[\text{m}^3]$
W	*Work*	$[\text{Kw}]$
X	*Concentration percentage*	$[\%]$

Greek symbols

η	*Efficiency*	$[\%]$
ρ	*Density*	$[\text{kg/ m}^3]$
μ	*Dynamic viscosity*	$[\text{Pa. s}]$

Dimensionless numbers

Pr	*Prandtl number*	
Re	*Reynolds number*	

Subscripts and indices

a, abs	*absorber*	
c	*condenser*	
e	*evaporator*	
g	*generator*	
h	*high*	
L	*low*	
m	*medium*	

Most used chemical symbols

CO_2	*carbon dioxide*
H_2O	*water*
NH_3	*ammonia*

Abbreviations

ANSYS	*commercial CFD software*
ABS	*absorption chiller*
AC	*air conditioning*
ADS	*adsorption chiller*
COP	*coefficient of performance*
DEC	*desiccant evaporative cooling*
EER	*energy efficiency ratio*
ETC	*evacuated tube collector*
FPC	*flat plate collector*
PTC	*parabolic trough collector*
SAT	*single-axis tracking solar collector*
SAHC	*solar air heating collector*

Chapter 1

1 Introduction

Energy-efficient, sustainable cooling and heating system technologies play a crucial role in addressing the megatrends of resource efficiency and the globalization of technologies. In particular, cooling and heating cycles, using renewable energy or waste heat rather than conventionally generated electricity, contribute to sustainably addressing issues like industrial or comfort cooling with a significantly reduced carbon footprint. In this context, absorption chillers, or heat pumps, represent a promising technology. In Western countries, consumption related to heating and cooling of buildings accounts for about 40% of primary energy needs. In the European Union, more than 25% of the energy consumed is used for the summer and winter air-conditioning of buildings [5]. Especially concerning summer cooling, the market has high growth potential. The increased demand for cooling systems technologies comes from the countries of southern Europe. However, in recent years, due to global warming and the increasing use of work equipment in enclosed spaces, the demand has also increased in northern European countries [6, 7]. The use of solar energy for heating buildings is a mature and well-known technology. However, lately, there has been an increased interest in technologies that can exploit the solar source for the cooling of buildings, realizing installations of solar cooling. Widespread use of these plants could prevent or mitigate a sharp increase in CO_2 emissions due to the increase in electricity consumption to meet the summer needs of growing buildings.

The Middle East and Northern Africa (MENA) region follows the worldwide trend of a continuously increasing demand for both primary energy and electricity for cooling purposes. The current energy demand is primarily fulfilled by relying on fossil fuels, with oil accounting oil for 50%, natural gas for 22%, and coal for 28% [8]. In the face of both global warming and limited conventional energy sources, the future challenge will be to find ways of meeting the growing cooling demand through renewable energy means. In Iraq, for example, it is now known that the peaks of electricity demand take place in the summer season and the demand for cooling and air conditioning is more than 50–60% of total electricity demand (48% in the residential

sector) [9], because of the simultaneous operation of millions of small air conditioners. Hence, it seems clear that fossil fuels contribute to global warming and their burning is harmful to the environment. Therefore, it is necessary to implement environmentally friendly energy sources that can be renewed in short periods, such as solar, wind, water, and others. In this context, the use of solar thermal energy for solar cooling is increasingly becoming an interesting topic. Solar cooling takes advantage of the fact that the hours of the day when there is the greatest cooling capacity needed for the air-conditioning of buildings coincide or almost coincide with the maximum availability of solar radiation. However, the major ecological advantage of solar thermal cooling systems lies not in the cooling side but in the multiple uses of water for heating and heating support, which means that, calculated for solar thermal cooling systems in Iraq, most of the CO_2 savings can be achieved [10–12].

Today, technological developments have made refrigeration by absorption an effective and economical alternative to vapor compression cycles. Rising electricity costs and problems with environmental conditions have made these heat-driven cycles more attractive for both industrial and residential applications. Absorption systems are widely used in air conditioning applications, in part because they can be operated by hot water, steam, and direct flame natural gas, among others, instead of electricity [13]. Absorption refrigeration systems have gained popularity because, first, they can be operated with environmentally friendly refrigerants in accordance with the Kyoto and Montreal protocols. Second, they take advantage of the use of low-cost alternative energy sources such as geothermal, biomass, solar energy, or waste heat from by-products. As a result, research in recent years has focused on improving absorption refrigeration systems. The main ways to improve efficiency are through thermodynamics analysis and the optimization of these systems [14–16]. Absorption systems can be divided into different groups regarding the working fluid, design, heat source, and heat rejection of the system. Two absorbent-refrigerant pairs commonly used in absorption systems are water-lithium bromide (H_2O-LiBr) and water-ammonia (H_2O-NH_3). The use of LiBr in air conditioning systems is very common since not only is the H_2O refrigerant from these systems available anywhere, but it is also inexpensive and non-toxic. Its latent heat of vaporization is high, which enables it to produce a considerable cooling capacity. On the other hand, the absorbent in these systems does not evaporate, and unlike H_2O-NH_3 systems, they do not require the use of a rectifier.

From today's perspective, the currently installed solar thermal cooling systems do not represent the technologically possible optimum. There is considerable potential to reduce costs

and/or increase performance through technological improvements or new developments in the basic materials (heat-substance transfer, working material pairs), at the component level (heat exchangers, re-cooling), and at the system level (overall plant optimization). Despite the fact that absorption refrigeration systems use waste heat in an energy-efficient manner, their environmental impact is significant. Solar air conditioning is not yet economically competitive with the currently prevailing electric air conditioning systems. The reason lies in the higher investment and low prices for conventional fuels and electrical energy, respectively. Therefore, thermodynamic analysis (energetic and exergetic) and economic insights are the most important ways to improve economic efficiency and coefficient of performance (COP).

In this regard, various research works have been carried out on the use of solar energy for cooling with absorption chillers. The mathematical modeling and optimization of thermal solar cooling systems are presented in [17–21]. More recently, thermo-economic analysis [22-26] has been applied to thermal absorption systems, combining exergy analysis and economic principles. To my knowledge, none of the above studies in the preceding survey have investigated the comparison of different configurations of solar absorption air-conditioning systems for commercial buildings in Iraq in the frame of thermo-economic analysis has not been addressed yet. Therefore, this Ph.D. dissertation aims to fill this gap. Here, different configurations of LiBr-H_2O and NH_3-H_2O solar absorption air-conditioning technology are discussed in detail.

This Ph.D. thesis is structured into four main sections. Next, the objective of the thesis is presented, followed by the problem statement. The section that follows will discuss the state of the art of thermal absorption cooling systems. In the third section the mathematical model, optimization, and energy analysis are presented. Finally, the conclusions of the work are drawn, and future works are mentioned.

1.1 Objectives

The overall objectives of the dissertation are to design, model, and compare different configurations of solar absorption air-conditioning systems for buildings in the framework of optimization and thermo-economic analysis. The main specific objectives are as follows:

- *Develop a technology road map for how to use and design solar thermal cooling in Iraq. This should include an analysis of the system's energy use and how well it works in terms of temperature.*

- *Modify the model of the solar thermal cooling system to include the flash tank for steam generation.*

- *Design and thermo-economic evaluation of a single-effect H_2O-LiBr absorption cycle with different types of solar thermal collectors.*

- *Design and thermo-economic evaluation of a single-effect NH_3-H_2O absorption cycle with different types of solar thermal collectors.*

- *Obtain mathematical correlations that allow optimization of the absorption cycle under different operation conditions.*

  - *Optimization of single effect H_2O-LiBr absorption cycle.*

  - *Optimization of single effect NH_3-H_2O absorption cycle.*

- *Comparison of different configurations of absorption cooling systems based on the use of various solar thermal collectors*

1.2 Challenge Statement

Global energy consumption has shown significant growth in recent years due to rising population numbers and continued high demand for primary energy by industrial and household users in Asia, Europe, and the USA. The high cooling demand combined with the huge supply of solar resources in Iraq, and more generally in the Middle East, suggests that solar energy for cooling is an extremely practical concept. On the other hand, electricity consumption in this region is increasing significantly and will exceed the planned generation capacity. Solar thermal cooling has gained importance in recent years because of its potential to provide efficient cooling at low costs without generating CO_2 emissions. One approach to meeting the growing global demand for efficient, intelligent air conditioning and refrigeration concepts for air conditioning and refrigeration is primarily to answer the question of the optimal design of solar-assisted absorption cycles. The conventional single-stage absorption cycle must be thermos-economically analyzed and optimized to reduce the cost, which would make the previously mentioned systems with solar cooling feasible, especially in countries where compression refrigeration systems dominate due to a lack of alternatives.

In the proposed approach in this work, all models are built according to the design calculation method. The system border streams (outlet temperature, ambient temperature, inlet cooling water temperature, etc.) are assigned by the user, and the entire design data (area,

length, volume, mass flow rate, etc.) are then calculated. Thus, a user would first assign the amount of required cooling load to the evaporator, and then all possible data for all the system units would be calculated in sequence. By specifying the system cooling load, the required thermal load is calculated. In addition, the required design limits and performance calculations would be passed out instantly. The objective of this work is to determine the optimal design and associated operating conditions. The optimization process has been carried out in order to bring down the costs and achieve techno-economic solutions. Moreover, to efficiently use the energy used in these systems, an energy analysis is performed to determine the energy demand of the system.

Chapter 2

2 State of the Art

2.1 Current State of Solar Cooling

Current economic development is based on the use of fossil fuel energy resources, causing great environmental impact and socioeconomic imbalances. These two impacts make it necessary to define a new model of sustainable development. Sustainable development means ensuring economic growth, social progress, and the rational use of resources are fulfilled simultaneously. In order to achieve sustainable development, the European Union has set a target of 12% of the primary energy demanded to be covered by renewable energy by 2010. The demand for air conditioning has increased in recent years, as people spend more time working in comfortable conditions inside buildings, reaching 6 MW in Europe. Therefore, the use of air conditioning systems based on compression technology has increased, leading to a significant increase in electricity demand in the summer, reaching, in many cases, the limits of grid capacity and the production of blackouts [27]. In the last 30 years, and especially in the last 10 years, researchers have been trying to find new ways to use solar energy to build air conditioning systems that are better for the environment.

Absorption machines are currently available on the market with a wide range of capabilities. All of them are fed with hot water, steam, or combustion gases. Despite the different types of absorption machines mentioned, the purpose of the vast majority is to produce chilled water for the cooling of buildings. In the last 30 years, and especially in the last decade, research efforts have focused on the development of environmentally friendly air-conditioning systems based on innovative, energy-efficient technologies that use solar energy. In this work, we focus on solar thermal absorption cooling systems, since they are currently the most widely used [28].

2.2 Solar Thermal Cooling

Solar thermal cooling processes can generally be divided into electrical and thermal systems. Electrical systems use photovoltaically generated electricity to drive the chiller. Thermal systems use heat generated by solar collectors to drive the thermal chiller. The present work considers only the technological development of solar thermal cooling and air conditioning. Thermally driven cooling processes use the process of physical sorption, i.e., a gaseous substance (refrigerant) is either adsorbed on a solid, porous substance (adsorption) or taken up in a liquid (absorption) and condensed in the process. With the addition of heat, the sorbent is "dried" (desorption), and the bound substance is evaporated and thus released again. Serial or simultaneous use of sorption and desorption, results in a continuously operating refrigeration system.

Depending on the type of process control, a distinction is made between open-cycle and closed-cycle refrigeration processes. In the refrigeration process of the closed cycle (absorption and adsorption chillers), primarily cold water is produced. At a low-temperature level, the chilled water absorbs the heat from the building to be cooled or air-conditioned and transfers it to the thermal cooling process. The thermal refrigeration machine achieves a temperature rise from the level of the useful cold to the level of the environment through high drive temperatures. The classical compression refrigeration process uses a mechanically driven compressor to produce chilled water, while the absorption and adsorption chillers require drive heat for a "thermal compressor." Typically, both the drive heat and the useful cold are dissipated into the environment or ambient air. According to the first law of thermodynamics, the sum of the heat fluxes given off to the environment is the sum of the heat absorbed at a high-temperature level and the heat absorbed into the cooling process at a low-temperature level (useful cooling). **Figure 1** *illustrates the heat balance of a thermal refrigerating machine, including the three different temperature levels.*
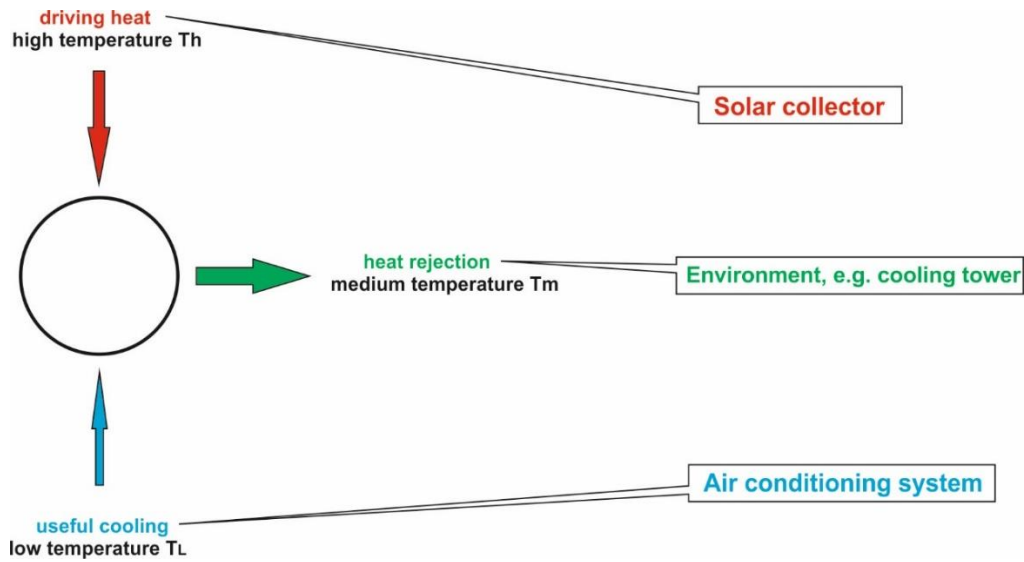
Figure 1: Energy balance of a thermal refrigeration process

The useful cold is produced at a low-temperature level, T_l. The driving heat is supplied at a high-temperature level, T_h. Both heat fluxes flow into the machine and have to be rejected at a medium temperature level, T_m. As a key figure for the characteristic of the energetic behavior of a thermally driven refrigeration machine, the COP (Coefficient of Performance) (or also $EER_{thermal}$: Thermal Energy Efficiency Ratio) is defined (see equation 1). The COP corresponds to the ratio of usable cooling energy to input drive heat.

$$COP(EER_{thermal}) = \frac{Useful\ cold\ at\ low\ temperature}{Driving\ heat\ at\ high\ temperature} \qquad\qquad (1)$$

Unlike in closed systems, the refrigerant (water) in open systems has contact with the atmosphere. While closed systems can be used not only for air conditioning but also for refrigeration, the application of open systems is limited to air conditioning of buildings. Table 1 [29] shows an overview of how solar thermal energy can be used for cooling or air conditioning, as well as a few specific system characteristics.

Table 1: Overview of thermally driven cooling systems based on sorption technology

Type of system	Water chillers (closed thermodynamic cycles)						Direct air treatment (open thermodynamic cycles)	
Physical phase of sorption material	*Liquid*			*Solid*			*Liquid*	*Solid*
Sorption material	*Water*	*Lithium-bromide*		*Zeolite*	*Silica gel*	*Lithium-chloride*	*Lithium-chloride*	*Silica gel (or zeolite), cellulose matrix with lithium-chloride*
Refrigerant	*Ammonia*	*Water*		*Water*	*Water*	*Water*	*Water*	*Water*
Type of cycle$^{(1)}$	*1-effect*	*1-effect*	*2-effect*	*1-effect*	*1-effect*	*1-effect*	*Cooled sorption process*	*Desiccant rotor*
EER$_{thermal}$ range	*0.5-0.75*	*0.65-0.8*	*1.1-1.4*	*0.5-0.75*	*0.5-0.75*	*0.5-0.75*	*0.7-1.1*	*0.6-0.8*
Driving temperature range, °C	*70-100 120-180$^{(2)}$*	*70-100*	*140-180*	*65- 90*	*65-90*	*65 - 90*	*60-85*	*60 -80*
Solar collector technology $^{(3)}$	*FPC, ETC SAT (2)*	*FPC, ETC*	*SAT*	*FPC, ETC*	*FPC, ETC*	*FPC, ETC*	*FPC, ETC, SAHC*	*FPC, ETC, SAHC*

Comments:
(1) 1-effect: single-effect thermodynamic cycle (no internal heat cascade); 2-effect: double-effect thermodynamic cycle (with internal heat cascade)
(2) Valid for production of cold at temperatures significantly below the freezing point of water, i.e., < 0°C
(3) Abbreviations for solar thermal collector types: FPC = flat plate collector; ETC = evacuated tube collector; SAT = single-axis tracking solar collector (e.g., parabolic trough collectors or Fresnel type collectors); SAHC = solar air heating collector

2.3 Currently Used Technologies

2.3.1 Absorption Chiller - Working Principle

Absorption refrigeration systems are considered three-phase cycles. They operate at three temperature levels: T_L, T_m, and T_h (verifying $T_L < T_m < T_h$). They produce cold only from a supply of heat at a temperature of T_h, i.e., without any exchange of work with the outside. The two temperatures, Tm and Tb, require two pressure levels.

- *Ph: High Pressure at the condenser and generator level,*
- *P_L: Low pressure at the level of the evaporator and the absorber.*

   Absorption refrigeration cycles work due to the ability of certain liquids to absorb and desorb vapors. They also take advantage of the fact that the solubility of this vapor in the liquid depends on the temperature and pressure. Thus, these systems use a binary mixture as a working fluid, where one of the components is much more volatile than the other and constitutes the refrigerant. The most commonly used pairs are Ammonia-Water (NH_3/H_2O, where ammonia is the refrigerant), and Water-Lithium Bromide ($H_2O/LiBr$, water being the refrigerant). The first solution allows the generation of negative refrigeration for air-conditioning or industrial refrigeration needs while the second can only generate positive refrigeration (the triple point at $0\ °C$), and is therefore exclusively suitable for building cooling. There are other solutions, but their use is still in the field of research and development or leads to poorer performance than the most common solutions.

   Figure 2 *shows a single-effect absorption cycle operating with the $H_2O/LiBr$ pair and its various components. An absorption system like the vapor compression cycle initially consists of a condenser, an expansion valve, and an evaporator through which only the pure refrigerant flows. The condenser is connected to the driving part of the process, which is responsible for changing the state of the evaporated refrigerant to make it condensable at the ambient temperature. The implementation of such a cycle requires the following active components:*

- *Condenser: a component similar to that of the vapor compression cycle. The condenser temperature is Tm, which determines the temperature of condensation and thus the pressure in the generator (desorber)/condenser unit (high-pressure P_h). Condensation requires the rejection of the heat of condensation Q_c at the temperature T_m. The corresponding path (7-8) includes a de-superheating phase, condensation as well as a possible sub-cooling.*
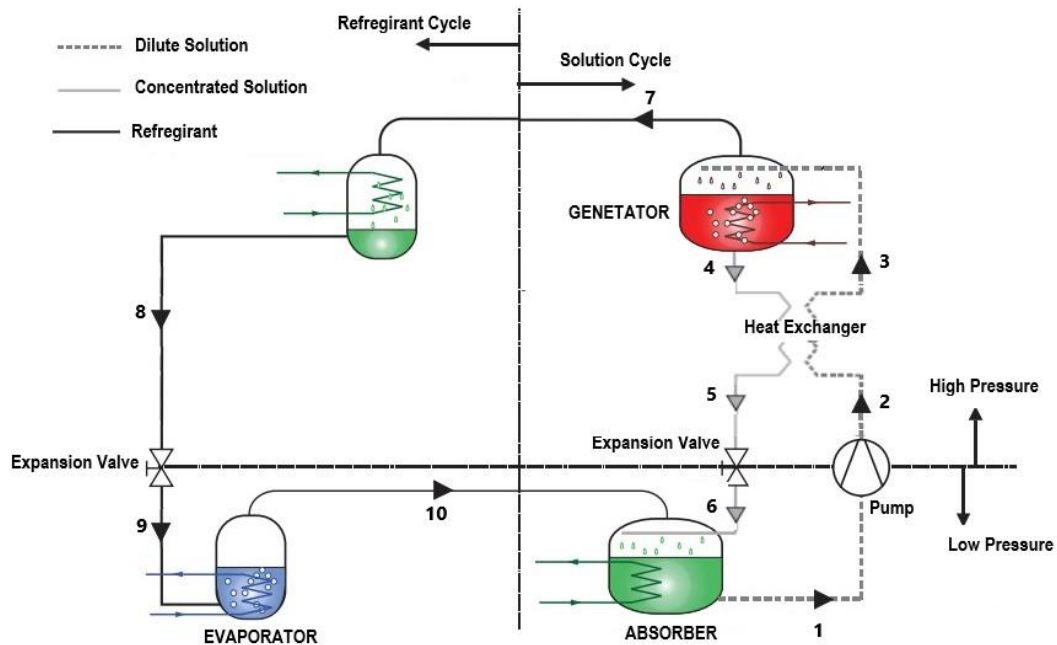
Figure 2: *Structure of absorption refrigeration cycle.*

- *Evaporator: At the outlet of the condenser (8), the liquid refrigerant undergoes a throttling through the expansion valve (8-9). Subsequently, the liquid evaporates due to the heat of the medium to be cooled, generating the cooling capacity Q_e (9-10). The temperature T_L of the refrigeration source determines the total pressure (low-pressure P_L) in the evaporator/absorber.*

- *Absorber: The vapor from the evaporator (10) meets the concentrated solution inside it (poor in refrigerant) coming from the desorber (6). This solution absorbs the vapor and is enriched with refrigerant. During this transformation, heat Q_a is released, which is discharged at the temperature T_m. At the outlet of the absorber (1), a diluted solution (rich in refrigerant) is obtained. This component performs refrigerant enrichment.*

- *Generator (desorber): The diluted solution (3) receives the quantity of heat Q_g at a temperature T_h in the desorber, thus causing the desorption of part of the refrigerant dissolved in the solution. Subsequently, the desorber produces water vapor (7) and a concentrated lithium bromide solution (4). This device performs a depletion of the refrigerant.*

To create a difference in pressure between the absorber/evaporator (P_L) and the desorber/condenser (P_h), you also need:

- *an expansion valve on the refrigerant circuit (7-8)*

- ▪ *an expansion valve on the concentrated solution circuit (poor in refrigerant) (5-6)*
- ▪ *a pump for the diluted solution circuit (rich in refrigerant) (1-2).*

It should be noted that the fluid passing through the pump is a liquid. The mechanical work done by the pump is very small compared to the thermal power required in such a cycle.

A heat exchanger may be added between the absorber and the generator, whose mission is to take advantage of the heat solution coming out of the generator in preheating the solution coming from the absorber. This reduces the amount of heat that must be supplied to the generator and separates the absorbent from the refrigerant.

2.4 Comparison between Absorption and Mechanical Compression Refrigeration Cycles

The principle of an absorption refrigeration machine's schematic design is largely similar to that of a mechanical compression machine, with a condenser, evaporator, and expansion valve (see **Figure 3***).*
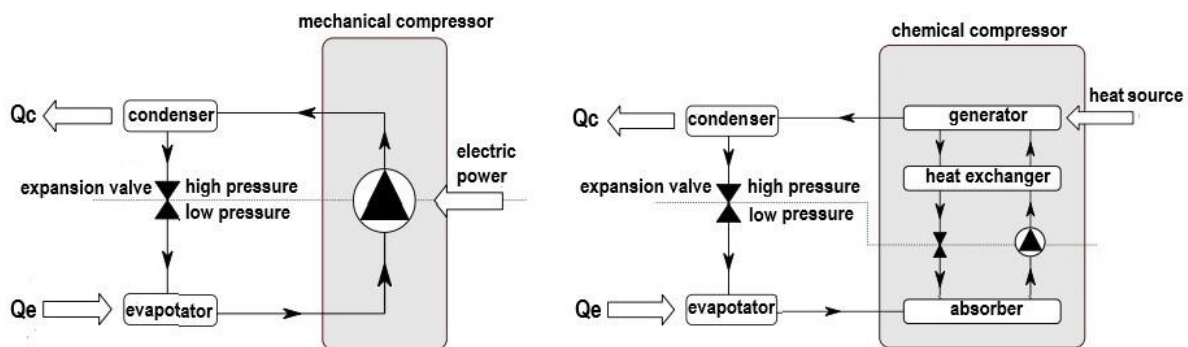

Figure 3: *Comparison between absorption and mechanical compression cooling systems*

From an overall point of view, the two systems appear identical except for the compression section, which is represented by a grey rectangle; a chemical compressor replaced by the mechanical compressor with an electric motor. Unlike the latter, the chemical compression cycle uses a refrigerant-absorbent pair such as a concentrated salt solution of lithium bromide salts (LiBr) and water (H_2O), or water (H_2O) and ammonia (NH_3). However, the chemical compression cycle is necessarily maintained under a vacuum; some machines may have a pump that allows for a vacuum draw which leads to an increase in the total electricity consumption of the machine. The Dühring diagram (see **Figure 4***) is a useful tool for understanding the behavior*

of the machine. In this diagram, it can be seen that the mechanical compression cycle has two distinct temperature levels (T_1, T_2); however, the chemical compression cycle has an additional level of temperature (T_1, T_2, T_3).

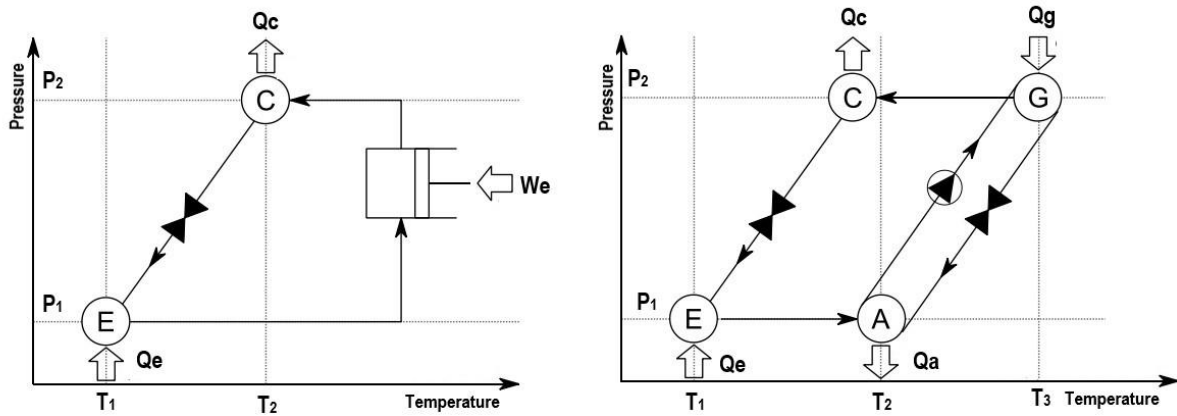**Figure 4:** *Dühring diagram for mechanical compression and chemical compression refrigeration cycles*

2.5 Suitable Collector Technologies

Solar thermal cooling systems are combined with different collector technologies depending on the required drive temperature for thermal cooling or air conditioning processes. If the thermal cooling systems are operated with drive temperatures in the range between about 60°C and 110°C, standard collector technologies can be used. **Figure 5** *shows the assignment of collectors based on their typical efficiency curves at typical drive temperatures of the various thermal cooling or air conditioning processes. In general, as the collector efficiency decreases with increasing operating temperatures and for thermal cooling or air-conditioning processes with high drive temperatures, it is necessary to use collector technologies with low thermal losses to the environment.*

From a technical standpoint [30], the following list serves as an initial guide to which collector technology is suitable for which thermal refrigeration or air conditioning process:

- *For the open process of sorption-assisted air conditioning DEC, stationary compound parabolic concentrator (CPC) collectors, flat-plate collectors, and solar air collectors deliver high sufficient temperatures to regenerate the sorption material.*
- *Adsorption chillers (ADS) can be powered by flat plate collectors, stationary CPC collectors, or evacuated tube collectors that collect heat from the sun.*

- *Stationary CPC collectors, evacuated tube collectors, and efficient flat plate collectors are mostly used to drive single-stage absorption chillers (1-ABS).*

- *The operation of two-stage absorption chillers (2-ABS) requires high drive temperatures, which forces the use of efficient evacuated tube collectors. In addition, concentrating collector technologies such as parabolic trough collectors or Fresnel collectors, with single-axis or even two-axis tracking, are used here.*
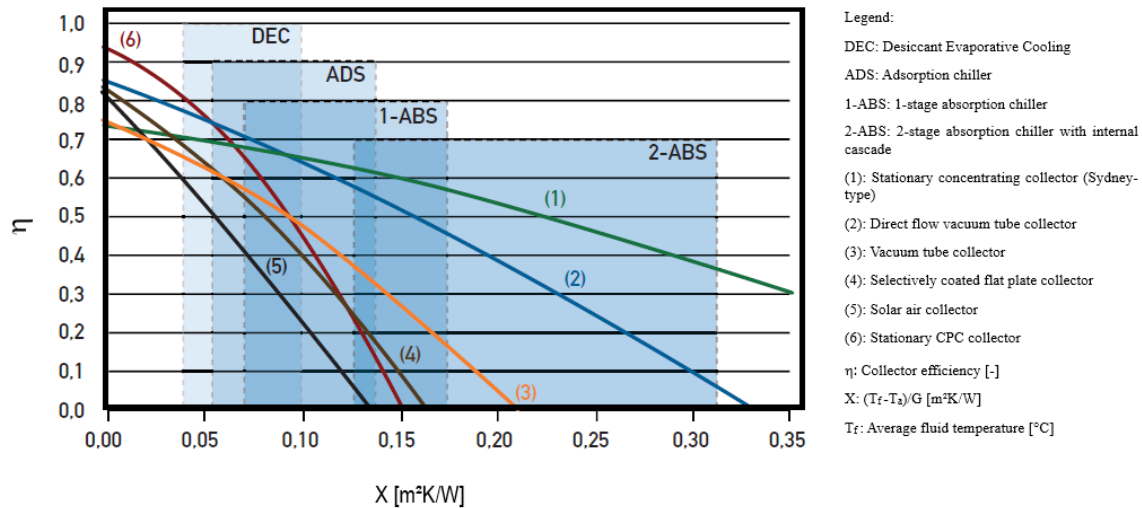
Legend:

DEC: Desiccant Evaporative Cooling

ADS: Adsorption chiller

1-ABS: 1-stage absorption chiller

2-ABS: 2-stage absorption chiller with internal cascade

(1): Stationary concentrating collector (Sydney-type)

(2): Direct flow vacuum tube collector

(3): Vacuum tube collector

(4): Selectively coated flat plate collector

(5): Solar air collector

(6): Stationary CPC collector

η: Collector efficiency [-]

X: $(T_f - T_a)/G$ [m²K/W]

T_f: Average fluid temperature [°C]

Figure 5: *Collector characteristics of different solar thermal collectors and their application as a drive for thermal cooling processes [30]*

The efficiency of a collector indicates the percentage of solar radiation reflected on the surface of the collector that can be transformed into useful thermal energy. If an optical efficiency of 80% is assumed, the maximum power of a collector surface of one square meter is equal to 0.8 kW. , However, this value is rarely reached in normal use. The maximum power is only important to find out how big the safety devices have to be.

Chapter 3

3 Thermodynamic Analysis

3.1 Thermodynamic Analysis of Absorption Cycles

In recent years a lot of research has been devoted to the improvement of solar absorption systems. The main ways to improve the efficiency of the absorption cycle are through thermodynamic analysis (energetic and exergetic) and optimization [31, 32]. Energy analysis concerns the application of the first law of thermodynamics which describes the conservation of energy within the different elements of the absorption cycle. The optimization of the first law leads to maximization of the coefficient of performance (COP) of the cycle [33], thus ensuring maximum heat dissipation with minimum input power. The first law of thermodynamics remains the most common method for the analysis of thermal systems, including absorption chillers. Several works in this vein have been completed [34-37].

3.2 Exergy Analysis of Absorption Cycle

Energy, like many other properties, should not only be evaluated in its quantity but also its quality. In conventional energy analysis based on the first law of thermodynamics, energy is evaluated mainly quantitively. Energy analysis based on the second law of thermodynamics considers the quality of energy. In the literature, several studies have addressed the concept of exergy analysis. [38, 39] provide a comprehensive discussion of exergy and thermo-economic analysis of thermal systems. In particular, exergy destruction analysis and evaluation of the exergetic efficiency of water-LiBr absorption cycles are available in [40-43]. Ammonia-water absorption cycles are discussed in [44, 45]. It is widely accepted that energy analysis provides more significant information when evaluating the performance of energy conversion systems, thus providing significant efficiencies and identifying locations of thermodynamically inefficient quantities and sources in their systems.

Energy analyses have two advantages over the conventional heat method for the analysis of the design and performance of systems related to energy. This allows greater precision of the actual inefficiencies in the systems and the true location of these inefficiencies. And also, it provides a real measure of system efficiency for more complex systems. For refrigeration cycles with heat balance analysis, it is not possible to determine the actual losses. For example, in an expansion valve, there are no energy losses, but there are pressure drops during the process. There is a loss of potential and inefficiencies in the system and the true location of these inefficiencies. From the heat balance, it is possible to conclude that the greatest losses in a cycle are in the condenser. But where exactly the actual losses occur and how these are reduced can be found only through exergetic analysis. Because of the low Carnot efficiency of refrigeration systems, the application of exergetic analysis can provide information with which the conservation of effective energy can be estimated [21].

This analysis is very important to implement to assess what capacity or availability we can obtain from different refrigeration systems by absorption and how to achieve low temperatures more efficiently without the need to use conventional compression systems, which require a lot of energy expenditure. To my knowledge, the energy and energy analysis that compares different configurations of absorption cycles integrated with various solar collectors is not covered. Hence, to fill this gap, an exergetic analysis of different absorption refrigeration systems is performed to achieve an increase in COP and exergetic efficiency.

3.3 Modeling of Absorption Cycles

The development, manufacture, and marketing of absorption systems has been accompanied by quite intense research and development activity concerning absorption. The modeling and simulation of such systems have led to a lot of work in recent years. Since we are interested in building a model not only of the system but also of the solar cooling system, we thought it would be useful to look into previous works in this field. Globally, there are two types of model applications, depending on whether the estimation of performance according to specifications in terms of temperature is targeted (we will then talk about the static model) or, on the contrary, that the objective is the evolution over time of the behavior of the system under varying conditions. In this case, we speak of a dynamic model. A final distinction should be made depending on the nature of the model used.

3.4 Selection of the Simulation Software Used

There are numerous programs for calculating thermal loads and building energy simulation. They are used for the dimensioning of air conditioning systems, but they are not intended for energy analysis. The next level is occupied by programs that allow calculating the energy required to maintain the conditions of premises. If the programs incorporate modeling teams from air conditioning would be changed to the denomination quite broadly in the principle of simulation. Some manufacturers have developed specific programs in this area, that include performance curves of their sales teams: HAP^{TM} has been developed by CARRIER [46], and TRACE^{TM} by TRANE [47]. Another type of program is one of a legal nature, used for the energy rating of buildings LIDER [48] and CALENER [49] have been developed to support the implementation of the European directive on energy efficiency at the national level, among others arising as alternative procedures. On the other hand, there are simulation programs at a high scientific level that are used fundamentally in the university environment. They are usually simulation programs that require a high level of effort and understanding but allow the analysis of countless factors. The emergence of increasingly comprehensive user interfaces has made it easier to expand the profile of users who use them.

In short, a wide variety of existing programs is observed. An interesting review study [50], conducted by the United States Department of Energy, highlights 20 the main important programs: BLAST, BSim, DeST, DOE-2.1E, ECOTECT, Ener-Win, Energy Express, Energy-10, EnergyPlus, Equest, ESP-r, IDA ICE, HAP, HEED, Power Domus, SUNREL, Tas, TRACE, and TRNSYS. Some are freely accessible and others require a license payment. Although there is no common language to describe the capabilities of each program, three fundamental characteristics stand out in the concept of modeling and simulation: Resolution scheme (sequential or simultaneous), resolution procedure (iterative implicit or explicit), and simulation time interval. Simultaneous simulation is suitable for a comprehensive analysis of the building (coupling the system and the building) and uses time steps in the simulation sufficiently small to bring simulation results closer to actual behavior. Currently, we are investigating whether there are powerful simulation tools that encompass both concepts (EnergyPlus, TRNSYS, ESP-r). There is a significant amount of research on solar-assisted absorption air conditioning systems that use the transient system simulation tool TRNSYS [51-54]. This program was developed by the University of Wisconsin and is widely used in the field of renewable energy and building simulation due to its extensive library of energy components [55, 56]. Therefore, this program

was used as a tool for the simulation of the proposed system in [1] and CARRIER software for building thermal load calculation. TRNSYS is a program originally developed in 1975 to study solar energy systems. Over time it has become a powerful tool for engineering research that can be used to solve transitory systems [57-58]. The structure of the program is modular so that it recognizes the description of the system in which the user specifies the constituent components (with their corresponding parameters) as well as the connections among them. The graphical interface of TRNSYS, Simulation Studio, allows the construction of the systems simply. Each component is a black box that has a mathematical model with a series of inputs, outputs, and parameters that characterize. It contains a library of components commonly found in solar thermal systems, and electrical, as well as a set of routines that allow you to enter certain additional functions.

The proposed system components configuration in [2, 3, and 4] are modeled and simulated depending on both the first and second laws of thermodynamics using a Matlab/Simulink environment. As a first step in modeling this system, the study is implemented depending on the steady-state basis at a constant value of solar radiation intensity. Matlab is an interactive system with an array as its basic data element that does not need to be dimensioned. Matlab is the industry standard for high-productivity research, development, and analysis. It can model linear and nonlinear systems in continuous time, sampled time, or a combination of both. Systems can also be modeled at multiple rates, with different parts sampling or updating at different rates. Simulink is a general-purpose dynamic system software program. This program was chosen for the task of modeling and simulation of solar cooling systems because it has great performance qualities for designing control algorithms. Simulink encourages consumers to explore and figure things out. Users can easily create models from scratch or customize existing models. Besides definitions of modeling, Simulink includes a graphical user interface (GUI) for creating models as block diagrams with mouse click-and-drag operations. Simulink can also take advantage of many Matlab features. Matlab is a high-performance programming language used in engineering computing. It combines computation, visualization, and programming in a user-friendly environment in which problems and solutions are expressed in familiar mathematical notation. Algorithm creation, data collection, analysis, visualization, modeling, simulation, scientific and engineering graphics application development, including graphical user interface design are common applications in Mathematics and computation.

The proposed model is operated under the design mode of modeling technique, which calculates unknown parameters such as areas, dimensions, mass flow rates, energy streams, exergy, cost streams, and the entire process temperatures or any other calculated physical properties. It is quite important to minimize power consumption because it has a direct effect on the cost and area. Therefore, best-operating conditions, assumptions, and considerations should be assigned to optimize power consumption.

Chapter 4

4 Conclusions and Perspectives

The thesis presents research on solar cooling technology using absorption chillers and thermal solar collectors for air conditioning applications. The number of existing solar cooling installations has increased significantly in recent years, especially in the small-scale sector. Many national and international projects have addressed and continue to work on the subject. But despite this, there are still barriers that make it difficult to implement this technology on a large scale. Among the obstacles that stand out is the lack of extensive knowledge of the system's choice, dimensioning, control logic, and components, as well as the fact that the cost of this type of equipment, although it has been significantly reduced, is still high compared to conventional systems. The diversity of configurations and design parameters justifies the interest in the selection of the most promising qualitatively and their subsequent quantitative comparison by simulation of different configurations of solar-assisted absorption air conditions. The configurations selected for simulation are divided into two blocks: On the one hand, only solar water-LiBr absorption configurations with hot water, cold water accumulation, and an auxiliary support system are considered in paper A [1]. On the other hand, the configurations include flash tanks located directly between the solar part and the absorption cycle. The demand for air conditioning not supplied by the solar system is provided by an independent auxiliary system. The first two simulated configurations include a water-LiBr absorption cycle integrated with different types of solar thermal collectors (paper B [2]). The rest of the configurations have an ammonia-water absorption cycle with ETC or PTC (paper C [3]). To select the best system configuration in (papers B and C [2, 3]). A detailed comparison of all simulated configurations is presented in paper D [4]. The system configuration combines a solar field (PTC/ETC), a flashing tank, and an absorption chiller (H_2O-LiBr/NH_3-H_2O). A similar base case is defined in Baghdad between configurations, although it is subsequently analyzed for the influence of certain

parameters on dimensioning, operating parameters, energy destruction rate, and cost. The conclusions withdrawn from the successive work are listed below:

- *Results of the energy analysis contribution of the water-LiBr absorption cycle integrated with ETC during the summer season in Baghdad, Iraq showed that the amount of energy incident was 178,023 kWh, while the total energy harvested was 96,073 kWh, which implies that the efficiency of ETC collectors during the cooling season is about 54%. It was also found that the solar energy supplied by the solar tank was 34,730 kWh and the energy delivered by the boiler was 26,025 kWh, indicating that the total seasonal solar coverage was about 58%. However, August presented the highest performance. The relevant average COP achieved a value of 0.52 while the solar fraction was 59.4% and the optimal inclination presented a higher solar fraction during the summer season, occurring between 15º and 25º.*

- *Optimization of the operating conditions such as temperatures has been performed for all configurations of H_2O-LiBr absorption air conditioning cycles. The following values of operating conditions are considered the best related to design aspects, COP, exergy destruction rate, and cost:*
  - *$T_a=35\,{}^oC$*
  - *$T_c=43\,{}^oC$*
  - *$T_e=7{\sim}10\,{}^oC$*
  - *$T_g=85{\sim}90\,{}^oC$*
  - *ETC $T_{high}=150{\sim}200\,{}^oC$*
  - *PTC $T_{high}=250{\sim}300\,{}^oC$*

- *According to the case study results, PTC/H_2O-LiBr is the best based on design and hourly costs. The required solar area is in the range of 2000~2500 m², while the total hourly costs are in the range of 4~5\$/h, which is quite attractive. The configuration with the lowest exergy destruction and flashing tank design aspects is PTC/H2O-LiBr The values are in the range of 930~1000 kW and the flashing tank dimensions are width 0.4~0.5 m, height 0.8 m, and volume 0.11m³. ETC/H_2O-LiBr comes next, with a total flashing tank equal to 1 m3. In general, the PTC system is thought to be the best choice for the H2O-LiBr solar cooling system, which has amazing results in terms of energy, design, and cost.*

- *Results of energy, exergy, and cost analysis configurations of solar-assisted NH_3-H_2O absorption refrigeration confirm that design aspects, such as solar area and flashing tank volume, were found to have a great influence on the cycle cost. PTC/NH3-H2O was recorded as the best based on design and hourly costs for the case study, with a cooling load in the range of 700 to 800 kW. The required solar area was in the range of 2000–2500 m^2. while the total hourly costs were in the range of USD 11.3-12.6/h. The PTC/NH_3-H_2O exergy destruction rate results are in the range of 4600–5000 kW and the lowest flashing tank design aspects are (width, 1.343 m; height, 2.743 m, and volume, 3.883 m^3). ETC/NH_3-H_2O comes next, with a total flashing tank equal to ~7.276 m^3. The best operating temperature for configurations is (T_a = 35 °C, T_c = 43 °C, T_e = 710 °C, T_g = 8590 °C, ETC T_{high} = 150-200 °C, PTC T_{high} = 250-300 °C).*

- *The introduction and study of different solar-assisted absorption air conditioning (AAC) cycle configurations that make up the installation are carried out. The results comparing the mathematical models of the configurations show that the design aspects such as solar area and flashing tank volume were found to greatly influence the cycle cost. The type of collector has a crucial influence on the results, mainly in cooling, since the collector works at higher temperatures, which is where the most performance difference is between the performance curves. Among all the configurations, PTC-H_2O-LiBr gives a remarkable result compared to the ETC. PTC-H_2O-LiBr was recorded as the best based on design and hourly costs, with a catchment area in the range of 2000~2500 m^2. Meanwhile, the total hourly cost was in the range of 4~5 \$/h, which is quite attractive.*

- *The solar field recorded a larger amount of exergy destruction rates for all configurations due to the large area and mass flow rate effect. PTC-H_2O-LiBr resulted in a 930~1000 kW exergy destruction rate compared to PTC-NH_3-H_2O, which resulted in a value of 4600~5000 kW.*

- *The thermo-economic cost is almost the same for all configurations in the range of 0.14-0.16 \$/GJ, with an advantage for the H_2O-LiBr configuration.*

- *The absorption chiller coefficient of performance was in the range of 0.5 to 0.9.*

- *When the cooling load goes up, the size of the solar field and the flow rate of the heat transfer fluid also have to go up.*

- *It is quite clear that PTC-H_2O-LiBr, followed by ETC-H_2O-LiBr has remarkable results in terms of energy, design, and cost. Generally, the PTC system is considered the best choice for H_2O-LiBr or NH_3- H_2O.*

The following points should be kept in mind for the future works:

- *Carry out energy and thermo-economic analysis for different configurations and stages of absorption cycles.*
- *Improving the absorption cycle performance by using other working pairs*
- *Study and analyze different alternative sources of heat rejection.*
- *Carry out more price feasibility studies on the design of solar absorption cooling systems.*
- *Study the effect of adding a tracing system to the solar thermal collector to increase the collector's solar radiation capture.*
- *The model of the absorption cycle could be extended to include environmental impact.*
- *The solar absorption cooling system can be modified to include other types of solar collectors with different arrangements, considering possible configurations.*
- *Carry out a more detailed analysis of the use of solar energy available in Iraq for this type of technology.*

Bibliography

1. *Al-Falahi, A., Alobaid, F., & Epple, B. (2020). A new design of an integrated solar absorption cooling system driven by an evacuated tube collector: A case study for Baghdad, Iraq. Applied Sciences, 10(10), 3622.*

2. *Al-Falahi, A., Alobaid, F., & Epple, B. (2020). Design and thermo-economic comparisons of large scale solar absorption air conditioning cycles. Case Studies in Thermal Engineering, 22, 100763.*

3. *Al-Falahi, A., Alobaid, F., & Epple, B. (2020). Thermo-Economic Evaluation of Aqua-Ammonia Solar Absorption Air Conditioning System Integrated with Various Collector Types. Entropy, 22(10), 1165.*

4. *Al-Falahi, A., Alobaid, F., & Epple, B. (2021). Thermo-Economic Comparisons of Environmentally Friendly Solar Assisted Absorption Air Conditioning Systems. Applied Sciences, 11(5), 2442.*

5. *Casals XG. Solar absorption cooling in spain: Perspectives and outcomes from the simulation of recent instalations. Renewable Energy 2006;31:1371.*

6. *Balaras CA, Grossman G, Henning HM, Ferreira CAI, Podesser E, Wang L, et al. Solar air conditioning in Europe: an overview. Renewable and Sustainable Energy Reviews 2007; 2:299.*

7. *Henning HM. Solar assisted air conditioning of buildings - an overview. Applied Thermal Engineering 2007;27:1734.*

8. *Commission of the European Communities C. Towards a European strategy for the security of energy supply. Tech. Rep.; 2000.*

9. *S. Rashid, "Electricity Problem in Iraq, Academia, p. 22, 2012.*

10. *Rosiek S, Batlles FJ. Integration of the solar thermal energy in the construction: Analysis of the solar-assisted air-conditioning system installed in ciesol building. Renewable Energy 2009;34:1423.*

11. *Doukas H, Patlitzianas KD, Kagiannas AG, Psarras J. Renewable energy sources and rationale use of energy development in the countries of GCC: Myth or reality? Renewable Energy 2006;34:755.*

12. *Jaruwongwittaya T, Chen G. A review: Renewable energy with absorption chillers in thailand. Renewable and Sustainable Energy Reviews 2009;14:1437.*

13. *DONATE, Marina; RODRIGUEZ, Luis; DE LUCAS, Antonio; RODRIGUEZ, Juan F. Thermodynamic evaluation of a new absorbent mixtures of lithium bromide and organic salts for absorption refrigeration machines.International Journal of Refrigeration 29 (2006) 30-35.*

14. *KILIC, Muhsin; KAYNAKLI, Omer. Second law-based thermodynamic analysis of water-lithium bromide absorption refrigeration system. Energy 32 (2007) 1505-1512.*

15. *SÖZEN, A. Effect of heat exchangers on performance of absorption refrigeration systems. Energy Conversion and Management 42 (2001) 1699-1716.*

16. *SUN, Da Wen. Comparison of the performances of NH_3-H_2O, NH_3-$LiNO_3$ and NH_3-$NaSCN$ Absorption Refrigeration Systems. Energy Conversion and Management 39 (1998) 357-368.*

17. *Siddiqui, F. R., El-Shaarawi, M. A. I., & Said, S. A. M. (2014). Exergo-economic analysis of a solar driven hybrid storage absorption refrigeration cycle. Energy Conversion and Management, 80, 165-172.*

18. *Mazzei, M. S., Mussati, M. C., & Mussati, S. F. (2014). NLP model-based optimal design of LiBr-H_2O absorption refrigeration systems. International journal of refrigeration, 38, 58-70.*

19. *Chen, Q., & Zhao, T. (2019, July). Heat current method based modeling and optimization of a solar driven absorption chiller for residential houses. In Energy Sustainability (Vol. 59094, p. V001T01A001). American Society of Mechanical Engineers.*

20. *Mansouri, R., Boukholda, I., Bourouis, M., & Bellagi, A. (2015). Modelling and testing the performance of a commercial ammonia/water absorption chiller using Aspen-Plus platform. Energy, 93, 2374-2383.*

21. *Xu, Y. J., Zhang, S. J., & Xiao, Y. H. (2016). Modeling the dynamic simulation and control of a single effect LiBr-H_2O absorption chiller. Applied Thermal Engineering, 107, 1183-1191.*

22. *Asadi, J., Amani, P., Amani, M., Kasaeian, A., & Bahiraei, M. (2018). Thermo-economic analysis and multi-objective optimization of absorption cooling system driven by various solar collectors. Energy Conversion and Management, 173, 715-727.*

23. *Jalili, Mohammad, Ata Chitsaz, and Mohammad Alhuyi Nazari. "Investigating the fuel type influence on the thermo-economic performance of absorption refrigeration systems: a comparative study." Journal of Thermal Analysis and Calorimetry (2021): 1-18.*

24. *Rad, E. A., & Davoodi, V. (2021). Thermo-economic evaluation of a hybrid solar-gas driven and air-cooled absorption chiller integrated with hot water production by a transient modeling. Renewable Energy, 163, 1253-1264.*

25. *Assareh, E., Assareh, M., Alirahmi, S. M., Jalilinasrabady, S., Dejdar, A., & Izadi, M. (2021). An extensive thermo-economic evaluation and optimization of an integrated system empowered by solar-wind-ocean energy converter for electricity generation-Case study: Bandar Abas, Iran. Thermal Science and Engineering Progress, 25, 100965.*

26. *Bhowmick, A., & Kundu, B. (2021). Thermo-economic optimization and comparison study of LiBr-H2O and LiCl-H2O working pair in absorption cooling systems based on genetic algorithm. International Journal of Energy Research, 45(3), 3938-3954.*

27. *Desideri, U., Proietti, S., Sdringola Paolo, 2009, Solar-powered cooling systems: Technical and economic analysis on industrial refrigeration and air-conditioning applications, Applied Energy, Vol. 86, pp.1376-1386.*

28. *Kima, D.S, Infante Ferreira, C.A., 2008, Solar refrigeration options - a state-of-the art review, International Journal of Refrigeration, Vol.31, pp.3-15.*

29. *Henning, H. M. (2011). Solar cooling position Paper. IEA SHC Task, 38.*

30. *Henning H.-M., et al., Solar-Assisted Air-Conditioning in Buildings, Handbook for Planners, Springer Verlag, Wien, New York, ISBN 3-211-00647-8, Page 49, 2004.*

31. *Sözen, A. (2001). Effect of heat exchangers on performance of absorption refrigeration systems. Energy conversion and management, 42(14), 1699-1716.*

32. *Misra, R. D., Sahoo, P. K., & Gupta, A. (2006). Thermoeconomic evaluation and optimization of an aqua-ammonia vapour-absorption refrigeration system. International Journal of Refrigeration, 29(1), 47-59.*

33. *Muhsin Kilic, Kaynakli O. 2007. Second lawbased thermodynamic analysis of waterlithium bromide absorption refrigeration system. Energy, **32**: 1505-1512.*

34. *Kim, D. S., & Ferreira, C. I. (2006). A Gibbs energy equation for LiBr aqueous solutions. International Journal of Refrigeration, 29(1), 36-46.*

35. *Yumrutaş, R., Kunduz, M., & Kanoğlu, M. (2002). Exergy analysis of vapor compression refrigeration systems. Exergy, An international journal, 2(4), 266-272.*

36. *Grossman, G., Wilk, M., & DeVault, R. C. (1993). Simulation and performance analysis of triple-effect absorption cycles (No. CONF-940104-13). Oak Ridge National Lab., TN (United States).*

37. *Lee, S. F., & Sherif, S. A. (2000). Second law analysis of multi-stage lithium bromide/water absorption heat transformers. Univ. of Florida, Gainesville, FL (US).*

38. *Kotas, T. J. (1995). The Exergy Analysis Method of Thermal Plant Analysis, Krieger. Melbourne, Australia.*

39. *Bejan, A., Tsatsaronis, G., & Moran, M. J. (1995). Thermal design and optimization. John Wiley & Sons.*

40. *Anand, D. K., Lindler, K. W., Kennish, W. J., & Schweitzer, S. (1984). Second law analysis of solar powered absorption cooling cycles and systems. ASME Journal of Solar Energy and Engineering, 106, 291-298.*

41. *Koehler, W. J., Ibele, W. E., Soltes, J., & Winter, E. R. (1988). Availability simulation of a lithium bromide absorption heat pump. Heat Recovery Systems and CHP, 8(2), 157-171.*

42. *Talbi, M. M., & Agnew, B. (2000). Exergy analysis: an absorption refrigerator using lithium bromide and water as the working fluids. Applied Thermal Engineering, 20(7), 619-630.*

43. *Kilic, M., & Kaynakli, O. (2007). Second law-based thermodynamic analysis of water-lithium bromide absorption refrigeration system. Energy, 32(8), 1505-1512.*

44. *Ataer, Ö. E., & Göğüs, Y. (1991). Comparative study of irreversibilities in an aqua-ammonia absorption refrigeration system. International Journal of Refrigeration, 14(2), 86-92.*

45. *Best, R., Islas, J., & Martinez, M. (1993). Exergy efficiency of an ammonia-water absorption system for ice production. Applied energy, 45(3), 241-256.*

46. *http://www.commercial.carrier.com/commercial/hvac/general/0,,CLI1_DIV12_ETI496_MID4 355,00.html*

47. *http://www.trane.com/TRACE.*

48. *http://www.codigotecnico.org/index.php?id=33.*

49. *http://www.mityc.es/energia/desarrollo/EficienciaEnergetica/CertificacionEnergetica/Programa Calener/Paginas/DocumentosReconocidos.aspx.*

50. *US Department of Energy, Crawley D.; Energy Systems Research Unit University of Strathclyde in Glasgow, Hand J.; University of Wisconsin-Madison, Kummert M.; National Renewable Energy Laboratory- Colorado USA, Griffith B; "Contrasting the capabilities of building energy performance simulation programs".*

51. *Sparber W., Napolitano A., Eckert G., Preisler A., 2009. State of the art on existing solar heating and cooling systems'. International Energy Agency Technical Report 2009-11-12.*

52. *Hans-Martin Henning, 2011. Status and Perspectives of Solar Air-Conditioning and Refrigeration. 4th International Conference Solar Air-Conditioning.*

53. *D2.5: Summary of report on specification of component costs. Solarcombi+, Athens, February 2009 Edited by Dr Yannis Vougiouklakis, Ms Myrto Theofilidi.*

54. *http://www.iea-shc.org/*

55. *http://www.iea-shc-task25.org/english/index.html*

56. *http://www.iea-shc.org/task38/index.html*

57. *http://sel.me.wisc.edu/trnsys/*

58. *http://www.trnsys.com/*

Paper A

A New Design of an Integrated Solar Absorption Cooling System Driven by an Evacuated Tube Collector: A Case Study for Baghdad, Iraq

Adil Al-Falahi *, Falah Alobaid and Bernd Epple

Institut Energiesysteme und Energietechnik, Technische Universität Darmstadt, Otto-Berndt-Straße 2, 64287 Darmstadt, Germany; falah.alobaid@est.tu-darmstadt.de (F.A.); bernd.epple@est.tu-darmstadt.de (B.E.)

* Correspondence: adil.al-falahi@est.tu-darmstadt.de; Tel.: +49-6151-16-20724; Fax: +49-6151-16-22690

Abstract: The electrical power consumption of refrigeration equipment leads to a significant influence on the supply network, especially on the hottest days during the cooling season (and this is besides the conventional electricity problem in Iraq). The aim of this work is to investigate the energy performance of a solar-driven air-conditioning system utilizing absorption technology under climate in Baghdad, Iraq. The solar fraction and the thermal performance of the solar air-conditioning system were analyzed for various months in the cooling season. It was found that the system operating in August shows the best monthly average solar fraction (of 59.4%) and coefficient of performance (COP) (of 0.52) due to the high solar potential in this month. Moreover, the seasonal integrated collector efficiency was 54%, providing a seasonal solar fraction of 58%, and the COP of the absorption chiller was 0.44, which was in limit, as reported in the literature for similar systems. A detailed parametric analysis was carried out to evaluate the thermal performance of the system and analyses, and the effect of design variables on the solar fraction of the system during the cooling season.

1. Introduction

There is growing demand for air conditioning in hot climate countries (due to increase in internal loads in buildings), and greater demand for thermal comfort by its users; thus, it is becoming one of the most important types of energy consumption [1]. Accordingly, the consumption of electrical power by refrigeration equipment begins to cause problems in the supply network on the hottest summer days.

Most buildings are provided with electrically driven vapor compression chillers. Currently, the energy for air conditioning is expected to increase tenfold by 2050 [2]. In Iraq, the demand for cooling and air conditioning is more than 50%–60% of total electricity demand (48% in the residential sector) [3]; thus, it contributes to increased CO_2 emissions, which could increase by 60% by 2030, compared to the beginning of the century (even though we urgently need to reduce) [4]. On the other hand, mechanical compression chillers utilize various types of halogenated organic refrigerants, such as HCFCs (hydrochlorofluorocarbons), which still contribute to the depletion of the ozone layer; this is why many of these refrigerants have been banned or are in the process of being banned.

To enhance a building's energy efficiency, solar-driven cooling systems seem to be an attractive alternative to conventional electrical driven compression units, as they achieve primary energy savings and reduce greenhouse gas emissions for solar fractions higher than about 50% [5]. They use refrigerants that do not harm the ozone layer and demand little external electric power supply.

The simulations of lithium bromide (LiBr)/water (H_2O) absorption cooling systems have a long history, but a general model for all circumstances is still elusive. Bani Younes et al. [6] presented a

simulation of a LiBr–H$_2$O absorption chiller of 10 kW capacity for a small area of 100 m^2 under three different zones in Australia. They concluded that the best system configuration consists of a 50 m^2 flat plate collector and a hot water storage tank of 1.8 m^3. In Tunisia, a feasibility and sensitivity analysis of the solar absorption cooling system was conducted by Barghouti et al. [7] using TRNSYS (University of Wisconsin-Madison, Madison, WI, USA, 1994) and EES software. They concluded that a house of 150 m^2 required 11 kW of absorption chiller, with 30 m^2 of flat plate solar collectors and a 0.8 m^3 storage tank to cover the cooling load.

For their part, Martínez et al. [8] compared the simulation of a solar cooling system using TRNSYS software, with real data from a system installed in Alicante, Spain. The air-conditioning system was composed of a LiBr–H$_2$O absorption chiller with 17.6 kW capacity and 1 m^3 hot storage tank. The results show an approximation between the measured and simulated data, where the coefficient of performance (COP) of the absorption chiller from the experimental data was 0.691 while the COP of the simulated system reached a value of 0.73.

Burckhartyotros [9] described a 250 m^2 field of vacuum tube solar thermal collectors, which provided hot water at temperatures of about 90 °C, to drive lithium bromide/water absorption chiller with a capacity of 95 kW, utilized to cover the thermal loads for a building of 4000 m^2, which included offices, laboratories, and a public area.

Ketjoy et al. [10] evaluated the performance of a LiBr–H$_2$O absorption chiller with 35 kW cooling capacity, integrated with 72 m^2 of evacuated tube collectors (ETC) and an auxiliary boiler. They found that the solar absorption system had high performance with a ratio of 2.63 m^2 of collector area for each kW of air-conditioning.

A solar parabolic trough collector has been used beside a single effect LiBr–H$_2$O absorption chiller [11]. Peter Jenkins [12] studied the principles of the operation of the solar absorption cooling system. The total solar area was 1450 m^2. Wang [13] investigated the effect of large temperature gradients and serious nanoparticles, photothermal conversion efficiency on direct absorption solar collectors.

Hamza [14] studied the development of a dynamic model of a 3TR (Ton of Refrigeration) single-effect absorption cooling cycle that employs LiBr–water as an absorbent/refrigerant pair, coupled with an evacuated tube solar collector and a hot storage unit.

Rasool Elahi [15] studied the effect of using solar plasma for the enhancement operation of solar assisted absorption cycles. Behi [16] presented an applied experimental and numerical evaluation of a triple-state sorption solar cooling module. The performance of a LiCl–H$_2$O based sorption module for cooling/heating systems with the integration of external energy storage has been evaluated. Special design for solar collectors was investigated by Behi [16]. Related to thermo-economics, Salehi [17] studied the feasibility of solar assisted absorption heat pumps for space heating. In this study, single-effect LiBr–H$_2$O and NH$_3$-H$_2$O absorption, and absorption compression-assisted heat pumps were analyzed for heating loads of 2MW (Mega Watt). Using the geothermal hot springs as heat sources for refrigerant evaporation, the problem of freezing was prevented. The COP ranged between 1.4 and 1.6. Buonomano et al. [18] studied the feasibility of a solar assisted absorption cooling system based on a new generation flat plate ETC integrated with a double-effect LiBr–H$_2$O absorption chiller. The results of the experiment show that maximum collector efficiency is above 60% and average daily efficiency is about 40%, and they show that systems coupled with flat-plate ETC achieve a higher solar fraction (77%), in comparison with 66.3% for PTC (Parabolic Through Collector) collectors.

Mateus and Oliveira [19] performed energy and detailed economic analysis of the application of solar air conditioning for different buildings and weather conditions. According to their analysis, they consider that the use of vacuum tube collectors reduces the solar collector surface area of about 15% and 50% in comparison with flat solar collectors. According to the final report of the European Solar Combi+ project, the use of evacuated tube collectors allows for greater energy savings (between 15% and 30%) but the investment increases significantly [20].

Shirazi et al. [21] simulated four configurations of solar-driven LiBr–H$_2$O air-conditioning systems for heating and cooling purpose. Their simulation results revealed that the solar fraction of 71.8%

and primary energy conservation of 54.51% could be achieved by the configuration that includes an absorption chiller with a vapor compression cycle as an assistance cooling system.

Vasta et al. [22] analyzed the performance of an adsorption cycle under different climate zones in Italy. It was concluded that the performance parameters were influenced significantly by the design variables. They found that with the dry and wet cooler, the solar fraction could archive values of 81% and 50% at lower solar collector areas. In addition, it was found that the COP could reach 57% and 35% in the same collector arrangement.

In recent years, research projects on solar refrigeration have been carried out to develop new equipment, reducing costs and stimulating integration into the building air conditioning market.

Calise et al. [23] carried out a transitional simulation model using the TRNSYS software. The building was 1600 m^2 building; the system included the vacuum tube collectors of 300 m^2 and a LiBr–H$_2$O absorption chiller. It was found that a higher coefficient of performance (COP) was 0.80; optimum storage volume of 75 L/m^2 was determined when the chiller cooling capacity was 157.5 kW.

Djelloul et al. [24] simulated a solar air conditioning system for a domestic house using TRNSYS software. They indicate that to cover the cooling load of a house of 120 m^2 the best air-conditioning system configuration consisted of a single-effect Yazaki absorption chiller of 10 kW, 28 m^2 flat plate collectors with 35° inclination, and a hot storage tank of 0.8 m^3. They concluded that the ratio of the collector area per kW cooling was 2.80 m^2/kW.

In Iraq, the conventional electricity grid is not working well as the country struggles to recuperate from years of war [25]. However, Iraq is blessed with an abundance of solar energy, which is evident from the average daily solar irradiance, ranging from 6.5–7 kWh/m^2 (which is one of the highest in the world). This corresponds to total annual sunshine duration ranging between 2800–3000 h [26]. Accordingly, solar cooling technology promotion in Iraq appears to be of high importance, concerning development, and is part of the government's new strategy for promoting renewable energy projects.

It is clear from the literature that solar energy has a great influence on refrigeration and/or air conditioning processes. Different types and configurations of solar collectors have been applied for such purposes. The most used type was the evacuated tube collector (ETC). Moreover, it was noticed that LiBr–H$_2$O have been used for most of the research activities in this regard [27,28].

The aim of this work is to provide (1) a valuable roadmap related to solar-driven cooling systems operating under the Iraq climate to allow for sustained greenhouse gas emission reductions in the residential air conditioning sector, and (2) energetic performance analysis of solar driven cooling systems to investigate the best system design parameters.

2. Design Aspects

2.1. Thermal Solar Cooling System Description

Solar cooling technology uses the solar hot water system as an energy resource for the sorption cycle. The solar absorption cooling system (SACS) under investigation contains two main parts (see Figure 1): the heat medium production and cold medium production. The heat medium production includes solar thermal collectors, a solar tank, auxiliary boiler, two pumps, and a distribution cycle. The cold medium production integrates an absorption chiller, a cooling tower, and two circulating pumps connected, respectively, to the absorber and evaporator. The energy harvested from the incident solar radiation heats the water in a field of the evacuated tube collector (ETC). Then, the hot water flows into a solar tank and is subsequently transported to the absorption chiller through the auxiliary boiler to produce chilled water, which circulates through a conventional distribution system of individual fan coils to deliver cold air to the building. An auxiliary heater is activated if the hot water temperature is not sufficient to drive the chiller. The cooling water dissipates the heat of the absorber and condenser of the chiller through the cooling tower. Figure 1 shows all of the elements that will be taken into account in the simulation and is described, in detail, in the following subsections.
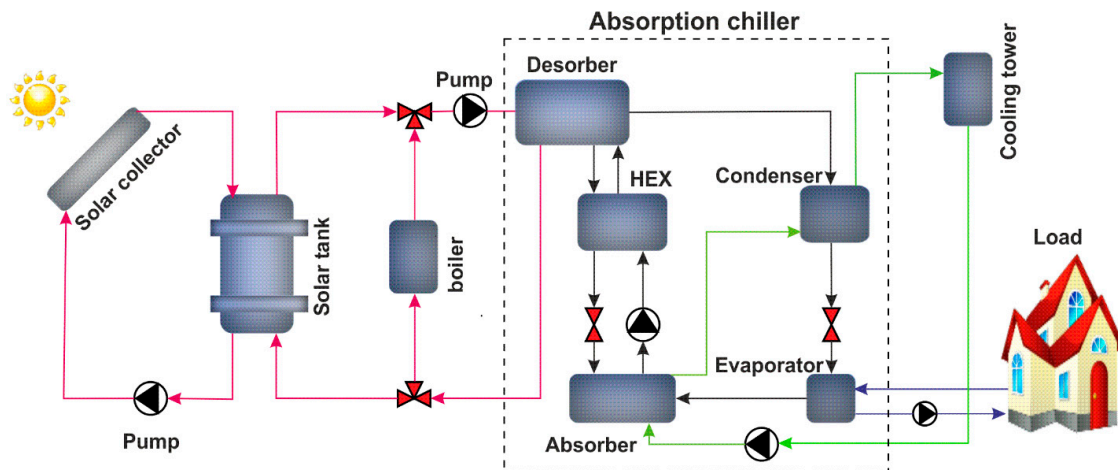
Figure 1. Solar absorption cooling system components.

2.1.1. Solar Collector

The evacuated tube collector (ETC) is the most popular solar collector in the world and excels in cloudy and cold conditions. The Apricus ETC-30 solar collector has been selected in this study [29]. The ETC is made up of two concentric glass tubes; the interior acts as a collector and the exterior as a cover. The elimination of air between the tubes reduces energy loss. An advantage of flat absorber vacuum tubes, from architectural integration, is that they can be installed on a horizontal or vertical surface, and the tubes can be rotated so that the absorber is at the appropriate inclination [30]. The collector thermal efficiency η_c is given in Equation (1):

$$\eta_c = \eta + a_1 \frac{\Delta T}{I_T} - a_2 \frac{(\Delta T)^2}{I_T} \tag{1}$$

where: η is the optical efficiency, a_1 and a_2 present, respectively, loss coefficient, ΔT refers to the difference between the average water temperature through solar collector T_m and the ambient temperature T_a and I_T is the total radiation incident on the absorber surface, for modeling the evacuated tube collectors (ETCs) in TRNSYS, needs an external file of incidence angle modifier (IAM) both longitudinal and transversal, which can be gained from manufacturer catalog. The performance specifications of the ETC are listed in Table 1 [29].

Table 1. Technical specifications of the Apricus evacuated tube collector (ETC)-30 solar collector [29].

Variable	Units	Value
Absorber area	m^2	2.4
Optical performance (η)	-	0.845
Loss coefficient (a_1)	W/(m^2·K)	1.47
Loss coefficient (a_2)	W/(m^2·K)	0.01

2.1.2. Solar Tank

The capacity of the hot storage tank is a decisive step in the solar system design and depends on the type of installation of three factors: the installed area of collectors, the operating temperature, and the time difference between the capture and storage. In installations for solar cooling, some authors have used values of 25 to 100 L/m^2 of the collector area [21]. For the calculation of the solar tank,

we will assume that the hot water is stratified. The stratified storage tank comprises N nodes, the *i* node energy balance is given in Equation (2) [31]:

$$M_i C_P \frac{dT_i}{dT} = \dot{m}_s C_P (T_{i-1} - T_i) - \dot{m}_L C_P (T_{i+1} - T_i) - UA_i (T_i - T_a) \tag{2}$$

where: M_i is the fluid mass at the node *i*, C_P is the fluid specific heat, $\dot{m}_s$ is the mass flow rate from the heat source side, $\dot{m}_L$ is the mass flow rate of the load side, U is the overall losses from the solar tank to the environment, A_i is the surface transfer area, T_i is the node temperature, and T_a is the ambient temperature. An overall heat transfer coefficient for heat loss between the storage tank and the environment of 1.5 kJ/(h·m²·K) will be assumed, close to that used by Barghouti et al. [31].

2.1.3. Auxiliary Boiler

To operate the absorption chiller when the captured radiation is insufficient and the solar tank is depleted, an auxiliary system is employed to maintain the thermal energy at the desired level to drive the thermal chiller, the thermal energy $\dot{Q}_{aux}$ supplied by the auxiliary boiler can be calculated by Equation (3):

$$\dot{Q}_{aux} = \frac{\dot{m} C_P (T_{set} - T_{in}) + UA_{aux} (T_{aux} - T_o)}{\eta_{aux}} \tag{3}$$

where: T_{in} is the fluid inlet temperature, T_{set} is the thermostat set temperature, UA_{aux} refers to the overall coefficient of loss to the environment, η_{aux} is the auxiliary heater efficiency, and T_{aux} is the average temperature can be calculated by Equation (4):

$$T_{aux} = \frac{(T_{set} - T_{in})}{2} \tag{4}$$

In this work, a boiler with a nominal power of 60 kW ($Q_e/COP = 35/0.70 = 50\ KW$) has been selected, and a performance of 90%, which will be assumed constant. For the auxiliary boiler, the parallel arrangement is preferred to prevent its operation from contributing to the heating of the water in the storage tank.

2.1.4. Heat Rejection System: Cooling Tower

A heat rejection system is attached to the thermal absorption chiller in order to evacuate the heat from the absorber and the condenser of the chiller and eject it to the ambient air. In this paper, the counterflow mechanical wet cooling tower was selected with the Baltimore Aircoil Company (BAC, Madrid, Spain) [32], The selected tower is the FXT-26 model, which has the nominal operating conditions listed in Table 2 and it is capable of dissipating all the heat evacuated by the absorption chiller under any environmental conditions in the location of installation (in our case, Baghdad, Iraq). The counterflow, the forced draft-cooling tower can be modeled in TRNSYS, based on the number of transfer units (NTU) [33]:

$$NTU = c \left[\frac{\dot{m}_a}{\dot{m}_w} \right]^{(n+1)} \tag{5}$$

where: $\dot{m}_w$ and $\dot{m}_a$ are the mass flow rates of water and air, respectively, *c* and *n* are the coefficients of mass transfer constant and exponent; their values are given by the manufacturer's curves in this paper, the selected values of *c* and *n* are 0.5 and −0.856 respectively.

Table 2. Technical characteristics of the FXT-26 cooling tower [32].

Characteristics	Value	Units
Cooling tower capacity	105	kW
Wet temperature	25	°C
Cooling water temperature	35-30	°C
Airflow rate	16	m^3/h
Electrical power	0.75	kW

2.1.5. Cooling Cycle: Absorption

The proposed chiller simulated here is the single-effect LiBr–H$_2$O absorption chiller YAZAKI WFC-SC10 (Yazaki Energy Systems Inc., Plano, TX, USA) with a nominal coefficient of performance (COP) of 0.70 and nominal cooling capacity $\dot{Q}_e$ of 35 kW. The technical specifications of the chiller are listed in Table 3 [34]. For the analysis of facilities, we will always assume a maximum demand capable of being satisfied by this chiller to cover the cooling load (in our case the maximum demand will be 25 kW). The simulation program required data from the chiller catalog that describes the chiller's operating map in order to determine the operating variables. The absorption machines are usually characterized by two basic parameters:

→   COP nominal. COP$_{nom}$. (0.7 for Yazaki WFC-10, Yazaki Energy Systems Inc., Plano, TX, USA)
→ $\dot{Q}_e$ Nominal evaporator power $\dot{Q}_{e,nom}$. (35 kW for Yazaki WFC-10, Yazaki Energy Systems Inc., Plano, TX, USA)

Table 3. Specifications of the YAZAKI WFC-SC10 absorption chiller [34].

Characteristic	Unit	Value
Cooling capacity	kW	35
Chilled water outlet /inlet temp.	°C	7/12.5
Cooling water outlet /inlet temp.	°C	35/31
Heating water outlet /inlet temp.	°C	88/83
Chilled water flowrate	m^3/h	11
Cooling water flow rate	m^3/h	36.7
Heating water flow rate	m^3/h	17.3
Electric power consumption	kW	0.21

From these, the nominal generator power $\dot{Q}_{g,nom}$ is immediately available by simply dividing the nominal cooling power $\dot{Q}_{e,nom}$ by the nominal coefficient of performance COP$_{nom}$. The TRNSYS model also requires entering the target temperature to be obtained at the outlet of the evaporator $T_{e,set}$, as well as the temperatures and flows entering the three external circuits: evaporator T_{ei}, condenser T_{ci} and generator T_{gi}. In this way, the model can determine the load regime in which the chiller works. Under these conditions, two situations can occur: if there is sufficient output power available on the evaporator, the set temperature will be reached. If not, the lowest possible value will be reached with the available power.

The instant heat $\dot{Q}_{remove}$ that should be removed from the incoming flow of the child as well as the load fraction f_{Load} are determined by Equations (6) and (7).

$$\dot{Q}_{remove} = \dot{m}_e C_{p,e} (T_{ei} - T_{e,set}) \qquad (6)$$

$$f_{Load} = \frac{\dot{Q}_{remove}}{\dot{Q}_{e,nom}} \tag{7}$$

With the load fraction and the temperatures indicated above (set, evaporator, condenser, and generator) it is possible to access the configuration file, whose structure will be commented on later, and which has been made from the chiller operation curves offered by the manufacturer for a set of operation points, establishing two basic parameters:

→　Fraction capacity $f_{capacity}$: is the ratio of the evaporator's output power to the nominal power of the chiller. With the manufacturer's data for each of the established operating points, the quotient between the output power it has in each of these conditions and the nominal power of the evaporator is evaluated.

$$f_{capacity} = \frac{\dot{Q}_e}{\dot{Q}_{e,nom}} \tag{8}$$

where $\dot{Q}_e$ is the output power under the particular conditions;

→　Energy input fraction $f_{Energyinput}$: is the ratio of the generator power to the nominal generator power necessary to satisfy the evaporator power. Similarly, it is obtained from the operation curves as:

$$f_{Energyinput} = \frac{\dot{Q}_g}{\dot{Q}_{g,nom}} = \frac{\dot{Q}_e}{\dot{Q}_{e,nom}} \cdot \frac{COP_{nom}}{COP} \tag{9}$$

where $\dot{Q}_g$ and COP are the values for the particular evaluation conditions obtained from the manufacture's curves. The maximum output power $\dot{Q}_{e,max}$ that the chiller will be able to offer on the evaporator for each of the conditions evaluated is calculated from Equation (10).

$$\dot{Q}_{e,max} = f_{capacity} \cdot f_{Energyinput} \cdot \dot{Q}_{e,nom} \tag{10}$$

On the other hand, the output power of the evaporator will be the minimum between the maximum power it is capable of offering in each of the conditions, and the demand is given by Equation (11).

$$\dot{Q}_e = Min\ of\ \left(\dot{Q}_e, \dot{Q}_{remove}\right) \tag{11}$$

With this evaporator power value, the flow rate, and the inlet temperature, the outlet temperature of the evaporator T_{eo} can be determined. Logically, at partial loads.

$$T_{eo} = T_{ei} - \frac{\dot{Q}_e}{\dot{m}_e \cdot C_{pe}} \tag{12}$$

The generator demand is taken from the energy input fraction $f_{Energyinput}$ (whose value has been given by the operating curve file for the operating conditions), multiplied by the standardized generator power.

$$\dot{Q}_g = f_{Energyinput} \cdot \dot{Q}_{g,nom} = f_{Energyinput} \cdot \frac{\dot{Q}_{e,nom}}{COP_{nom}} \tag{13}$$

The output temperature is an immediate value, the input temperature, and the generator flow rate are known as shown in Equation (14):

$$T_{go} = T_{gi} - \frac{\dot{Q}_g}{\dot{m}_g \cdot C_{pg}} \tag{14}$$

If it is assumed that the machine is adiabatic and, therefore, has no heat loss or gain; the power in the condenser is equal to the sum of the generator plus the evaporator:

$$\dot{Q}_c = \dot{Q}_e + \dot{Q}_g \tag{15}$$

The output temperature of the condenser T_{co} is calculated in the same way as for the evaporator and the generator:

$$T_{co} = T_{ci} - \frac{\dot{Q}_c}{\dot{m}_c \cdot C_{pc}} \tag{16}$$

Finally, The COP of the chiller is determined by Equation (17) [35]:

$$COP = \frac{\dot{Q}_e}{\dot{Q}_g + \dot{Q}_{aux}} \tag{17}$$

2.2. Meteorological Data

This section will highlight the analysis of potential solar data in Baghdad, Iraq. The main reason for this is to discover the potential power of renewable energy available at the location of operation. The meteorological conditions of Iraq correspond to a warm and dry climate during the summer season. Iraq has abundant solar energy capability with a significant amount of sunlight throughout the year as it is located in the Global Sunbelt. Solar energy can be widely deployed throughout two-thirds of Iraq. In the western and southern areas, daily average radiation ranges between 2800 and 3000 h, with relatively high average daily solar radiation of 6.5–7 kWh/m^2. The direct and global solar irradiation is given in Figure 2, [26]. Thence, the study location has great potential for solar energy, allowing sufficient use of solar thermal power as a main prime mover for the absorption cooling system.
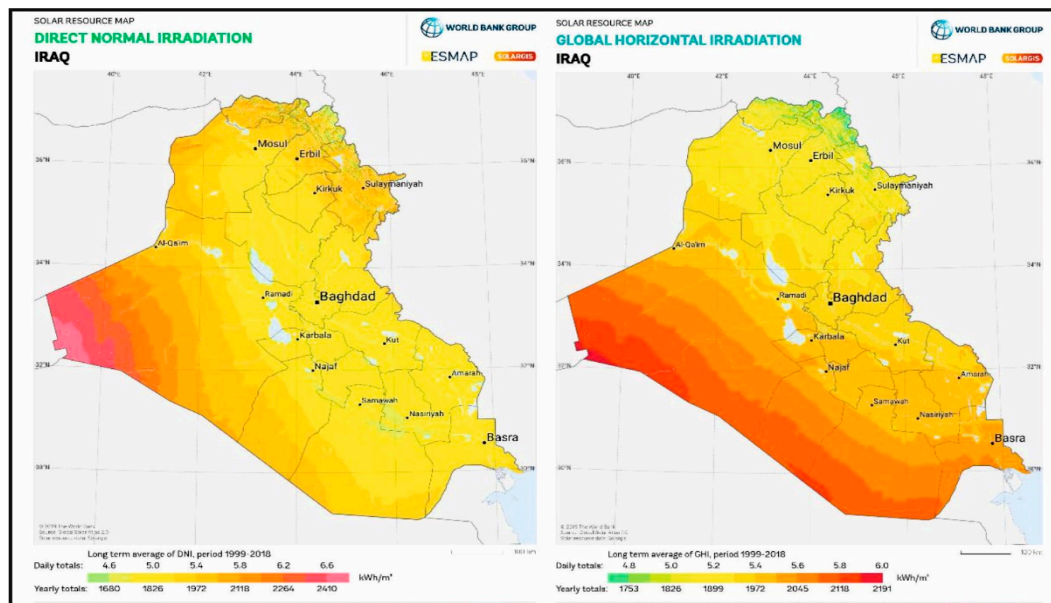
Figure 2. Iraq solar annual direct normal and global horizontal Irradiation map © 2019 The World Bank, Source: Global Solar Atlas 2.0, Solar resource data: Solargis [26].

The solar radiation data and environmental conditions used correspond to the TMY2 (typical meteorological year) format for Baghdad, the capital of Iraq (latitude is 33.3 N, longitude is 44.6 E, and Altitude 3.8 m). These data are provided by TRNSYS and have been obtained with Version 5 of the Meteonorm program.

Solar insolation varies according to the time of year. The daily highest solar irradiation of the globe is almost 8 kWh/m^2 and the daily highest temperature reaches over 45 °C (sometimes in summer

season, the temperatures exceed 50 °C). A cooling effect is needed for seven months (April–October). During these months, the sunshine lasts for almost 10 hours per day, with an average total daylight of 13 hours per day [36].

2.3. House Profile and Cooling Loads

The proposed methodology was applied to a residential house located in Baghdad, Iraq. The house layout, wall layer details, and various construction components are given in Appendix A. As for the design of the house: the windows are on the north, east, and west walls; overhangs have a projection factor (overhang depth/window height) of 0.6. Two doors are on the north and east sides. Windows and doors are not specified on the south wall (to minimize heat gain through radiation). The window-to-gross-wall area is kept at 29%. The zone temperature is specified as 25 °C; the new design envelope specifications are as follows:

- The window-to-gross-wall area should not be greater than 35%.
- Overhangs should be placed on the east, west, and south windows of the building with a projection factor (overhang depth/window height) of greater than 0.5.
- Lighting devices should have an efficiency of 60 lumens/W.
- Specific lighting, 15 W/m^2.
- Specific gain (equipment and people), 15 W/m^2.
- Occupation rate 0.05 occupants/m^2.

Concerning the house under study, the monthly cooling demand of the house is variable during the summer season. An enormous portion of that variable is involved in the cooling load configuration due to the (transient) storage nature inherent in the cooling load. The sum of the components of the cooling load gives the total load of the house building. The calculation of the cooling demand was carried out using CARRIER software, version 4.04 (Carrier Software Systems, Syracuse, NY, USA, 2015), based on weather data for Baghdad. The inside conditions: temperature 25 °C and relative humidity 50%, ambient summer design dry-bulb temperature 48 °C, coincident wet-bulb 26 °C and 18.9 °C (daily range). Solar insolation varies according to the time of year, especially from April to October. The house's peak load occurs in August at 4 p.m., where the maximum outside temperature is about 49 °C. This value should be adopted for design purposes. Figure 3 illustrates the design temperature profiles for August; the maximum total cooling load according to CARRIER software is 25 kW was in August. Figure 4 shows the percentage of the various peak cooling load components.
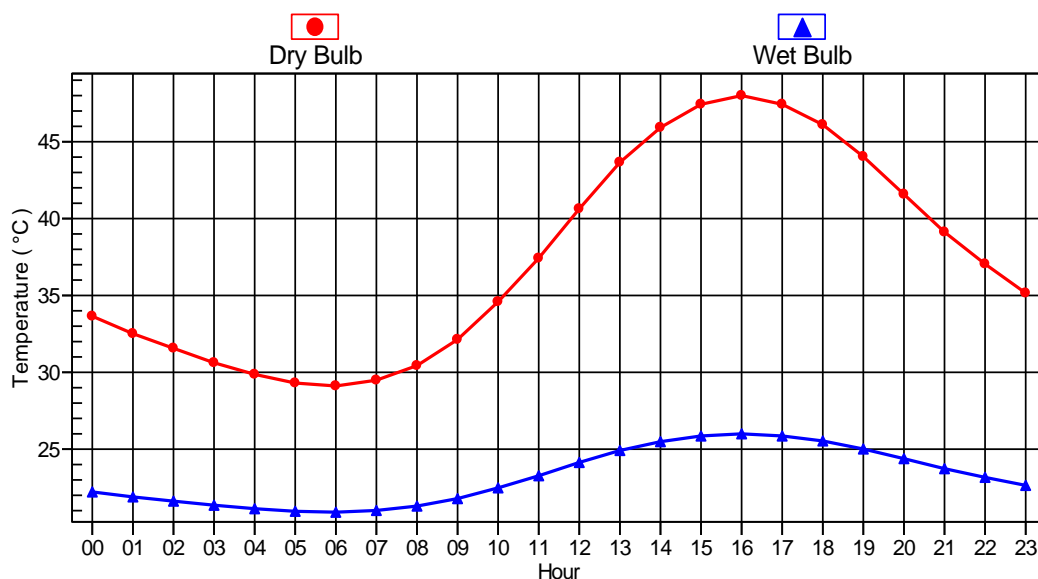

Figure 3. Design temperature profiles for August.

2.4. System Modeling

The TRNSYS library includes modules (TYPES) that represent the equipment commonly used in energy systems, modules for processing meteorological data, and modules for processing simulation results. The modular structure of TRNSYS gives great flexibility to analyze different types of energy systems. The representation of SACS in TRNSYS, described in the previous section, is illustrated in Figure 5. Table 4 provides information about the most important components of the system, the type of module that represents them, and provides some parameters of the basic design. Figure 5 and Table 4 do not include other components and flows of less importance. The period of simulation in TRNSYS was seven months (cooling season) from 1April 1 (2160 h) until the end of October (7296 h), with a step time simulation of one minute. Baghdad meteorological data was gained from TMY2.
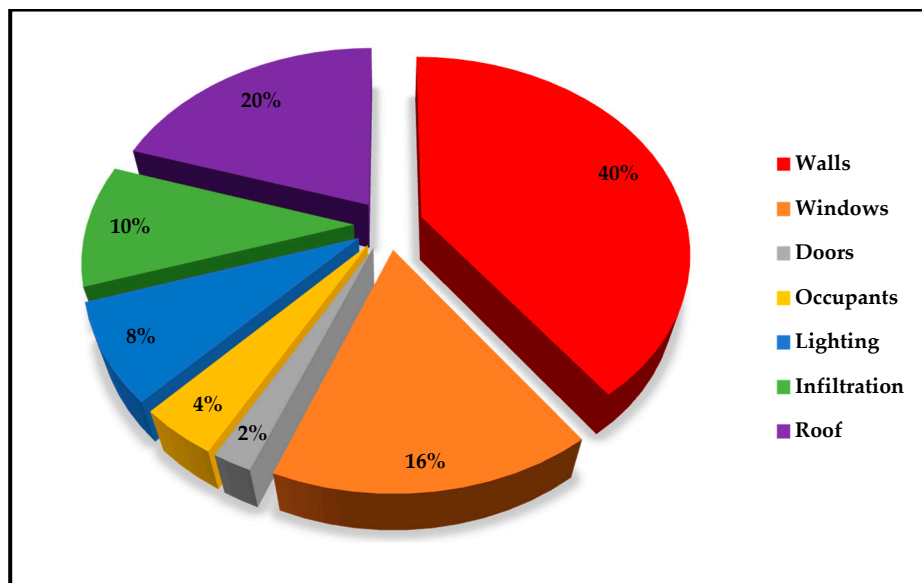
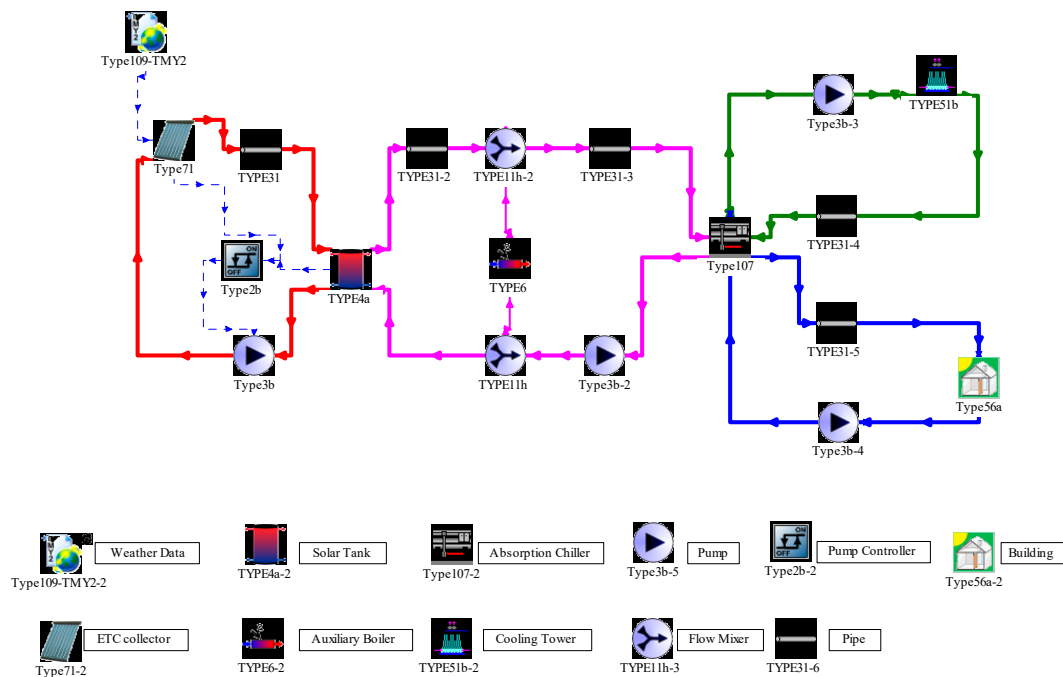**Figure 4.** Contribution of the various cooling load component.

Figure 5. Diagram of the TRNSYS model of the solar absorption cooling system (SACS).

Some of the simplifying assumptions used in the calculation are indicated below:

- The electrical energy consumed by the pumps is neglected.
- Pumps are not supposed to transmit thermal energy to the fluid.
- When the pumps are running the mass, flows remain constant.
- The limit capacity of the chiller is assumed to correspond to a cooling water temperature of 27 °C.

In developing the model, the recommendations by some authors who have simulated the behavior of solar absorption cooling systems with TRNSYS, or other applications, have been taken into account [19,31].

Table 4. List of the most important components of the TRNSYS model.

Component	Type TRNSYS	Parameters (Base Design Values)
Solar Collector	TYPE 71a	Apricus ETC-30 (Table 3) Number of collectors (12) Inclination (30°)
Hot water tank	TYPE 4a	Volume (50 L/m^2 collector)
Auxiliary boiler	TYPE 6	Efficiency (90%)
Absorption chiller	TYPE 107	YAZAKI WFC SC10 (Table 5)
Cooling tower	TYPE 51b	B.A.C. FXT-26 (Table 4)
Weather data	TYPE 109—TMY2	Location: Baghdad, Iraq
Collector pump	TYPE 3b	Flow rate 50 (L/h)/m^2 of collector
Collector pump control	TYPE 2b	Maximum accumulator temperature (90 °C) Minimum collector gain (5 °C)
Pipe	TYPE 31	
Flow mixer	TYPE 11h	
Building	TYPE 56a	

3. Performance Analysis

3.1. Solar Fraction

The SACS performance can be evaluated using solar fraction (solar coverage). This factor demonstrates the solar energy contribution in chilled water production [37]; the following equation enables the calculation of the solar fraction.

$$SF = \frac{\dot{Q}_s}{\dot{Q}_S + \dot{Q}_{aux}} \tag{18}$$

where $\dot{Q}_s$ solar gained energy and $\dot{Q}_{aux}$ is energy from the auxiliary heater. Q_s can be calculated by:

$$\dot{Q}_s = \dot{Q}_c - \sum \dot{Q}_{loss} \tag{19}$$

where $\dot{Q}_c$ is useful collectors' energy and $\dot{Q}_{loss}$ is the system losses energy.

3.2. Primary Energy Saving

The primary energy (PE) savings is the saved primary energy, electric, and fossil. These values are mathematically described below, in order to evaluate the primary energy consumption of a solar system and a conventional one:

$$PE_{save} = \Delta PE_{fossil} + \Delta PE_{eletricity} \tag{20}$$

$$\Delta PE_{fossil} = \left(\frac{Q_{heat\,fossil,ref} - Q_{aux,total}}{\eta_{boiler}\cdot C_{con,fossil}}\right) \tag{21}$$

$$\Delta PE_{ele} = \left(\frac{P_{el,ref,tot} - P_{el,sc,tot}}{C_{con,elec}}\right) \tag{22}$$

$$Relative\ PE_{save} = \frac{PE_{save}}{PE_{ref}} \tag{23}$$

$$PE_{ref} = \frac{Q_{heat\,fossil,ref}}{\eta_{boiler}\cdot C_{con,fossil}} + \frac{P_{el,ref,tot}}{C_{con,ele}} \tag{24}$$

where:

η_{boiler} is the efficiency of auxiliary boiler 0.9;

$Q_{heat\,fossil,ref}$ is required heat for both space heating and DHW (Domestic Hot Water) in the conventional system (kWh).

$Q_{aux,total}$ is the produced energy by auxiliary heater (kWh).

$C_{con,fossil}$, $C_{con,ele}$ are the primary energy conversion factors for heat and electricity from fossil fuel, 0.95 kWh$_{heat,fossil}$/kWh$_{PE}$ and 0.5 kWh$_{elec,fossil}$/kWh$_{PE}$.

3.3. Electric Efficiency of the Total System

The electric efficiency is the relationship of the total heating and cooling energy generation to the required electricity for this production. The total system electrical efficiency $\eta_{ele,tot}$ is given by:

$$\eta_{ele,tot} = \frac{(Q_{cold})}{\left(P_c + P_{cw} + P_{el,chiller} + P_{el,CT} + P_{el,PS} + P_{el,boiler}\right)} \tag{25}$$

where:

P_c is the consumed electricity by a pump that feeds the chiller (kWh).

P_{cw} is the consumed electricity by cooling water loop pump (kWh).

$P_{el,chiller}$ is the consumed electricity by the chiller (kWh).

$P_{el,CT}$ is the electrical power of fan cooling tower (kWh).

$P_{el,PS}$ is the consumed electricity by solar loops pumps (kWh).

$P_{el,boiler}$ is the consumed electricity by boiler (kWh).

4. Results and Discussion

4.1. House Energy Balance Analysis

In this section, the thermal energy balance of SACS for the house under study was established through the evaluation of harvested solar energy, the delivered energy from a hot solar tank, the energy from the auxiliary boiler, and the necessary energy to satisfy the load. Table 5 shows the important and vital information efficiency parameters (result of SACS) for the summer season.

Table 5. Most relevant data and results for the cooling season operation (kWh).

Month	Incident Energy	Collected Energy	Solar Tank Energy	Aux. Boiler Energy	Load Energy	Collector Efficiency (%)	COP	Solar Fraction (%)
April	17,329	9489	2350	1760	4110	54.75	0.39	57.17
May	19,624	11,346	3642	1954	5596	57.81	0.41	65.08
June	30,632	16,358	6243	4720	10,963	53.40	0.45	56.94
July	33,685	18,509	7496	5153	12,649	54.94	0.51	59.26
August	35,173	19,245	7889	5391	13,280	54.71	0.52	59.40
September	29,627	15,296	4948	4430	9378	51.62	0.40	52.76
Oct.	11,953	5830	2162	2617	4779	48.77	0.40	45.23
Total	178,023	96,073	34,730	26,025	60,755	53.96	0.44	57.16

Figures 6 and 7 show, respectively, the energy contribution of the integrated gas boiler and solar field during the cooling season. The analyses results show that the useful energy of the solar field was 34,730 kWh and the energy delivered by the boiler was 26,025 kWh, indicating that the total season solar fraction (also called solar coverage) to the load was about 58% (see Figure 7). It is clearly seen that the system operating in May had the highest average solar fraction (a value of about 65%) due to the higher value of captured energy and the lower cooling load. Contrarily, the system presenting the lowest average value of solar fraction (45%) operated under October weather conditions. This is because of the lower energy supplied by the storage tank and lower harvested energy by ETC collectors (see Table 5). This outcome reflects the effect of solar irradiation on the energy performance of SACS.
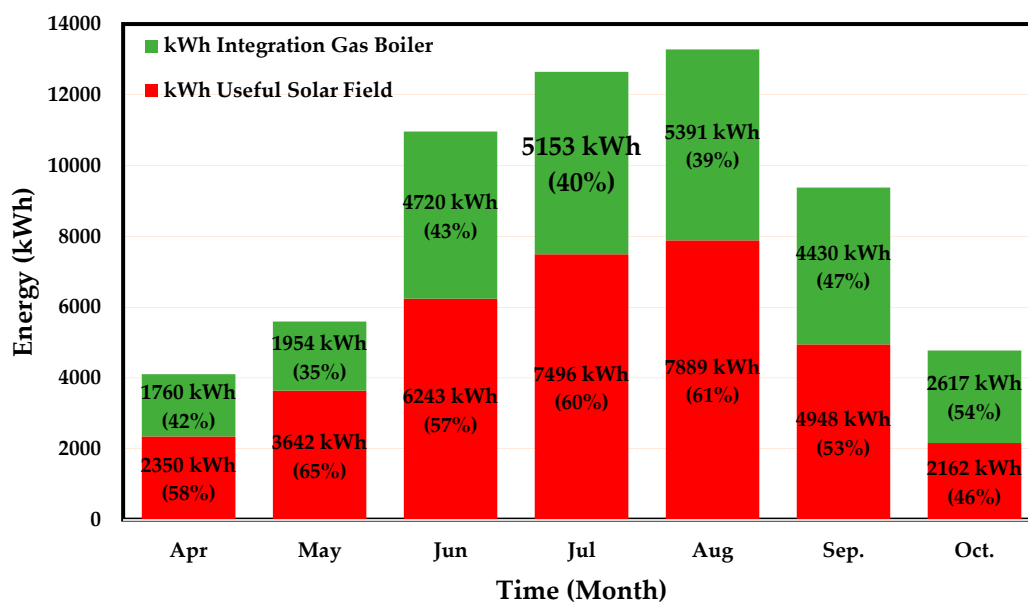

Figure 6. Energy contribution of integration gas boiler and solar field.

It is also clear that there is a significant impact on the solar fraction from the weather data each month, particularly, solar irradiation that has a direct influence on the energy generated by the ETC field. It is possible to observe this by referring to Equation (18).

Figure 8 shows the energy contribution of solar irradiation, energy from solar collectors, and solar tank. The average monthly values of incident solar radiation energy on the solar collectors was 178,023 kWh, while the total captured solar energy was 96,073 kWh, and the energy from the solar tank was 34,730 kWh, which implies that the efficiency of ETC collectors during the cooling season was about 54% (see Table 5).
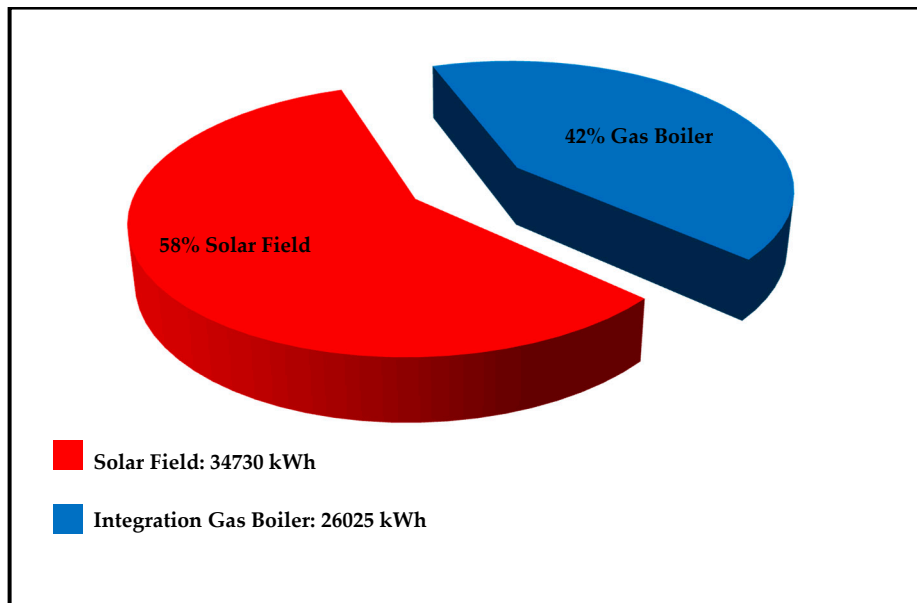
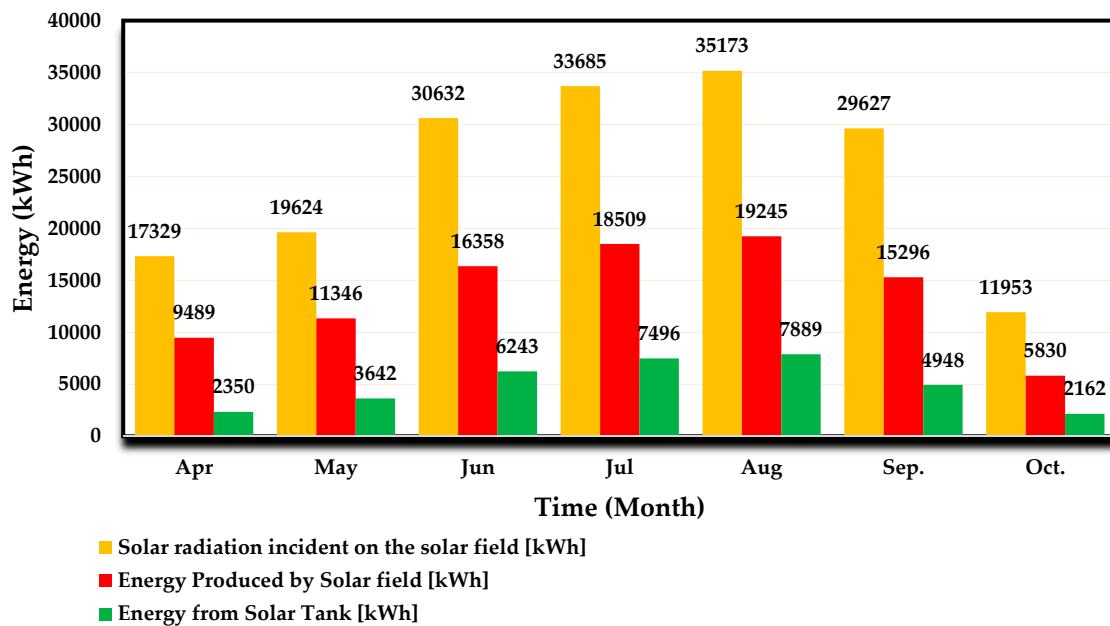**Figure 7.** Solar coverage during cooling season.

Figure 8. Energy contribution of solar field and solar tank.

Table 5 outlines the evaluation of the COP over six months, indicating that the average COP of SACS ranges between 0.39 and 0.52. It was also found that the system, operating in July and August, has the best average COP (a value of 0.51 and 0.52), respectively, due to a large amount of captured energy by ETC and a large cooling load that is led to higher solar coverage. Moreover, the lowest average COP (0.39) was recorded in April. Based on Equation (17), we can conclude that the variation in COP (see Table 5) through the six months is directly reported to the thermal energy at the input and output of the generator, and evaporator of the absorption chiller. The COP strongly depends on the flows of energy in these two parts. In general, the generator is influenced by the solar radiation of each month, while the evaporator is affected by building a cooling load, which depends on the ambient outdoor temperature of each month.

4.2. Primary Energy Analysis

The target of this analysis is to find the configuration that optimizes the system performance. Sensitivity analysis is presented under a different number of collectors (areas) and solar tank sizing. The number of collectors, and storage size, in the base case is 12 (30 m^2) and 50 L/m^2 (1500 L), respectively, compared with the base case. The sensitivity analysis includes changing the surface collector area from 25 m^2 to 35 m^2; the solar tank volume varied from 1000 l to 2000 l. The results are displayed in Table 6.

Table 6. Primary energy performance for various collector areas and solar tank volume.

		Number of Collectors			Solar Tank Volume L		
		10 (25 m^2)	12 (30 m^2)	14(35 m^2)	1000	1500	2000
	Solar Fraction%	53.1	62.3	70.2	61.5	62.3	63.9
	$\eta_{ele,total}$	11.2	11.5	11.9	11.6	11.9	12.1
PE save	PEsave kWh$_{PE}$	1361	3759	5661	4669	5761	6342
	PEref (Primary Energy References) kWh$_{PE}$	15,469	15,545	15,666	15,628	15,666	15,306
	Relative %	8.8	24.8	36.8	29.9	36.8	40.6

It is shown that, with a greater collector area, the best results were obtained. A 16.6% increase in collector surface area is followed by an increase in the solar fraction and relative PE saved, 12.6% and 48.3%, respectively. Regarding solar tank volume, it is clearly seen that variation of tank volume does not present a significant influence on solar fraction, electrical efficiency, and PE relative; a solar tank volume increasing of 33.3% reflects on increasing in a solar fraction of about 2.5%, and PE relative around 10.3%. From the previous results, it can be recommended to use a collector area of 35 m^2 and a storage tank volume of 2000 L in order to achieve better performance than that reached in the base case.

4.3. Parametric Analysis

In this section, a parametric analysis has been carried out, taking into consideration the main important design parameters: the collector slope, water flow rate through the collector, number of collectors, and the solar tank size. In all analyses carried out below, the value of a single parameter is modified keeping the rest in the value corresponding to the base design.

4.3.1. Effect of Collector Slope

The inclination angle of the collector has a significant impact on the overall SACS performance. Figure 9 shows the variation in solar coverage with the collector field inclination in Baghdad. The evaluation based on a change in the tilt angle from 5° to 50° by a step of 5° was carried out in order to compute the optimum angle of the solar field that provides the highest solar fraction. The change in this variable shows that the tilt angles (15°, 20°, 25°, 30°) give a higher solar fraction, contrarily to the last three angles where solar fraction decreases. The reason for this difference is solar radiation perpendicularity that provides optimal results during summer with low tilt angle values, which help capture more solar radiation, as reported by Shariah and Elminir [38,39]. The optimum tilt values giving higher solar fraction are between 15° and 25°; therefore, operating at optimum value for tilt angles can readily expand the amount of solar energy incident and, thus, enhance both the thermal and economic efficiency of the SACS.
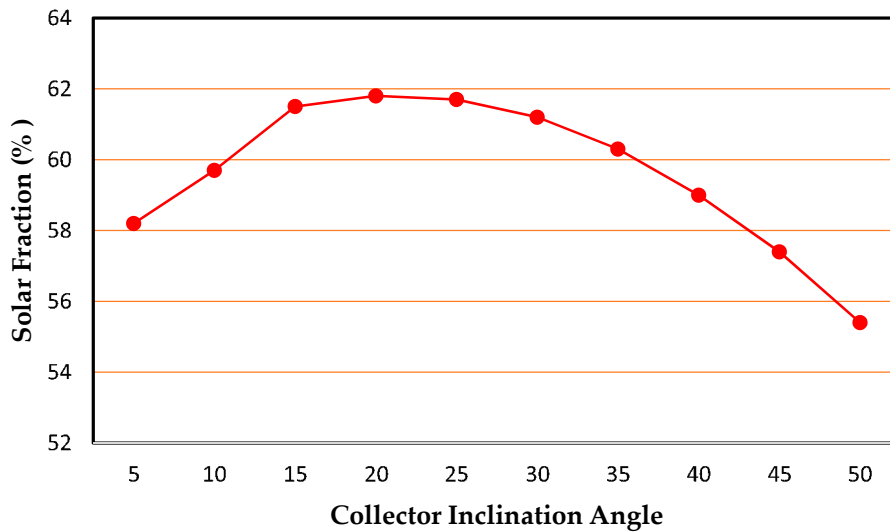
Figure 9. Solar coverage variation with the solar collector tilt.

4.3.2. Effect of Water Flow Rate

In the literature, the hot water flow rate values through solar collectors range from 20 to 80 L/h per m^2 of collector area are recommended for panels connected in parallel, as in our case. The variation of the solar fraction, with the hot water flow rate through the solar collector array, is indicated in Figure 10. The water flow rate varied from 20 to 55 $(L/h)/m^2$ of collector area. A change of water flow from 20 to 40 $(L/h)/m^2$ causes only a 0.9% increase in solar fraction; increasing the flow rate over an optimum value (40 $(L/h)/m^2$) will lead to drops in a solar fraction of about 0.2%. It is evident that the results obtained depict small changes in solar fraction and allow us to affirm that this parameter does not present a significant impact on solar coverage; it is in alignment with the results obtained by Beckman [40,41].
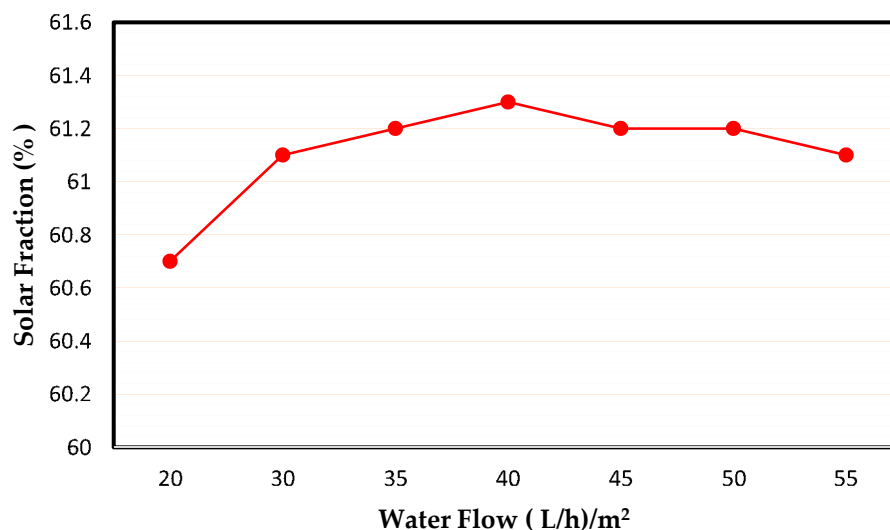

Figure 10. Variation of the solar fraction with the flow of water circulating through the collector.

4.3.3. Effect of Solar Field Area

The area and the number of solar collectors play an important role in determining the optimal configuration of the capture solar system. The collector surface has a decisive effect on the efficiency and feasibility of SACS. The simulation was carried out to establish the influence of this parameter on the overall performance of SACS under study, based on the collector's tilt angle 20°. The area of each collector was 2.5 m^2, the water flow rate was 40 L/h per m^2, the solar tank volume was 30 L/m^2;

the lower and upper solar tank temperatures were T$_{lower}$ = 75 °C, T$_{upper}$ = 90 °C. Figure 11 depicts the variation of the solar fraction with the number of collectors installed. The evaluation involves changing the number of a collectors from 4 to 24 (10 m^2 to 60 m$^{2)}$) by a step of 2 (2 m^2). It is clear that an increase in the collector surface area tends to enhance solar coverage due to the proportion between the captured energy from the ETC field and solar fraction, according to simulation results displayed in Figure 11. It is predicted that the solar coverage stays constant, especially at the higher solar surface field (>55 m^2). As an example, an evacuated tube collector operating in Baghdad, inclination angle 30 degrees, presents a solar coverage of about 88.1% for 22 collectors (55 m^2) and 88.3% for 24 collectors (60 m^2). The stability in solar fraction SF (Solar Fraction), which was also achieved in published works Bahria and Assilzadeh [42,43], indicates that the system achieves its optimum level, and any additional increase in the surface field leads to overproduction of thermal energy, which can cause technological problems and significantly increase the initial investment. Therefore, with equal investment costs, the best design will be the one that offers the greatest coverage.
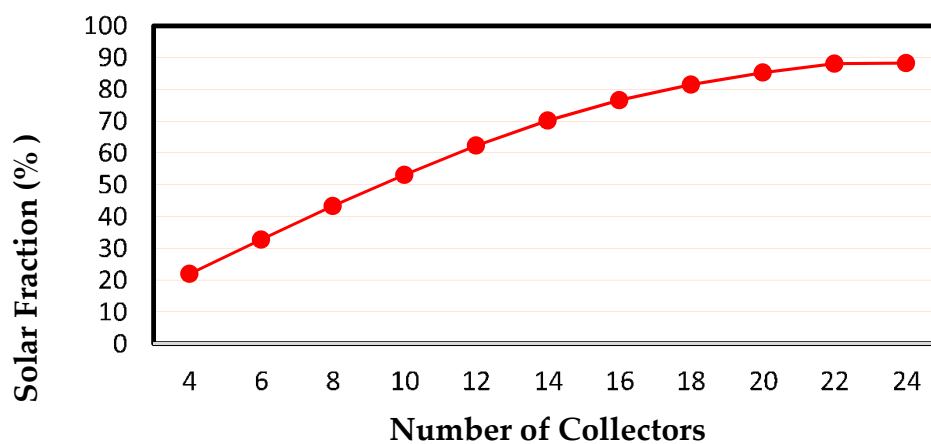

Figure 11. Solar coverage as a function of the number of collectors.

4.3.4. Effect of Solar Tank Capacity

This section examines the influence of the solar tank capacity on the solar fraction. The literature recommends values of storage solar tank capacity from 20 to 100 L/m^2 of collector area for installations where the time delay between collection and consumption does not exceed 24 h. The solar fraction is not significantly affected by the change in storage tank capacity, as shown in Figure 12. It is clear that increasing the solar tank capacity has a slight effect on the solar fraction. A change in solar accumulator capacity from 10 to 55 L/m^2 of the collector area obtains an increase in solar coverage of only 60.6% to 61.1%, respectively, with this difference (0.5%) observed—that the effect of the solar tank size on solar coverage is not significantly high. The optimum capacity of the solar tank, 30 L/m^2, gives solar coverage of 61.6%. Figure 12 depicts that the oversized solar tank will cause a decrease in solar fraction due to increases in thermal losses. The result in Figure 12 is in alignment with that of Beckman [40,41]. Therefore, it is not surprising that the optimal accumulator capacity is at the lower values of the recommended range.
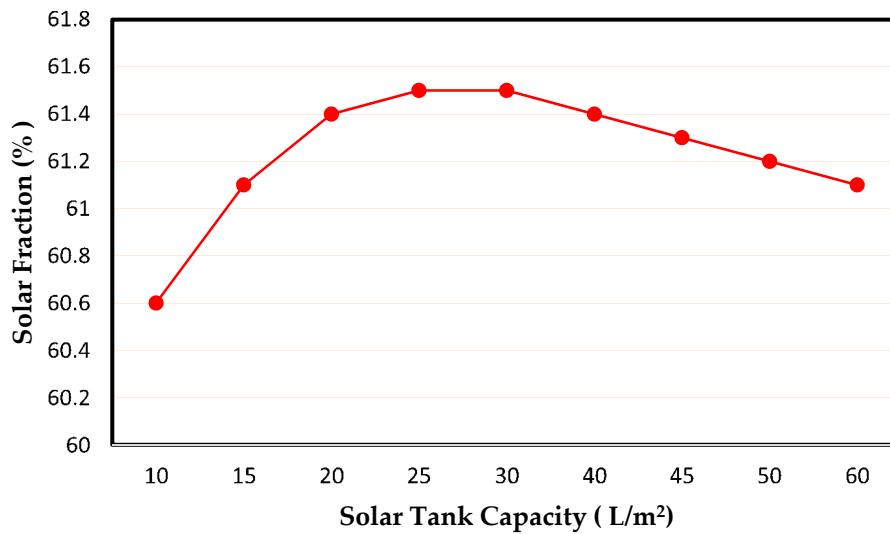
Figure 12. Solar coverage as a function of storage tank volume.

4.3.5. Effect of Solar Tank Temperature

Tables 7 and 8 present the results obtained for the variation of the solar fraction with the lower and upper temperatures of the solar tank that defines the operating of the absorption chiller with solar heat. The absorption chiller will operate with water from the solar accumulator tank when the upper temperature of the storage tank is between these limits and it is possible to completely cover the cold demand. Concerning the upper temperature, the value of 90 °C used in the basic design seems reasonable; a higher value of top solar tank temperature would improve the solar coverage somewhat, but it should be taken into account that the limit of 95 °C, imposed by the absorption chiller, cannot be exceeded. In fact, tank temperature affects, as well, the inlet temperature of the generator, since the hot water directly supplies the chiller generator. As for the lower temperature, the advantage of using values as small as possible is clear. This is because more solar heat can be used and the efficiency of the collector can be improved.

Table 7. Variation of the solar coverage with the lower temperature of the solar tank.

Temperature °C	70	72.5	75	77.5	80
Solar Fraction%	63.1	62.2	61.2	59.9	57.9

Table 8. Variation of solar coverage with an upper temperature of the solar tank.

Temperature °C	85	87.5	90	92.5	95
Solar Fraction%	60.7	61.0	61.2	61.3	60.6

5. Conclusions

This article presented a detailed analysis of the performance of a solar driven-absorption cooling system as alternative technology for air conditioning of a house, under hot and dry climate in Baghdad, Iraq. Various parameters influencing the solar fraction and the solar cooling performance of the proposed system have been discussed.

Based on the results of the simulation performed in this work, it was revealed that weather conditions have a significant effect on the performance of the solar absorption air conditioning system, with peak loads during the summer months. August presented the highest performance. The relevant average COP achieved a value of 0.52 while the solar fraction was 59.4%.

The results (of energy analysis contribution) during the summer season showed that the amount of energy incident was 178,023 kWh, while the total energy harvested was 96,073 kWh, which implies

that the efficiency of ETC collectors during the cooling season is about 54%. It was also found that the solar energy supplied by the solar tank was 34,730 kWh and the energy delivered by the boiler was 26,025 kWh, indicating that the total seasonal solar coverage was about 58%.

The results of the primary energy analysis evidenced the use of a collector area of 35 m^2; a storage tank volume of 2000 L presented better performance than that reached in the base case.

Parametric analysis results showed the best configuration for the design of SACS. It was found that the solar collector tilt angle is significantly affected by the incident solar irradiation. An optimal value (between 15° and 25°) of the inclination presented a higher solar fraction. It was also found that increasing the water flow rate through the collectors does not indicate a significant effect on solar coverage.

The surface collector analysis revealed that, in general, the increase of the installed surface of the collector field leads to improve the solar fraction values. It was also found that the solar fraction remained the same for an area larger than 55 m^2. Therefore, it is concluded that the appropriate collector surface selection should be carried out together with economic and technical feasibility (mainly cost analysis and land availability) in order to achieve the best profitability of the system.

Moreover, the change in the size of the solar tank has no significant impact on the solar fraction (60.6% and 61.1% for 10 L/m^2 and 55 L/m^2 of collector area, respectively). Increasing the upper solar tank temperature improves the solar coverage, but it should be <95 °C.

Finally, this work provides a roadmap for designers, in particular, to ensure that all of the operating and design variable effects are taken into consideration when developing a solar air-conditioning cycle under the Iraq climate. Additionally, the model can be employed to carry out thermo-economic comparisons of the system using various types of collectors.

Author Contributions: Conceptualization, A.A.-F.; methodology, A.A.-F.; validation, A.A.-F.; formal analysis, A.A.-F.; investigation, A.A.-F.; data curation, A.A.-F.; writing—original draft preparation, A.A.-F.; writing—review and editing, F.A.; supervision, B.E. All authors have read and agreed to the published version of the manuscript.

Conflicts of Interest: The authors declare no conflict of interest.

Nomenclatures, Subscripts and Abbreviations

Nomenclatures

A	area (m^2)
a	loss coefficient
η	efficiency
I	radiation incident (W/m^2)
$\dot{m}$	mass flow rate (kg/s)
C_P	specific heat (kPa)
$\dot{Q}$	heat transfer rate (kW)
T	temperature (°C)
U	overall heat transfer coefficient (kW/m^2·K)
$\dot{W}$	power (kW)

Subscripts

a	Ambient
aux	Auxiliary
c	Condense
e	Evaporator
f	Fraction
g	Generator
i	Node
L	Load
nom	Nominal

min	Minimum
max	Maximum
o	Outlet
s	Source
set	Set
w	Water

Abbreviations

COP	Coefficient of performance
DHW	Domestic hot water
EES	Engineering Equation Solver
ETC	Evacuated tube collector
HVAC	Heating, ventilation, and air conditioning
IEA	International Energy Agency
IAM	Incidence angle modifier
NTU	Number of transfer unit
PE	Primary energy
SACS	Solar absorption cooling system
SF	Solar fraction
TMY	Typical meteorological year
TRNSYS	Transient System Simulation Program

Appendix A

The House under Study

The house building is double dwelling, connected by internal stairs, as shown in Figure A1 [37]. Each floor has an area of 97 m^2 and a height of 3 m. The ground floor includes an entrance, living room, bedroom, kitchen, and bathroom. The first floor contains the master room, bedrooms, and bathroom. The wall layer details and various construction components of the house are given in Tables A1 and A2.

The maximum total calculated cooling load, according to CARRIER software, is about 25 kW. Figure 4 shows the percentage of the various peak cooling load components estimated by CARRIER software. The load through the walls was 40% of the total cooling load due to the higher temperature difference between outdoor and indoor temperature; the heat envelope transmission aggravates cooling demand. The transmission losses could be reduced significantly with envelope higher thickness insulation. Additionally, ETC collectors mounted on the first floor roof of the house could reduce the cooling load due to shading, though not all are eliminated. The load on the roof is 20% of the overall cooling load. The actual total estimated cooling load would be about 21, which is in alignment with the data obtained in [37].

Table A1. Wall layers details.

Wall Details Outside Surface Color Dark Absorptivity 0.900 Overall U-Value 0.415 W/(m^2·K) Wall Layers Details (Inside to Outside)					
Layers	Thickness mm	Density kg/m^3	Specific Ht·kJ/(kg·K)	R-Value (m^2·K)/W	Weight kg/m^2
Inside surface resistance	0.000	0.0	0.00	0.00200	0.0
Cement bounded	12.000	1600.0	1.34	0.04200	19.2
Insulation	50.000	32.0	0.90	1.66600	1.6
Hollow block	200.000	1922.0	0.84	0.40000	384.4
13 mm gypsum board	12.700	800.9	1.09	0.07890	10.2
Outside surface resistance	0.000	0.0	0.00	0.00200	0.0
Air space	0.000	0.0	0.00	0.16026	0.0
Outside surface resistance	0.000	0.0	0.00	0.05864	0.0
Totals	274.700	-	-	2.40980	415.4

Table A2. Construction components of the house.

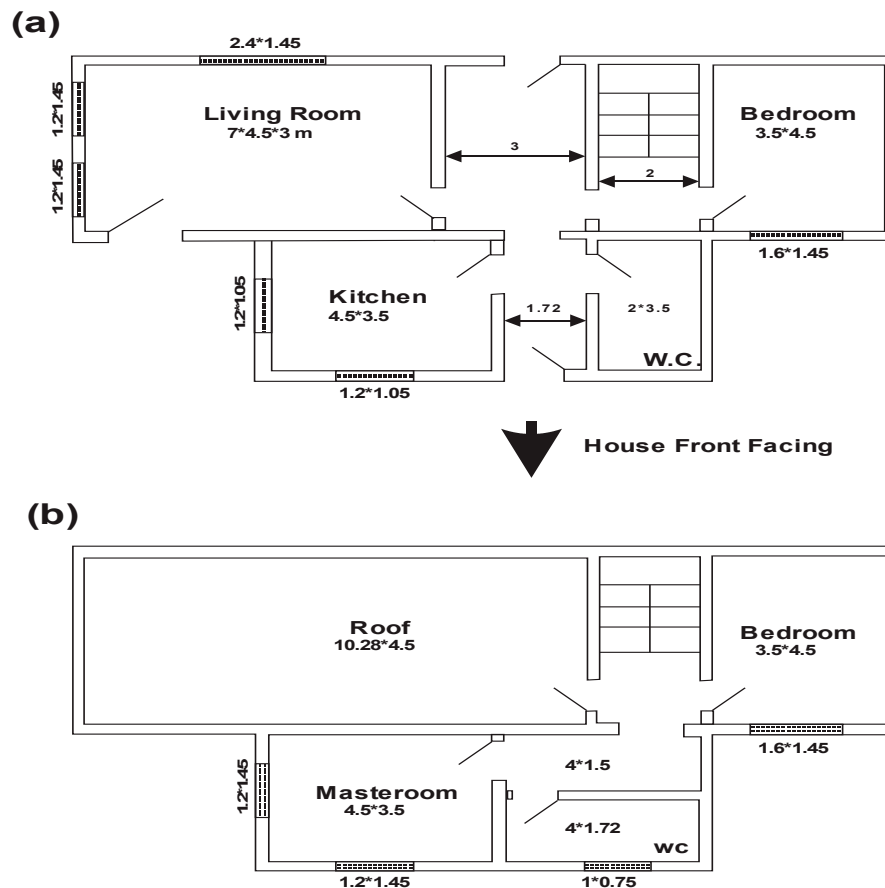| Component	Exterior Roof	Exterior Glass	Exterior Wooden Door	Exterior Steel Door
U value (W/m^2 °C)	1.670388	5.888993	2.087049	6.07040

Figure A1. Layout diagram of the modern domestic solar house (**a**) ground floor (**b**) first floor.

References

1. Allouhi, A.; El Fouih, Y.; Kousksou, T.; Jamil, A.; Zeraouli, Y.; Mourad, Y. Energy consumption and efficiency in buildings: Current status and future trends. *J. Clean. Prod.* **2015**, *109*, 118–130. [CrossRef]
2. Dahl, R. Cooling concepts: Alternatives to air conditioning for a warm world. *Environ. Health Perspect.* **2013**, *121*, a18–a25. [CrossRef] [PubMed]
3. Rashid, S.; Peters, I.; Wickel, M.; Magazowski, C. Electricity Problem in Iraq. In *Economics and Planning of Technical Urban Infrastructure Systems*; HafenCity Universität Hamburg: Hamburg, Germany, 2012.
4. Allouhi, A.; Kousksou, T.; Jamil, A.; El Rhafiki, T.; Mourad, Y.; Zeraouli, Y. Economic and environmental assessment of solar air-conditioning systems in Morocco. *Renew. Sustain. Energy Rev.* **2015**, *50*, 770–781. [CrossRef]
5. Petela, K.; Szlęk, A. Assesment of Passive Cooling in Residential Application under Moderate Climate Conditions. *Ecol. Chem. Eng. A* **2016**, *23*, 211–225.
6. Baniyounes, A.M.; Rasul, M.G.; Khan, M.M.K. Assessment of solar assisted air conditioning in Central Queensland's subtropical climate, Australia. *Renew. Energy* **2013**, *50*, 334–341. [CrossRef]
7. Balghouthi, M.; Chahbani, M.H.; Guizani, A. Feasibility of solar absorption air conditioning in Tunisia. *Build. Environ.* **2008**, *43*, 1459–1470. [CrossRef]
8. Martínez, P.J.; Martínez, J.C.; Lucas, M. Design and test results of a low-capacity solar cooling system in Alicante (Spain). *Sol. Energy* **2012**, *86*, 2950–2960. [CrossRef]

9.   Burckhart, H.J.; Audinet, F.; Gabassi, M.-L.; Martel, C. Application of a novel, vacuum-insulated solar collector for heating and cooling. *Energy Procedia* **2014**, *48*, 790–795. [CrossRef]

10. Ketjoy, N.; Rawipa, Y.; Mansiri, K. Performance evaluation of 35 kW LiBr H$_2$O solar absorption cooling system in Thailand. *Energy Procedia* **2013**, *34*, 198–210. [CrossRef]

11. Leiva-Illanes, R.; Escobar, R.; Cardemil, J.M.; Alarcón-Padilla, D.-C. Comparison of the levelized cost and thermoeconomic methodologies—Cost allocation in a solar polygeneration plant to produce power, desalted water, cooling and process heat. *Energy Convers. Manag.* **2018**, *168*, 215–229. [CrossRef]

12. Jenkins, P.; Elmnifi, M.; Younis, A.; Emhamed, A.; Alshilmany, M. Design of a Solar Absorption Cooling System: Case Study. *J. Power Energy Eng.* **2020**, *8*, 1–15. [CrossRef]

13. Wang, K.; He, Y.; Kan, A.; Yu, W.; Wang, D.; Zhang, L.; Zhu, G.; Xie, H.; She, X. Significant photothermal conversion enhancement of nanofluids induced by Rayleigh-Bénard convection for direct absorption solar collectors. *Appl. Energy* **2019**, *254*, 113706. [CrossRef]

14. Mukhtar, H.K.; Said, S.A.; El-Sharaawi, M.I. Dynamic performance of solar powered vapor absorption cooling system in dhahran—Saudi Arabia. In Proceedings of the 2018 5th International Conference on Renewable Energy: Generation and Applications (ICREGA), Al Ain, United Arab Emirates, 26–28 February 018.

15. Elahi, R.; Nagassou, D.; Trelles, J.; Mohsenian, S.; Trelles, J. Enhanced solar absorption by CO$_2$ in thermodynamic noneq. *Sol. Energy* **2019**, *195*, 369–381. [CrossRef]

16. Behi, M.; Mirmohammadi, S.A.; Ghanbarpour, M.; Behi, H.; Palm, B. Evaluation of a novel solar driven sorption cooling/heating system integrated with PCM storage compartment. *Energy* **2018**, *164*, 449–464. [CrossRef]

17. Salehi, S.; Yari, M.; Rosen, M.A. Exergoeconomic comparison of solar-assisted absorption heat pumps, solar heaters and gas boiler systems for district heating in Sarein Town, Iran. *Appl. Therm. Eng.* **2019**, *153*, 409–425. [CrossRef]

18. Buonomano, A.; Calise, F.; Dentice D'accadia, M.; Ferruzzi, G.; Frascogna, S.; Palombo, A.; Russo, R.; Scarpellino, M. Experimental analysis and dynamic simulation of a novel high-temperature solar cooling system. *Energy Convers. Manag.* **2016**, *109*, 19–39. [CrossRef]

19. Mateus, T.; Oliveira, A.C. Energy and economic analysis of an integrated solar absorption cooling and heating system in different building types and climates. *Appl. Energy* **2009**, *86*, 949–957. [CrossRef]

20. Fedrizzi, R.; Franchini, G.; Mugnier, D.; Melograno, P.N.; Theofilidi, M.; Thuer, A.; Nienborg, B.; Koch, L.; Fernandez, R.; Troi, A.; et al. Assessment of Standard Small-Scale Solar Cooling Configurations within the SolarCombi+ Project. In Proceedings of the 3rd International Conference Solar Air-Conditioning, Palermo, Italy, 30 September–2 October 2009.

21. Shirazi, A.; Taylor, R.A.; White, S.D.; Morrison, G.L. Transient simulation and parametric study of solar-assisted heating and cooling absorption systems: An energetic, economic and environmental (3E) assessment. *Renew. Energy* **2016**, *86*, 955–971. [CrossRef]

22. Vasta, S.; Palomba, V.; Frazzica, A.; Costa, F.; Freni, A. Dynamic simulation and performance analysis of solar cooling systems in Italy. *Energy Procedia* **2015**, *81*, 1171–1183. [CrossRef]

23. Calise, F.; d'Accadia, M.D.; Palombo, A. Transient analysis and energy optimization of solar heating and cooling systems in various configurations. *Sol. Energy* **2010**, *84*, 432–449. [CrossRef]

24. Djelloul, A.; Draoui, B.; Moummi, N. Simulation of a solar driven air conditioning system for a house in dry and hot climate of algeria. *Courr. Savoir* **2013**, *15*, 31–39.

25. Hassan, L.; Moghavvemi, M.; Mohamed, H.A.F. Impact of UPFC-based damping controller on dynamic stability of Iraqi power network. *Sci. Res. Essays* **2011**, *6*, 136–145.

26. The World Bank. Available online: https://solargis.com/maps-and-gis-data/download/iraq (accessed on 5 December 2019).

27. Nafey, A.S.; Sharaf, M.A.; García-Rodríguez, L. A new visual library for design and simulation of solar desalination systems (SDS). *Desalination* **2010**, *259*, 197–207. [CrossRef]

28. Sharaf Eldean, M.A.; Soliman, A.M. A new visual library for modeling and simulation of renewable energy desalination systems (REDS). *Desalin. Water Treat.* **2013**, *51*, 6905–6920. [CrossRef]

29. Available online: http://www.apricus.com/en/america/products/solar-collectors/ap-30/ (accessed on 6 December 2019).

30. Peuser, F.; Remmers, K.; Schnauss, M. *Solar Thermal Systems: Successful Planning and Construction*; Routledge: Abingdon, UK, 2013.

31. Balghouthi, M.; Chahbani, M.H.; Guizani, A. Solar powered air conditioning as a solution to reduce environmental pollution in Tunisia. *Desalination* **2005**, *185*, 105–110. [CrossRef]

32. Available online: http://www.BaltimoreAircoil.com (accessed on 16 December 2019).

33. ASHRAE. *Heating, Ventilating, and Air-Conditioning Systems and Equipment*, SI ed.; American Society of Heating, Refrigerating and Air-Conditioning Engineers, Inc.: Atlanta, GA, USA, 2012.

34. Available online: http://www.yazakienergy.com (accessed on 31 January 2020).

35. Rodríguez-Hidalgo, M.D.C.; Rodríguez-Aumente, P.A.; Lecuona, A.; Legrand, M.; Ventas, R. Domestic hot water consumption vs. solar thermal energy storage: The optimum size of the storage tank. *Appl. Energy* **2012**, *97*, 897–906.

36. Allouhi, A.; Kousksou, T.; Jamil, A.; Bruel, P.; Mourad, Y.; Zeraouli, Y. Solar driven cooling systems: An updated review. *Renew. Sustain. Energy Rev.* **2015**, *44*, 159–181. [CrossRef]

37. Joudi, K.A.; Dhaidan, N.S. Application of solar assisted heating and desiccant cooling systems for a domestic building. *Energy Convers. Manag.* **2001**, *42*, 995–1022. [CrossRef]

38. Shariah, A.; Al-Akhras, M.A.; Al-Omari, I.A. Optimizing the tilt angle of solar collectors. *Renew. Energy* **2002**, *26*, 587–598. [CrossRef]

39. Elminir, H.K.; Ghitas, A.E.; El-Hussainy, F.; Hamid, R.; Beheary, M.M.; Abdel-Moneim, K.M.; Elminir, H.K. Optimum solar flat-plate collector slope: Case study for Helwan, Egypt. *Energy Convers. Manag.* **2005**, *47*, 624–637. [CrossRef]

40. Duffie, J.A.; Beckman, W.A. *Solar Engineering of Thermal Processes*; John Wiley & Sons: Hoboken, NJ, USA, 1991.

41. Duffie, J.A.; Beckman, W.A. *Solar Engineering of Thermal Processes*; John Wiley & Sons: Hoboken, NJ, USA, 2013.

42. Bahria, S.; Amirat, M.; Hamidat, A.; El Ganaoui, M.; Slimani, M.E.A. Parametric study of solar heating and cooling systems in different climates of Algeria–A comparison between conventional and high-energy-performance buildings. *Energy* **2016**, *113*, 521–535. [CrossRef]

43. Assilzadeh, F.; Kalogirou, S.A.; Ali, Y.; Sopian, K. Simulation and optimization of a LiBr solar absorption cooling system with evacuated tube collectors. *Renew. Energy* **2005**, *30*, 1143–1159. [CrossRef]

Paper B
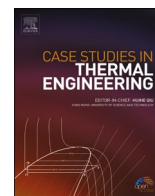
Design and thermo-economic comparisons of large scale solar absorption air conditioning cycles

Adil Al-Falahi [*], Falah Alobaid, Bernd Epple

Technische Universität Darmstadt, Institut Energiesysteme und Energietechnik, Otto-Berndt-Straße 2, 64287, Darmstadt, Germany

A B S T R A C T

Sustainable cooling absorption technologies, using renewable energy sources, and climate-friendly cooling liquids gain more and more attention. In this work, design and thermo-economic analyses are presented to compare between two different collector types (parabolic trough and evacuated tube) by Water-Lithium Bromide absorption systems. Generally, the main component of the entire system is the absorption refrigeration chiller, the plant will then consist of three subsystems. The first subsystem is the solar system for thermal power conversion. The second subsystem is represented by the condenser and chiller absorber that need to be cooled, using a cooling tower. The third subsystem is represented by the cold circuit and the terminals of the useful cooling power produced. A case study for a sports arena with 700–800 kW total cooling load is also presented. Results reveal that parabolic trough collector combined with H_2O–LiBr (PTC/H_2O–LiBr) gives lower design aspects and minimum rates of hourly costs (5.2$/h), while ETC/$H_2O$–LiBr configuration (5.6$/h). H_2O–LiBr thermo-economic product cost is (0.14$/GJ). The cycle coefficient of performance COP was in the range of 0.5–0.9.

1. Introduction

Nowadays, cooling systems are an essential technology in the domestic and industrial sectors, such as food preservation, air conditioning, air separation, natural gas liquefaction, and ice production [1]. The two most common refrigeration systems used in domestic and industrial applications are compression and absorption refrigeration systems. In compression cycles, an electrical compressor is used to increase the pressure of the refrigerant. In contrast, in absorption refrigeration systems, the refrigerant is absorbed into another fluid (absorbent) and pumped to the condenser pressure [2]. However, like any thermal systems, energy consumption should be considered and be manipulated. Furthermore, the growing requirements related to thermal comfort are also observed. Moreover, in the last several years there has been increasing attention to effective technologies in order to achieve both energy saving and CO2 emission reduction [3]. As a clean source of energy needed for refrigeration and air conditioning cycles, a growing interest in the use of solar thermal applications to produce renewable and sustainable energy, coupled with the remarkable progress being made in nanotechnology, many innovative solutions have been observed. Generally, cooling power production needs electrical or mechanical power, whereas absorption chillers can produce chilled water from low-temperature heat. Such heat can be provided by solar thermal collectors [4]. Solar-driven cooling systems are a sound alternative to conventional electrical driven compression units, as they achieve primary energy savings and reduce greenhouse gas emissions for solar fractions higher than about

* Corresponding author.
   E-mail address: adil.al-falahi@est.tu-darmstadt.de (A. Al-Falahi).

Nomenclature

A	Availability, kWArea, m^2
A_t	Tube cross-sectional area, m^2
A_f	Amortization factor, 1/y
AAC	Absorption Air Conditioning
C	Thermo-economic cost stream, \$/kJ
C_p	Specific heat capacity, kJ/kg^{o}C @ constant pressure
COP	Coefficient of Performance
D	Diameter, m
D_{env}	Collector glass envelope diameter, m
E	Exergy stream, kW
ETC	Evacuated Tube Collector
f	Function
FHP	Fan power, kW
H, h	Height, m, Enthalpy, kJ/kg
H_{dish}	Dish parabola height, m
I_s	Solar intensity, W/m^2
i	Interest rate, %
L	Length, m
L_m	Module length, m
LMT	Logarithmic Mean Temperature, ^{o}C
LPC	Levelized Power Cost, \$/kWh
LTp	Plant life time, y
M	Mass flow rate, kg/s
NOT	Number of Tubes
NOC	Number of Collectors
NOL	Number of Loops
P	Power, or Pressure, bar
ΔP	Pressure, bar
Q	Thermal power, kW
RPR	Relative Performance Ratio
Re	Raynold's Number
S, s	Entropy, kJ/kg^{o}C
T	Temperature, ^{o}C
U	Overall heat transfer coefficient, W/m^{2o}C
V, Vol	Volume, cm^3
v	Velocity, m/s
W	Power, Work, kW
W_c	Collector width, m
X	Concentration percentage, %
Z	Hourly cost, \$/h

Subscripts

a, abs	Absorber
air	Air
amb	Ambient
a-hex	From absorber to heat exchanger stream
c	Condenser
c-evp	From condenser to evaporator stream
col	Collector
cw	Cooling water
e	Evaporator
etc	Evacuated tube collector
e-abs	From evaporator to absorber stream
f	Liquid phase
fan	Fan
fsh	Flashing tank
fst	Flashing steam
g	Generator, vapor phase

g-hex	From generator to heat exchanger stream
i	Inlet
loop	Loop
o	Out
p	Pump
ptc	Parabolic trough collector
$p_{i,o}$	Pump inlet and outlet
q	Heat
r	Refrigerant
s	Steam
st	Steam
str	Strong
t	Turbine, total
w	Water
wk	Weak solution
Greek	
η	Efficiency, %
ρ	Density, kg/m^3
μ	Dynamic viscosity, Pa.s

50% [5]. N. Molero-Villar [5] dealt with the selection of the most suitable configuration for residential cooling systems with solar energy. Villar [5] used a TRNSYS model to compare a configuration with just hot storage (of typical capacity 40 L/m^2 of solar collector surface). Syed A.M [6] suggested an alternate design for a 24-h operating solar-powered absorption refrigeration technology that has been developed. Thermodynamic analysis of some designs has been investigated.

The analysis indicates that continuously operating a solar-powered aqua-ammonia absorption system with refrigerant storage was the most suitable alternative design for an uninterrupted supply of cooling effect. A. Aliane [7] demonstrated different case studies about solar thermal absorption systems. Ayman et al. [8] investigated by a developed model a proposed design for a pilot test unit of 10 kW electrical power, 1.7 m^3/day of desalinated water, and 3.6 TR cooling load capacity. The system showed how it was very effective to utilize solar energy for power generation, water desalination, and air conditioning systems. H$_2$O–LiBr was used for the air condoning cooling part [8]. In the same regard, Roberto Leiva [9] compared between the Levelized cost and the thermo-economic methods in their application to assess the performance of a solar polygeneration plant. The results show that the cost allocation method is proper when more precise analysis is required to evaluate the appropriate costs of different products.

One of the advantages of the absorption cycle is the possibility of using various heat sources as the input to the generator. Solar parabolic trough collector has been used beside a single effect H$_2$O–LiBr absorption chiller [9]. Tzivanidis and Bellos [10] researched the effects of various design parameters, such as mass flow rate and solar tank size on the performance of solar absorption cooling system comprises of parabolic through collectors (PTC) integrated with single-stage absorption chiller in the Athens climate, and found that utilizing harvested area of a 54 m^2 and a 1.35 m^3 storage tank, a maximum cooling load of 12.8 kW can be achieved. Wang [11] investigated the effect of large temperature gradients and serious nanoparticles photothermal conversion efficiency on direct absorption solar collectors. Olivier [12] presented dynamic modeling of a single-effect absorption chiller working with the H$_2$O–LiBr solution used in a solar cooling installation operating without any backup systems (hot or cold). In that case, the absorption machine is powered only by a solar collector field. Given the highly variable nature of solar radiation and the building loads, the range of the three source temperatures of the chiller can vary widely since there is no backup system. The system was operated for 30 kW of thermal cooling load.

In a recent study, Al-Falahi Adil [13] investigated the energy performance of a solar absorption air conditioning system integrated with evacuated tube collectors (ETC), in the climate of Baghdad, Iraq. It was concluded that the seasonal collector efficiency and solar fractions are 54% and 58%, respectively, and the absorption chiller COP was 0.44. Relevant to the H$_2$O–LiBr chiller we have used in this study, [13].

Rejeb et al. [14] studied the effect of different nanofluid types on the coefficient of performance (COP) solar air conditioning cycle using H$_2$O–LiBr chiller coupled with parabolic through collectors (PTC). The numerical results show that it is possible to achieve a maximum COP of 0.77 for the hottest day and there is no significant effect of nanofluid. Behi [15] presented an applied experimental and numerical evaluation of a triple-state sorption solar cooling module. The performance of a LiCl–H$_2$O based sorption module for cooling/heating system with the integration of external energy storage has been evaluated. Special design for solar collector was investigated by Behi [15]. Related to thermo-economics, Salehi [16] studied the feasibility of solar assisted absorption heat pumps for space heating. In Salehi [16]study, single-effect LiBr/H2O and NH$_3$–H$_2$O absorption and absorption compression-assisted heat pumps are analyzed for heating loads of 2 MW. Using the geothermal hot springs as heat sources for refrigerant evaporation, the problem of freezing is prevented. Salehi [16]COP was ranged between 1.4 and 1.6.

Marc [17] used 36 solar collectors of composed double-glazed flat-plate solar-type for a total capture area of 90 m^2. Zhai [18] used an evacuated tube solar field for 8 kW cooling capacity. The system consumed and amount of 92 m^2 of solar area. Khaled [19] studied an open absorption (liquid desiccant) system, capable of producing both cooling and dehumidification for air conditioning, utilizing

low-grade heat. The system includes a novel solution heat and mass exchanger designed to serve as a desiccant solution reservoir for both the absorber and desorber, enabling mass transfer between them with minimum heat transfer losses and eliminating the need for an external recuperative heat exchanger. Zambrano [20] presented a solar power system as a primary source of energy. Solar collectors were used to increasing the temperature of the circulating water. The solar field is composed of 151 m^2 of flat collectors which work in the range of 60–100 °C. The cooling system was an absorption machine that works with water as a cooling fluid and a water solution of lithium bromide (H$_2$O–LiBr). The operating procedure of the machine requires that its inlet temperature is within the range of 75–100 °C. Villada [21] compared different configurations based on energy consumption and efficiency. Three types of solar collectors have been compared.

It is clear from the literature that solar energy has a great influence on refrigeration and/or air conditioning processes. Different types and configurations of solar collectors have been applied for such purposes. The most type used was evacuated tube collector. Moreover, it has been noticed that H$_2$O–LiBr has been used for most of the research activities in this regard for conditioning applications. The aim of this work is to optimize and design H$_2$O–LiBr absorption air conditioning systems that are operated by two different types of solar collectors (ETC and PTC), based on energy, exergy, design, and cost. Selecting the best operating condition has also been the focus. The following general outlines are being proposed for this work:

✓ H$_2$O–LiBr absorption cycles have been studied under different operating conditions. The selection was made based on the best-operating conditions.
✓ Two different types of solar collectors (ETC and PTC) have been compared while combining with absorption cycles.
✓ A detailed mathematical model has been performed.
✓ The comparison is performed based on the terms of energy, exergy, design, cost, and thermo-economic. The design technique of modeling has been adopted in this study.
✓ Based on the optimized selection, a case study for a 700–800 kW (200–230 TR) cooling load has been performed.

2. Proposed system configuration

The solar absorption air-conditioning (AAC) system under study comprised of several important elements. One such element is the heat medium production cycle, which includes solar thermal collectors, a solar flash tank, a pump, and a distribution cycle. Another important element is the cold medium production cycle, which integrates an absorption chiller, a cooling tower, and two circulating pumps connected respectively to absorber and evaporator. The most important system elements are shown in Fig. 1. The energy obtained from the incident solar radiation heats the water in a field of solar thermal collectors, then the hot water flows into a solar tank, and subsequently transported to the absorption chiller to produce chilled water, which circulates through a conventional distribution system of individual fan coils to deliver cold air to the building. The cooling water dissipated the heat of the absorber and condenser of the chiller through the cooling tower. The currently proposed thermal cooling system is comprised of the following important elements:

➢ Evacuated tube collector (ETC) and/or parabolic trough collector (PTC) for thermal power generation. Water working fluid is the main fluid through the solar part.
➢ A flash evaporation tank is used for steam generation.
➢ The pumping unit has been used for flow circulation and pressure drop issues.
➢ The generator unit and this part is attached to the solar part. The flash evaporation tank will generate sufficient steam in order to drive on the generator unit.
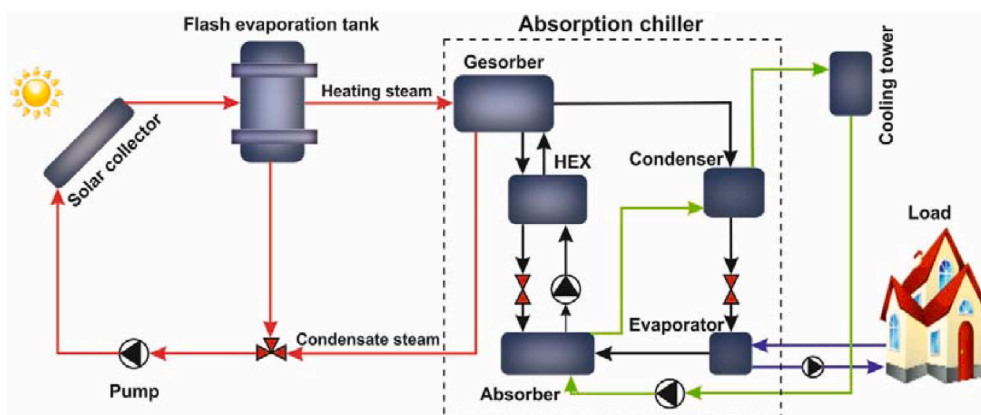➢ Absorber unit.

Fig. 1. Schematic drawing of solar absorption cooling system.

➢ Air conditioning as cooling load and this part is attached to the evaporator unit. The fan cooling unit is attached to the air cooler unit.

➢ Condenser unit for condensation process and will be cooled down by the use of the mechanical draft cooling tower.

➢ A mechanical draft crossflow cooling tower is used for the condenser unit. The water cooling cycle is passing through the absorber unit before cooling down the condenser unit.

Table 1

Data assumptions for the (ETC/PTC)H_2O–LiBr configurations.

Unit Process	Assigned Data	Calculated Data
Absorption air-conditioning cycle (AAC): (ETC/PTC) H_2O–LiBr	✓ Solar radiation:500 W/m^2 ✓ Ambient temperature:25 °C ✓ Average relative humidity: 15% ✓ ETC top temperature:100–200 °C ✓ PTC top temperature:200–300 °C ✓ Absorber temperature:30–35 °C ✓ Generator temperature:80–90 °C ✓ Condenser temperature:40–45 °C ✓ Hot air temperature:35 °C ✓ Target cooled air temperature: 20 °C ✓ Evaporator temperature:5–10 °C ✓ Cooling load:14–57 kW (50–200 TR) ✓ Condenser effectiveness:80% ✓ Cooling tower effectiveness: 60% ✓ Fan system efficiency:85% ✓ Pumping system efficiency:75% ✓ Plant life time:20 year ✓ Interest rate: 5% ✓ Load factor:90% ✓ Specific electric power cost:0.065 \$/kWh ✓ Water steam is the solar field working fluid	**Solar Field:** ➢ Solar field top pressure, bar ➢ Solar field pressure loss, bar ➢ Total solar field area, m^2 ➢ Solar field thermal load, kW ➢ Number of solar collectors, # ➢ Solar field mass flow rate, kg/s ➢ Solar field inlet temperature, °C ➢ Efficiency, % ➢ Exergy destruction, kW **Flash Tank:** ➢ *Flash tank design data ➢ Total mass flow rate, kg/s ➢ Dryness fraction, % ➢ Flash tank water flow rate, kg/s ➢ Steam flow rate, kg/s ➢ Exergy destruction, kW **Mechanical Draft Cooling Tower:** ➢ Cooling tower flow stream, kg/s ➢ Cooling tower approach, °C ➢ Cooling tower range, °C ➢ Fan power, kW ➢ *Design data **Absorption air-conditioning cycle (AAC) Unit:** ➢ Weak & strong solutions, kg/s ➢ *Design data ➢ Thermal power, kW ➢ Total cycle flow rate, kg/s ➢ Generator power, kW ➢ Cooling fan power, kW ➢ COP ➢ COPmax ➢ Relative performance ➢ Exergy destruction, kW **Pump:** ➢ Power, kW ➢ Outlet temperature, °C ➢ Exergy destruction, kW **Cost & Performance:** ➢ Units hourly costs, \$/h ➢ Total hourly costs, \$/h ➢ Total power, kW ➢ LPC, \$/kWh ➢ Thermo-economic cost, \$/GJ ➢ Total exergy destruction rate, kW
Notes:	• Data are run out based on steady-state operating conditions. • Ambient temperature is fixed as 25 °C for all process runs. • Solar radiation is fixed at 500 W/m^2. • *Design data means an area, length, width, etc …	

➢ The cycle is considered a closed cycle related to the working flowed through it.

3. Methodology, mathematical model and assumptions

The proposed configurations in this work are required iterative programming in order to calculate the complicated streams (recycle and backward streams). Hence; to develop a specific model for this innovative kind of plant. Simulink software, a Matlab work's product, has been chosen for its high versatility and capacity to handle unsteady situations. Two models were built according to the proposed configurations (ETC/H_2O–LiBr and PTC/H_2O–LiBr). The models were built according to the design calculation method. The system border streams (outlet temperature, ambient temperature, inlet cooling water temperature, etc.) are assigned by the user than the entire design data (area, length, volume, mass flow rate, etc.) Will then be calculated. Therefore; a user would assign the amount of needed cooling load on the evaporator then all possible data for all the system units would be calculated in sequence.

Specifying the system cooling load would calculate the required thermal load. Besides; the required design limits and performance calculations would be pass out instantly. The modeling assumptions are listed in Table 1. Saturated liquid and vapor phases of pressure, temperature, enthalpy, specific volume, and specific entropy are stored behind the modeled blocks and lookup tables. The source of physical properties is obtained from NIST [22] web chemistry book. Generally, the optimization process has been done in order to bring down costs and techno-economic solutions. Table 1 illustrates the design operating conditions and the assumptions that been considered in this work. The mathematical model that been used in this work is described in Appendix A in detail.

4. Results and comments

As illustrated earlier, the proposed cycles for the current study are two cycles. Therefore, it is very important to optimize the absorption air conditioning AAC cycle before the attachment with solar collectors. Such optimization would reduce the design aspects such as area. Meanwhile, lowering the cost values and the thermo-economic product cost goes to the end-user. For such optimization purposes, different operating conditions have been examined in this section. The optimization process addressed the effect of different operating conditions on COP, COP$_{max}$, Exergy destruction rate, mass flow rates, and design aspects such as areas and volume. For performance calculations, the C.O.P is calculated based on evaporator and generator thermal powers, $COP = \frac{Q_e}{Q_g}$, The COP strongly depends on the flows of energy in these two parts. In General, the generator is influenced by solar radiation, while the evaporator affected by building a cooling load which depends on the ambient outdoor temperature.

4.1. Optimization of H_2O–LiBr cycle

4.1.1. Evaporator temperature effect (H_2O–LiBr)

Fig. 2 shows the data results based on the effect of evaporator temperature on the other design parameters such as COP, COP$_{max}$, Exergy destruction rate, mass flow rates, and design aspects. Data has been obtained at different refrigerant loads (1-100 TR), and different values of evaporator operating temperature (5–10 °C). Figure (2-a) shows the effect of the evaporator temperature on the COP. Increasing the evaporator temperature would cause a slight increase in the COP. The same behavior has been noticed in Figure (2-b) as an effect on the COP$_{max}$. The reason for this was happened because of the following relation between the evaporator temperature
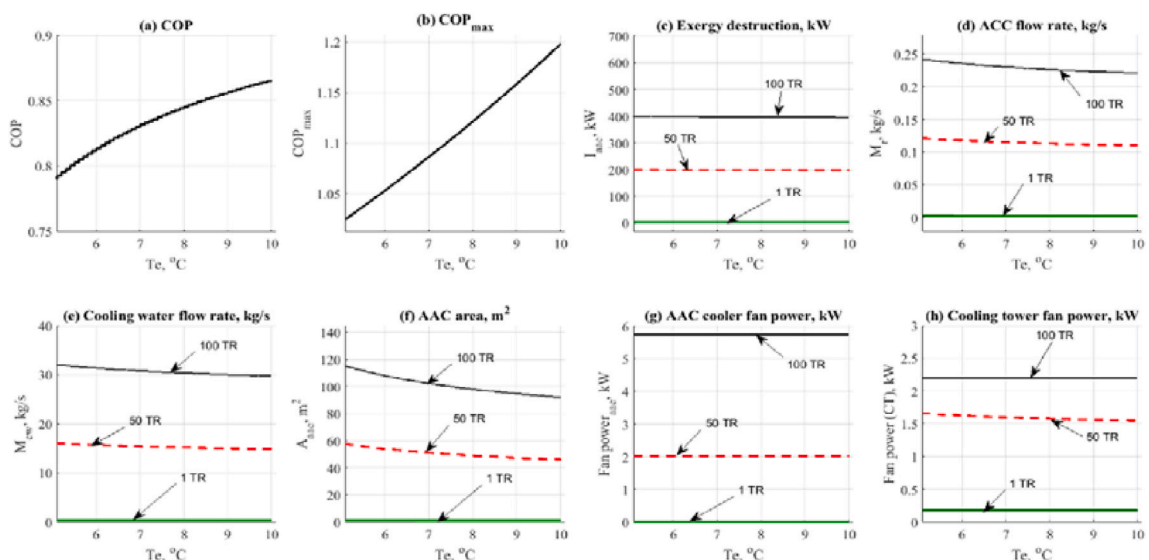

Fig. 2. H_2O–LiBr data results based on the effect of evaporator temperature parameter.

and the COP, and COP$_{max}$ ($COP_{max} = \frac{(T_e+273.15)\times(T_g-T_a)}{(T_g+273.15)\times(T_c-T_e)}$).

Increasing the load does not affect the COP and/or COP$_{max}$ as noticed. In general, the COP was in increasing range mode from 0.8 up to 0.85. Figure (2-c) shows that increasing the evaporator temperature has no remarkable effect on the exergy destruction rate which is quite beneficial to the system with regards to reducing or halting the exergy destruction rate. For example, at 100 TR load, the exergy destruction rate has been fixed at 400 kW. A decreasing behavior was noticed on the total mass flow rate as shown in Figure (2-d). The mass flow rate was in decreasing mode vs. the increase of evaporator temperature. The effect of evaporator temperature on the flow rate is not significantly high when viewed against the refrigerant load. Moreover, the effect is considered on the same line when viewed related to the cooling water flow rate Figure (2-e). The evaporator temperature would cause a decrease in the cooling flow rate which is considered recommended according to cost limitations. A slight reduction in the AAC area can be noticed in Figure (2-f) too. For instance, the total AAC area has been decreased from 117 m^2 down to 90 m^2 at 100 TR load. Figure (2-g) shows that there is no effect on the evaporator fan cooler unit. Figure (2-h) reflects the change in cooling tower mass flow rate by the cause of the evaporator temperature. The fan power has been decreased significantly. The increase in load would increase fan power. Increasing the evaporator temperature would slightly decrease the power in the cooling tower fan. Generally, increasing the evaporator temperature decrease the cost with a remarkable increase in performance too. A value of 7–10 °C would be recommended in this study for the evaporator unit.

4.1.2. Generator temperature effect (H$_2$O–LiBr)

Fig. 3 shows the data results based on the effect of generator temperature on the other design parameters such as COP, COP$_{max}$, Exergy destruction rate, mass flow rates, and design aspects. Data has been obtained at different refrigerant loads (50-150 TR) and different values of the generator operating temperature (80–90 °C). Figure (3-a) shows the effect of the generator temperature on the COP. Increasing the generator temperature would cause a remarkable increase in the COP. The same behavior can be noticed in Figure (3-b) as an effect on the COP$_{max}$. The reason for this was happened because of the following relation between the generator temperature and the COP, and COP$_{max}$ ($COP_{max} = \frac{(T_e+273.15)\times(T_g-T_a)}{(T_g+273.15)\times(T_c-T_e)}$).

Increasing the load does not affect the COP and/or COP$_{max}$ as noticed. In general, the COP was in increasing range mode from 0.7 up to 0.87. Figure (3-c) shows that increasing the generator temperature has a slight effect on the exergy destruction. For example, at 150 TR load, the exergy destruction rate was a little bit fixed at 600 kW. A remarkable decreasing behavior was noticed in the total mass flow rate as shown in Figure (3-d). The mass flow rate was in decreasing mode vs the increase in generator temperature. Moreover, the effect is considered on the same line when comparing it related to the cooling water flow rate Figure (3-e). The generator temperature would cause a decrease in the cooling flow rate which is considered recommended according to cost limitations. A slight reduction in the AAC area can be noticed in Figure (3-f) too. For instance, the total AAC area has been decreased from 110 m^2 down to 100 m^2 at 100 TR load. Figure (3-g) shows that there is no effect on the generator fan cooler unit. Figure (3-h) reflects the change in cooling tower mass flow rate by the cause of generator temperature. The fan power has been decreased significantly. The increase in load would increase fan power. Increasing the generator temperature would slightly decrease the power on the cooling tower fan. Generally, increasing the generator temperature is used to decrease the cost, with a remarkable increase in performance, too. A value of 85–90 °C would be recommended in this study for the generator unit.

4.1.3. Solar field top temperature effect (H$_2$O–LiBr)

Figures (4,5) show the data results based on the effect of solar collector temperature on the other design parameters such as mass flow rates, and design aspects. Data has been obtained at different refrigerant loads (50-150 TR) and different values of solar collector
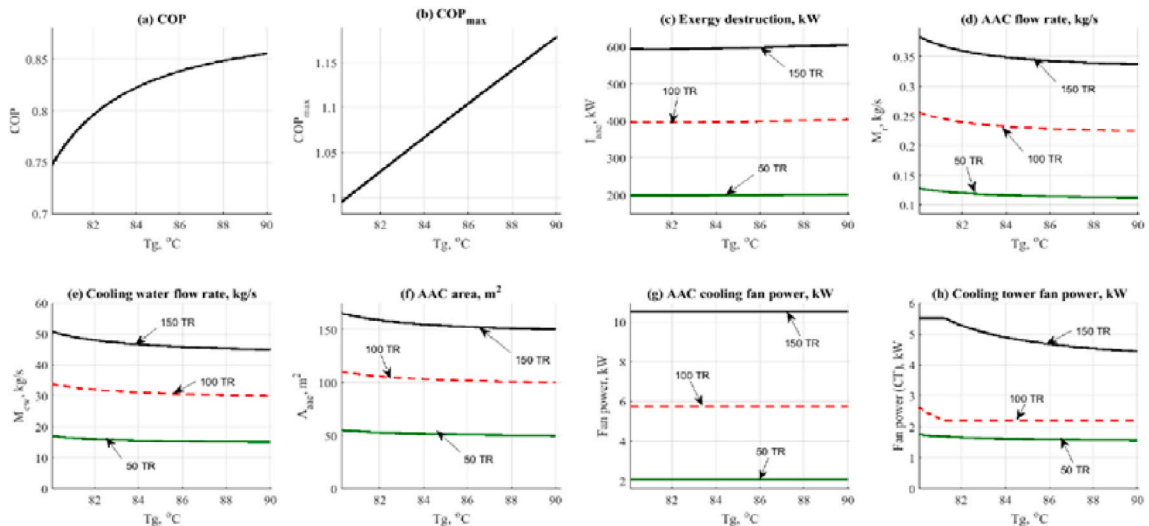

Fig. 3. H$_2$O–LiBr data results based on the effect of generator temperature parameter.

operating temperature (100–200 °C for ETC and 200–300 °C for PTC). Figures (4-a, 5-a) show the effect of solar collector temperature on the solar field mass flow rate. Increasing the solar collector temperature would cause a remarkable decrease in the solar field mass flow rate. The main reason for this is related to energy balance across the solar field as presented in this relation $Q_{th} = M_{col} \times C_p \times (T_o - T_i)$. The same behavior can be noticed in Figures (4-b, 5-b) as an effect on the total mass flow rate.

However, the PTC gives lower results in the total mass flow rate according to the increase in top temperature when compared against the ETC. Increasing the load does not affect the dryness fraction, as noticeable in Figures (4-c, 5-d). Generally, the dryness fraction X was in the increasing range from 5% up to 25% in the case of ETC and 24% up to 45% in the case of PTC. Increasing the dryness fraction means more steam could be used for the generator unit, which is probably a favorable effect. Figures (4-d, 5-e) shows that increasing the solar collector temperature has a massive effect on the flash tank volume. However, PTC recorded lower tank volume results comparing against the ETC. The solar field area has also an increasing effect based on temperature increasing. Figures (4-e, 5-f) represent that effect. It is quite clear that increasing the outlet temperature would increase the area of the solar field. However, PTC is recorded lower total area when compared against the ETC.

Figures (4-f, 5-g) represent the change in total thermal power based on the change in top solar field temperature. Figures (5-h, i) show the effect of top solar temperature of the performance indicators, such as efficiency and exergy efficiency. Increasing the top solar field temperature would decrease both efficiencies due to the increase of thermal exergy destruction rate across the solar field for both cases. A value of 150–200 °C and 250–300 °C would be recommended in this study for ETC and PTC solar collectors respectively. Based on the obtained results, it is quite interesting to assign the operating temperature as follows:

- ➢ $T_a = 35$ °C.
- ➢ $T_c = 43$ °C.
- ➢ $T_e = 7$–10 °C.
- ➢ $T_g = 85$–90 °C.
- ➢ ETC $T_{high} = 150$–200 °C.
- ➢ PTC $T_{high} = 250$–300 °C.

4.1.4. Cooling load effect (H_2O–LiBr)

The cooling load effect on ETC/H_2O–LiBr and PTC/H_2O–LiBr cycles is shown in Figures (6 & 7). Both figures address the effect on hourly costs, Levelized power costs, and thermo-economic product costs. As expected, the behavior in the figure was in increasing mode, due to the load and energy demand for all units. Solar collectors recorded the highest values of hourly costs among the other units as shown in Figures (6-a, 7-a).

However, PTC was recorded as lower by 12% than the ETC, related to the hourly costs parameter. The main reason for this is related to the increase in collector operating temperature (250 °C vs 150 °C). Increasing the collector temperature will generate more steam for the AAC unit. The cooling tower comes next by 2.2$/hr for both operations. AAC, pumps, and flashing tanks are shown in Figures (6-b, 7-b). It is clear in the figures that AAC is recorded a little bit higher than the pump and flashing tank, based on the total needed area.

Figures (6-c, 7-c) show the effect of cooling load on the Levelized power cost, $/kWh. The results are nearly the same based on the close results between the two configurations related to the pumping unit and the cooling tower. The Levelized power cost ranged between 0.15$/kWh to 0.35$/kWh. The same close behavior is noticeable when comparing thermo-economic product costs. Results were centralized around 0.08 to 0.14–0.16$/GJ for both configurations, with a minor advantage to the ETC Figures (6-d, 7-d). As
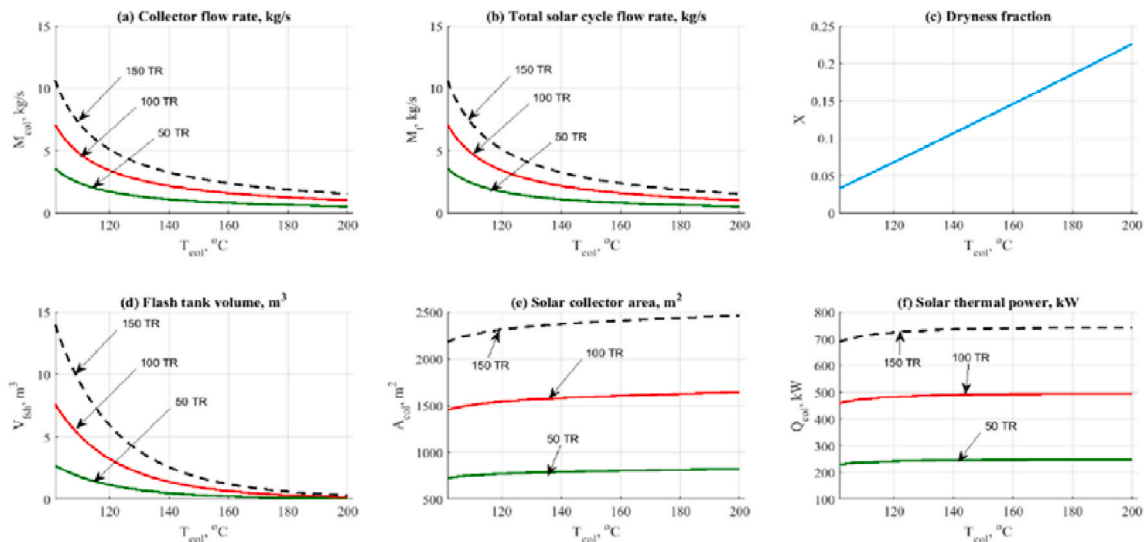

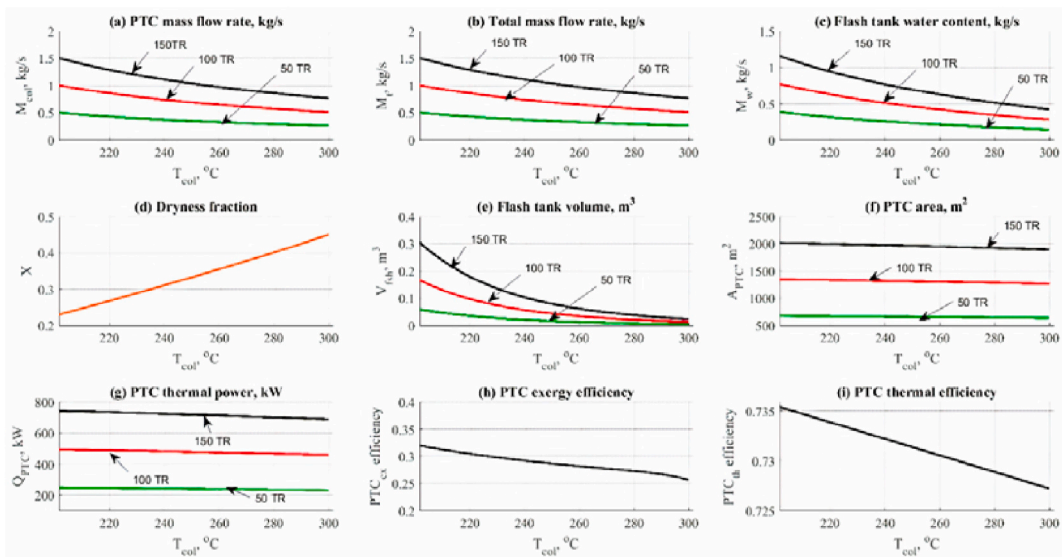Fig. 4. H_2O–LiBr data results based on the effect of ETC outlet top temperature.

Fig. 5. H$_2$O–LiBr data results based on the effect of PTC outlet top temperature.
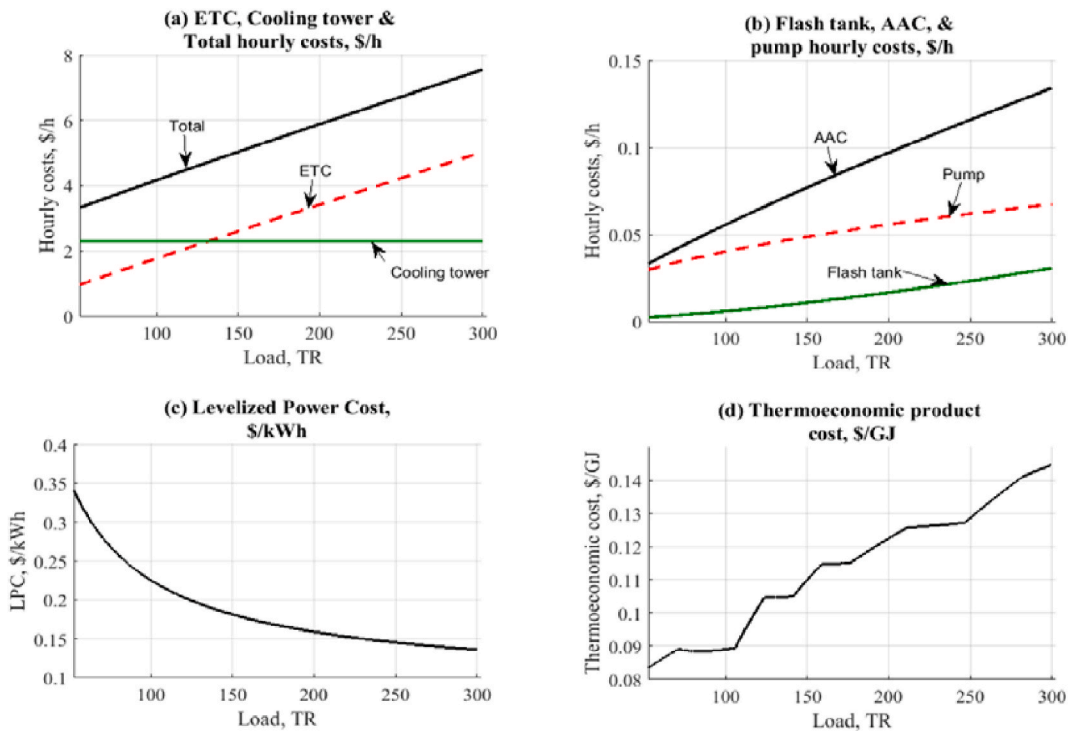

Fig. 6. ETC-H2O–LiBr data results based on the effect of cooling load.

anticipated, increasing the load would increase the cost of exergy. Solar PTC and/or ETC are considered the main cause of such an effect, related to the large area needed to cover the load.

4.2. Case study results

The case study presented in this section compares between two configurations at a specific load point. The case study was about a sports arena which is located in Baghdad, Iraq. The arena is USD14 million, a 3000-seat indoor sports facility focused around basketball, volleyball, and athletics. The whole project will be centrally air-conditioned by a 700–800 kW solar absorption cycle. The
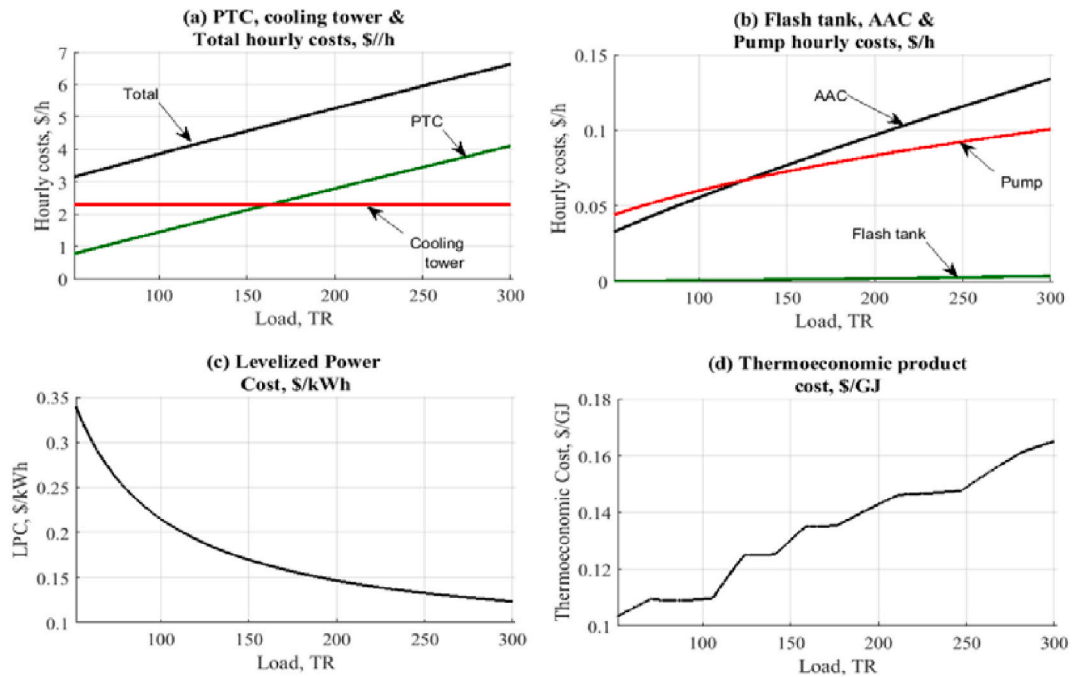
Fig. 7. PTC-H2O–LiBr data results based on the effect of cooling load.

evaporator will be designed to work between 7 and 12 °C. Table 2 shows the data results for two configurations in case of using the solar absorption cycle. A 200 TR cooling load has been selected as an example of such a comparison. Environmental operating conditions are fixed at a specific value for simplicity. For solar field results, PTC/H_2O–LiBr resulted in the lowest area needed, and it is quite important to reduce the needed area. ETC/H_2O–LiBr comes next. For design aspects such as flashing tank design, it was clear the operation of PTC/H_2O–LiBr gives the lowest results, which were the most favorable, at 0.11 m^3, followed by ETC/H_2O–LiBr with 1 m^3. The same behavior was also noticed related to the dryness fraction. The same behavior is also noticed related to the exergy destruction rate. The results reveal that PTC is considered an advantage to the cycle vs the ETC operation. Minimum driving steam was recorded by PTC/H_2O–LiBr (0.4 kg/s) which lead to low flashing tank volume and lower solar field area. COP was found remarkable related to the H_2O–LiBr cycle. For hourly costs, PTC/H_2O–LiBr is noted as the lowest among the rest. By achieving 5.2$/h, PTC/$H_2O$–LiBr is considered the best option for this case study. Lower hourly costs for the solar field is considered the vital term to judge the system cost. Thermo-economic cost is nearly the same for two configurations, within the range of 0.14–0.16$/GJ.

5. Conclusion

In this work, two configurations of solar assisted absorption air conditioning (AAC) cycles are presented. H_2O–LiBr absorption chillers have been considered. For the solar part, Evacuated Tube Collector (ETC) and Parabolic Trough Collector (PTC) technology as the main source of thermal power. The novelty of this work emerged from the connection type between the solar part and the absorption part. A flash evaporation tank has been used as an intermediate unit between both parts. Energy, exergy, cost analyses are presented in this work. According to the analysis results, the following conclusions can be drawn:

- A flashing tank has been used for two configurations. Water steam is considered the main working fluid through the solar cycle.
- Energy, exergy, and cost balances are performed for all units.
- Design aspects, such as solar area and flashing tank volume, were found to have a great influence on the cycle cost.
- Optimization of the operating conditions, such as temperatures, has been performed for two configurations. The following values of operating conditions are considered the best, related to design aspects, COP, exergy destruction rate, and cost:
  o $T_a = 35$ °C.
  o $T_c = 43$ °C.
  o $T_e = 7$–10 °C.
  o $T_g = 85$–90 °C.
  o ETC $T_{high} = 150$–200 °C.
  o PTC $T_{high} = 250$–300 °C.
- Among configurations, PTC/H_2O–LiBr gives remarkable results comparing to the ETC.

Table 2
Data results based on a 200 TR load case study.

Solar Radiation, W/m^2	500.	
T_{amb}, °C	25	
T_a, T_e, T_g, T_c, T_{col}, °C	30, 10, 90, 40, 175	30, 10, 90, 40, 250
Load, kW (TR)	58 (200)	
Target cooled air, °C	20	
Interest rate, %	5	
Load factor, %	95	
Plant life time, yr	20	
Electric cost, USD/kWh	0.065	
Fans efficiency, %	80–85	
Pumps efficiency, %	75	
Configuration:	ETC/H$_2$O–LiBr	PTC/H$_2$O–LiBr
Solar field:		
Total solar field area, m^2	3022	2433
Solar thermal power, kW	918.6	890
Inlet temperature, °C	91.64	92.66
Mass flow rate, kg/s	2.582	1.327
Inlet exergy, kW	1436	1136
Exergy destruction, kW	1191	930
Flash tank:		
Height/Width, m	1.742/0.852	0.837/0.41
Volume, m^3	0.9942–1	0.1106
Total flow rate, kg/s	2.582	1.327
Water content, kg/s	2.1	0.897
Dryness fraction	0.1667	0.324
Exergy destruction, kW	134.3	180.8
AAC unit:		
Q_a, kW	743.3	743.3
A_a, m^2	190.5	190.5
M_{str}, kg/s	1.391	1.391
M_{wk}, kg/s	1.092	1.092
X_{a-hex}	0.4893	0.4893
A_{hex}, m^2	1.313	1.313
Q_g, kW	787.8	787.8
A_g, m^2	4.299	4.299
Driving steam flow, kg/s	0.4034	0.4034
X_{g-hex}	0.6233	0.6233
Outlet cooling water, °C	30.5	30.5
Q_c, kW	747.8	747.8
A_c, m^2	37.45	37.45
M_r, kg/s	0.299	0.299
Q_e, kW	703.4	703.4
A_e, m^2	36.35	36.35
FHP, kW	29.33–30	29.33–30
M_{air}, kg/s	68	68
CT water flow rate, kg/s	116.5	116.5
CT fan power, kW	15	15
CT rang/approach, °C	3.29/2.2	3.29/2.2
CT dia/height, m	5.9/4	5.9/4
COP/COP_{max}	0.89/1.56	0.89/1.56
RPR	0.573	0.573
Exergy destruction, kW	729.9	729.9
Fan exergy destruction, kW	55.6	55.6
Pump unit:		
W_p, kW	3.204	7.338
Exergy destruction, kW	14.8	12.33
Cost and Thermo-economics:		
Z_{col}, USD/h	3.918	2.604
Z_{fsh}, USD/h	0.02	0.001
Z_{aac}, USD/h	0.121	0.121
Z_{p+f}, USD/h	0.055	0.1743
Z_{ct}, USD/h	2.295	2.295
Z_{tot}, USD/h	5.685	5.2
LPC, USD/kWh	0.165	0.1557
cp, USD/GJ	0.1474	0.1602

- A case study is presented in a sports arena located in Baghdad, Iraq, for which the needed cooling load was in the range of 700–800 kW. PTC/H$_2$O–LiBr was recorded the best based on design and hourly costs. The required solar area was in the range of 2000–2500 m^2, while the total hourly costs were in the range of 4–5$/h, which is quite attractive.

- PTC/H_2O–LiBr gives the lowest values related to exergy destruction rates for all units. Moreover, the exergy destruction rate for the AAC was in the vicinity of 55 kW. As expected, the solar filed would harvest greater exergy destruction rates for the two configurations due to the large area and mass flow rate effect. The PTC/H_2O–LiBr exergy destruction rate results are in the range of 930–1000 kW.
- PTC/H_2O–LiBr gives the lowest value of flashing tank design aspects, such as width 0.4–0.5 m, height 0.8 m, and volume 0.11 m^3. ETC/H_2O–LiBr comes next with a total flashing tank equal to 1 m^3.
- It is quite clear that PTC/H_2O–LiBr followed by ETC/H_2O–LiBr has remarkable results according to the terms of energy, design, and cost. Generally, the PTC system is considered the best choice for the H_2O–LiBr solar cooling system.

CRediT authorship contribution statement

Adil Al-Falahi: Conceptualization, Data curation, Methodology, Software, Writing - original draft. **Falah Alobaid:** Writing-Reviewing and Editing. **Bernd Epple:** Supervision.

Declaration of competing interest

The authors declare that they have no known competing financial interests or personal relationships that could have appeared to influence the work reported in this paper.

Acknowledgements

Appendix A. Detailed mathematical model

Mathematical model of the proposed configurations.
Solar filed (ETC and/or PTC):
For ETC, the efficiency is calculated based on the following relation [23]:

$$\eta_{etc} = 0.673 - \left(0.30 \times \left(\frac{\left(\frac{T_o + T_i}{2} \right) - T_{amb}}{I_s} \right) \right)$$

Where I_s in kW and ambient temperature T_{amb} in ^oC.
Thermal useful load on the ETC, kW:

$$Q_{th} = M_{col}^{\cdot} \times C_p \times (T_o - T_i)$$

Where, M_{col} in kg/s, C_p in kJ/kg^oC, and the temperature difference is in ^oC.
Total ETC area, m^2:

$$A_t = \frac{1000 \times Q_{th}}{\eta_{etc} \times I_s}$$

Solar field design:

$$A_{etc} = \pi \times D_t \times L_t \times NOT$$

ETC module area A_{etc}, m^2 can be calculated where, D_t is the tube diameter, m, and L_t is the tube length, m, and *NOT* is the number of tubes per one module. The total number of evacuated tube collectors *NOC* can be calculated from the following equation.

$$NOC = \frac{A_t}{A_{etc}}$$

The number of loops *NOL*, loop area A_{loop}, and the loop length, L_{loop} can be calculated by assigning the hydraulic mass flow rate M_{hyd}, kg/s. M_{col} will be calculated based on the load between the flash tank and the AAC unit.

$$NOL = \frac{M_{col}^{\cdot}}{M_{hyd}}$$

$$A_{loop} = \frac{A_t}{NOL}$$

$$L_{loop} = \frac{A_{loop}}{L_t}$$

The corresponding efficiency equation for the medium-high temperatures parabolic trough collectors (PTC) is given by Eq. (9). Where, T_o is the outlet collector top temperature, ^oC, and T_{amb} is the ambient temperature, ^oC [24].

$$\eta_{ptc} = \eta_o - a_{11}(T_o - T_{amb}) - a_{21}\left(\frac{T_o - T_{amb}}{I_s}\right) - a_{31}\left(\frac{T_o - T_{amb}}{I_s}\right)^2$$

where, a_{11} W/m^2=4.5 $\times$ 10^{-6}, a_{21} W/m^2 = 0.039, a_{31} W/m^2 = 3 $\times$ 10^{-4}, η_o = 0.75

The collector total area is estimated based on the collector energy balance equation as a function of collector efficiencies as;

$$A_{PTC} = \frac{Q_u}{\eta_{PTC} \times I_s}, \ m^2$$

Where Q_u is the collector's useful thermal power and (I_s) is the solar flux over the collector area, and A_{PTC} is the collector total area. The collector useful energy equation may exist according to the following relation;

$$Q_u = M_{col} \times \Delta h_{o-i}$$

Where Δh is the enthalpy difference across the collector in kJ/kg, and M_{col} is the total field mass flow rate in kg/s. The PTC total length is then calculated based on collector width, m, and glass envelope diameter, m.

$$L_{PTC} = \frac{A_{PTC}}{W_c - D_{env}}$$

By knowing the total mass flow rate which is calculated from the boiler heat exchanger load, and by assigning the hydraulic mass flow rate as an input, the total number of loops, loop area, loop width, and number of solar PTC's are then calculated as follows,

$$N_{loop} = \frac{M_{col}}{M_{hyd}}$$

$$A_{loop} = \frac{A_{PTC}}{N_{loop}}$$

$$W_{loop} = \frac{A_{loop}}{L_m}$$

where L_m is assigned as module length, m

$$N_{PTC's} = \frac{A_{PTC}}{L_m(W_c - D_{env})}$$

Total pressure losses are calculated based on major and minor losses along the field length. The general loss equation is performed as following [25,26],

$$P_{tloss} = N_{loop} \times \Delta P_{loop}$$

Where,

$$\Delta P_{loop} = \frac{32 \times f \times L_{loop} \times M_{hyd}^2}{\rho \times \pi^2 \times D_t}$$

D_t is the inner tube diameter, m

$$f = [(1.82 \times \log Re) - 1.64]^{-2}$$

$$Re = 4 \times \frac{M_{hyd}}{\mu \times \pi \times D_t}$$

Flashing tank:
Flash Cyclone tank design data are calculated as the following:
Tube Inlet and outlet tank steam area based on steam velocity V_{st}, m/s and vapor density, kg/m^3:

$$A_{t_i} = \frac{M_{st}}{\rho_v \times V_{st}}$$

Tube diameter, m:

$$D_t = \left(\frac{A_{t_i} \times 4}{\pi} \right)^{0.5}$$

Flash tank height, m [24]:

$$H_{fst} = 7.15 \times D_t$$

Flash tank width m:

$$W_{fst} = 3.5 \times D_t$$

Flash tank total volume, m3:

$$Vol_{fst} = \left(\frac{pi}{4} \right) \times W_{fst}^2 \times H_{fst}$$

Flashing enthalpy is equal to the well enthalpy coming from the solar collector, kJ/kg:

$$h_{fsh} = h_{col}$$

The flashing dryness fraction is calculated based on flashing enthalpy, liquid enthalpy, h_f, kJ/kg and dry vapor enthalpy, h_g, kJ/kg:

$$X_{fsh} = \frac{h_{fsh} - h_f}{h_g - h_f}$$

Total mass flow rate, kg/s:

$$M_{total} = \frac{M_{st}}{X_{fsh}}$$

Unvaporized water, kg/s:

$$M_w = \left(1 - X_{fsh} \right) \times M_{total}$$

Pump unit [26]:
Pump work kW:

$$W_p = M_{total} \times \frac{\Delta P}{\rho} \times \eta_p$$

Total pressure difference bar:

$$\Delta P = P_{high} + P_{loss}$$

Outlet pump enthalpy, kJ/kg:

$$h_{po} = \left(\frac{W_p}{M_{total}} \right) + h_{pi}$$

Absorption Air Conditioning (AAC) unit [27]:

1. **The absorber unit [27]:**

Solution concentration outlet to the heat exchanger, kg LiBr/kg solution, where, T_a is the absorber temperature, °C, and T_e is the evaporator temperature, °C:

$$X_{a\_hex} = \frac{49.04 + 1.125 \times T_a - T_e}{134.65 + 0.47 \times T_a}$$

Strong solution mass flow rate, kg/s is then calculated based on refrigerant mass flow rate, M_r, kg/s and the concentration stream comes from the generator unit $X_{g\,hex}$:

$$M_{str} = M_r \times \left(\frac{X_{g\_hex}}{X_{g\_hex} - X_{a\_hex}} \right)$$

Weak solution mass flow rate, kg/s is then calculated based on refrigerant mass flow rate, M_r, kg/s and the concentration stream comes from the generator unit $X_{g\,hex}$:

$$M_{wk} = M_r \times \left(\frac{X_{a\_hex}}{X_{g\_hex} - X_{a\_hex}} \right)$$

The enthalpy of LiBr/water solution of concentration X kg/LiBr kg solution at temperature T, °C outlet to the heat exchanger unit [29]:

$$H_{a\_hex} = f\left(X_{a_{hex}}, T_a\right)$$

where, can be calculated from the following correlation [24,29],

$$H = \left(42.81 - 425.92 \times X + 404.67 \times X^2\right) + \left(1.01 - 1.23 \times X + 0.48 \times X^2\right) \times T \times 4.186798$$

Absorber thermal power, kW:

$$Q_a = \left(M_{wk} \times H_{a\_hex}\right) + \left(M_r \times H_{e\_hex}\right) - \left(M_{str} \times H_{a\_hex}\right)$$

Outlet cooling water temperature from the absorber unit goes to the condenser unit based on absorber effectiveness, ^oC is then calculated based on inlet cooling water temperature, T_{acwo} and absorber temperature:

$$T_{a_{cwo}} = \left(\eta_{abs} \times \left(T_a - T_{a_{cwi}}\right)\right) + T_{a_{cwi}}$$

Cooling tower mass flow rate, kg/s is calculated based on the energy balance through the absorber tube [27]:

$$M_{cw} = \frac{Q_a}{H_{a_{cwo}} - H_{a_{cwi}}}$$

Where,

$$H = 421.2 \times exp(0.004008 \times T) - 435.9 \times exp(-0.007559 \times T)$$

Overall heat loss, kW/m^{2o}C [24]:

$$U_a = 1.9394 + 1.40562e - 3 \times T_a - 2.0752e - 4 \times T_a^2 + 2.3186e - 6 \times T_a^3$$

Log Mean Temp to find the absorber area, m^2:

$$LMT_a = \frac{T_a - T_{a_m}}{log\left(\frac{T_a - T_{a_{cwi}}}{T_a - T_{a_{cwo}}}\right)}$$

Where, T_{am} is the absorber mean temperature, ^oC

Absorber area, m^2:

$$A_a = \frac{Q_a}{U_a \times LMT_a} \ldots\ldots (41)$$

2. **Heat exchanger unit** [27]:

Outlet heat exchanger temperature to the absorber unit, ^oC:

$$T_{hex\_a} = T_g - \left(\eta_{hex} \times \left(T_g - T_a\right)\right)$$

Outlet heat exchanger temperature stream goes to the generator unit, ^oC:

$$T_{hex\_g} = T_a + \left(\eta_{hex} \times \left(\frac{X_{a\_hex}}{X_{g\_hex}}\right) \times \left(\frac{f_{cpLB}\left(X_{g\_hex}\right)}{f_{cpLB}\left(X_{a\_hex}\right)}\right) \times \left(T_g - T_a\right)\right)$$

Where, the specific heat capacity of lithium bromide/water solution of concentration X kg LiBr/kg solution is given by Ref. [29]:

$$f_{cpLB} = \left(1.01 - 1.23 \times X + 0.48 \times X^2\right) \times 4.186798$$

The enthalpy of LiBr/water solution of concentration X kg/LiBr kg solution at temperature T, ^oC outlet to the Absorber unit:

$$H_{hex\_a} = f\left(X_{g_{hex}}, T_{hex\_a}\right)$$

where, can be calculated from the following correlation [24,29], where

$$H = \left(42.81 - 425.92 \times X + 404.67 \times X^2\right) + \left(1.01 - 1.23 \times X + 0.48 \times X^2\right) \times T \times 4.186798$$

3. **Generator unit** [27]:

Solution concentration outlet to the heat exchanger, kg LiBr/kg solution:

$$X_{g_{hex}} = \frac{49.04 + 1.125 \times T_g - T_c}{134.65 + 0.47 \times T_g}$$

Where, T_c is the condenser temperature, °C

Outlet enthalpy from the generator to the condenser unit, kJ/kg:

$$H_{g\_cond} = f\left(T_g, T_c\right)$$

where

$$H = (572.8 + 0.46 \times T - 0.043 \times T_s) \times 4.186798$$

Generator thermal power, kW:

$$Q_g = \left(M_{wk} \times H_{hex_a}\right) + \left(M_r \times H_{g_{cond}}\right) - \left(M_{str} \times H_{a_{hex}}\right)$$

Inlet driving steam mass flow rate to the generator, kg/s:

$$Ms_{aac} = \frac{Qg}{\eta_g \times fl_s\left(T_g\right)}$$

where l_s is the latent heat, kJ/kg,

$$l_s = -1.714e - 009 \times T^5 + 1.324e - 006 \times T^4 - 0.0003829 \times T^3 + 0.044 \times T^2 - 4.279 \times T + 2519$$

The overall heat transfer coefficients in the evaporator is calculated as following [22,24,29]:

$$U_g = 1.9695 + \left(1.2057 \times 10^{-2} \times T_g\right) - \left(8.5989 \times 10^{-5} \times T_g^2\right) + \left(2.5651 \times 10^{-7} \times T_g^3\right)$$

Generator heat transfer area, m²:

$$A_g = Ms_{aac} \times \frac{fl_s\left(T_g\right)}{U_g \times T_g}$$

4. Condenser unit:

The enthalpy stream outlet from the condenser to the evaporator, kJ/kg of pure water liquid at temperature, °C:

$$H_{c\_evp} = (T_c - 25) \times 4.186798$$

Condenser thermal power, kW:

$$Q_c = M_r \times \left(H_{g_{cond}} - H_{c_{evp}}\right)$$

Inlet cooling water enthalpy, kJ/kg:

$$H_{c_{cwi}} = 421.2 \times exp(0.004008 \times T_{c_{cwi}}) - 435.9 \times exp(-0.007559 \times T_{c_{cwi}})$$

Outlet cooling water enthalpy, kJ/kg:

$$H_{c_{cwo}} = \left(\frac{Q_c}{M_{cw}}\right) + H_{c_{cwi}}$$

5. Evaporator unit:

The enthalpy, kJ/kg of saturated water vapor at temp, °C from the evaporator to absorber unit:

$$H_{e\_abs} = (572.8 + (0.417 \times T_e)) \times 4.186798$$

Thermal load on evaporator unit, kW [29]:

$$Q_e = Load_{TR} \times 3.517$$

Refrigerant mass flow rate, kg/s:

$$M_r = \frac{Q_e}{H_{e_{abs}} - H_{c_{evp}}}$$

6. Fan unit [24]:

Cooling air mass flow rate, kg/s is calculated based on thermal power (Q_e, kW), the specific heat capacity of the air, C_p, kJ/kg°C and the temperature difference between input and outlet cases, °C:

$$M_{air} = \frac{Load \times 3.517}{C_p(T_{a_m}) \times (T_{a_i} - T_{a_o})} \quad \text{..... (58)}$$

Airflow velocity, m/s based on air duct diameter, D_{ta}, m mass flow rate, and air density:

$$V_{air} = \frac{M_{air}}{\rho_a(T_{a_m}) \times \left(\left(\frac{\pi}{4}\right) \times (D_{ta}^2)\right)}$$

A pressure drop across the air-cooled condenser, kPa based on air density, air velocity, and mean air temperature, Ta_m, °C:

$$\Delta P = \frac{\sqrt{\left(\frac{V_{air} \times \rho_a(T_{a_m})}{0.85}\right)}}{2 \times 9.81 \times \rho_a(T_{a_m})} \quad \text{..... (60)}$$

Fan Power, kW:

$$FHP = \frac{\left(\left(\frac{\pi}{4}\right) \times D_{ta}^2\right) \times V_{air} \times \Delta P}{\eta_{fan}}$$

Exergy, Cost & Performance [28–30]:

For any system goes under steady-state, the mass, energy, and entropy balances equations under steady-state condition should be developed as follows;

$$\sum \dot{m}_{in} - \sum \dot{m}_{out} = 0, \, kg/s$$

$$\sum \dot{e}_{in} - \sum \dot{e}_{out} = 0, \, kJ/kg$$

$$\sum \dot{s}_{in} - \sum \dot{s}_{out} = 0, \, kJ/kgoC$$

The general form of the availability is defined by the following equation;

$$A_2 - A_1 = A_q + A_w + A_{fi} - A_{fo} - I$$

Where

$A_2 \text{-} A_1 = 0$

is the non-flow availability change in a steady-state condition,

$$A_q = \sum_J (1 - T_{amb}/T_J)Q_J$$

is the availability transfer due to the heat transfer between the control volume and its surroundings,

$$A_w = -W_{cv} + P_o(V_2 - V_1)$$

is equal to the negative value of the work produced by the control volume but in most cases, the control volume has a constant volume, therefore Aw can be further simplified. And

$I = T_{amb} \times S_{gen}$

is the availability of destruction in the process. The flow availability expressed as;

$$A_{fi,o} = \sum_{i,o} \dot{m}_{i,o} a_{fi,o}.$$

So the general form in steady-state condition would become;

$$0 = A_q + A_w + A_{fi} - A_{fo} - I$$

In conventional economic analysis, a cost balance is usually formulated for the overall system operating at steady state as following;

$$\sum_{out} \dot{C} = \sum_{in} \dot{C} + Z^{IC\&OM}$$

Where $\dot{C}$ the cost rate according to inlet and outlet streams, and $Z^{IC\&OM}$ is the capital investment and operating & maintenance costs. In exergy costing a cost is associated with each exergy stream. Thus, for inlet and outlet streams of matter with associated rates of exergy transfer $E_{i,o}$, power W, and the exergy transfer rate associated with heat transfer Eq it can write as following;

$$C_{i,o} = c_{i,o} \dot{E}_{i,o}$$

$$C_w = c_w \dot{W}$$

$$C_q = c_q \dot{E}_q$$

Where $c_{i,o}, w, q$ denote average costs per unit of exergy in $/kJ for inlet (*i*), outlet (*o*), power (*w*), and energy (*q*) respectively. For hourly costs estimation, the following correlations are considered:

For cost analysis, the amortization factor should be calculated first as presented here, Amortization factor, *1/y*

$$A_f = \frac{i.(1+i)^{LTp}}{(1+i)^{LTp} - 1}$$

Collector investment cost is calculated based on the following area correlation, $,

$$IC_{col} = 150 \times A_{col}^{0.95}$$

operating and maintenance cost is then calculated, $,

$$OMC_{col} = 0.15 \times IC_{col}$$

The total annual cost, *$/y* is then calculated based on operating & maintenance cost and investment cost parameters as following,

$$TAC_{col} = (IC_{col} + OMC_{col}) \times A_f$$

hourly costs are calculated, *$/h*,

$$Z_{col} = \frac{TAC_{col}}{OH \times 365}$$

Flashing tank cost is calculated based on the following total tank volume correlation, $;

$$IC_{fsh} = \frac{Vol_{fst} \times 6.3e3}{3.8}$$

The total annual cost, *$/y* is then calculated;

$$TAC_{fsh} = IC_{fsh} \times A_f$$

hourly costs are calculated, *$/h*,

$$Z_{fsh} = \frac{TAC_{fsh}}{OH \times 365}$$

Absorption cycle cost is calculated based on the following total area correlation, $,

$$IC_{aac} = 150 \times A_{aac}^{0.8}$$

The total annual cost, *$/y* is then calculated,

$$TAC_{aac} = IC_{aac} \times A_f$$

hourly costs are calculated, *$/h*,

$$Z_{aac} = \frac{TAC_{aac}}{OH \times 365}$$

Pump cost is calculated based on the following pump power correlation, $,

$$IC_p = 3500 \times W_p^{0.47}$$

The total annual cost, *$/y* is then calculated,

$$TAC_p = IC_p \times A_f$$

hourly costs are calculated, *$/h*,

$$Z_p = \frac{TAC_p}{OH \times 365}$$

Cooling tower hourly costs [31] is calculated based on the following wet-bulb temperature correlation, $,

$$Z_{ct} = -0.261 \times T_{wb}^1 + 8.82$$

The total annual cost, *$/y* is then calculated

$$TAC_{ct} = Z_{ct} \times OH \times 365$$

Total hourly costs *$/hr* is then calculated based on all parameters as following,

$$Z_{tot} = Z_{col} + Z_{fsh} + Z_{aac} + Z_p + Z_{ct}.$$

Total Plant Costs is also calculated based on the total annual costs for all unit, *$/y*,

$$TPC = TAC_{col} + TAC_{fsh} + TAC_{aac} + TAC_p + TAC_{ct}$$

The total thermo-economic equation is calculated based on the cost and exergy stream through the proposed cycles, *$/GJ*,

$$c_p = 1000 \times \left(\frac{(W_{tot} \times c_w) + \left(\frac{Z_{tot}}{3600} \right)}{Ex_{fo}} \right)$$

Where, c_p is the thermo-economic product cost, *$/GJ*, c_w is the power cost in \$/kWh ($\sim$0.065), and W_{tot} is the total cycle power, kW, Ex_{fo} is the exergy stream outlet from the system to the user, kW. For performance calculations, the C.O.P is calculated based on evaporator and generator thermal powers,

$$COP = \frac{Q_e}{Q_g}$$

where the Max COP is found as,

$$COP_{max} = \frac{(T_e + 273.15) \times (T_g - T_a)}{(T_g + 273.15) \times (T_c - T_e)}$$

and the relative performance ratio could be then estimated as,

$$RPR = \frac{COP}{COP_{max}}$$

References

[1] D. Moreno, V. Ferro, J. de Riva, R. Santiago, C.M.-A. Energy, Absorption Refrigeration Cycles Based on Ionic Liquids: Refrigerant/absorbent Selection by Thermodynamic and Process Analysis, Elsevier, 2018.
[2] M. Moran, H. Shapiro, Fundamentos de termodinámica técnica, 2004.
[3] Bittanti, S.; de Marco, A.; Giannatempo, M.; Prandoni, V. European Association for the Development of Renewable Energies, Environment and Power Quality (EA4EPQ) A Dynamic Model of an Absorption Chiller for Air Conditioning;.
[4] A. Mallah, M. Zubir, O. Alawi, K.N.-S.E.M, Plasmonic Nanofluids for High Photothermal Conversion Efficiency in Direct Absorption Solar Collectors: Fundamentals and Applications, Elsevier, 2019.
[5] N. Molero-Villar, J.C.-L.-S. energy, A Comparison of Solar Absorption System Configurations, Elsevier, 2012.
[6] S. Said, M. El-Shaarawi, Alternative Designs for a 24-h Operating Solar-Powered Absorption Refrigeration Technology, of, M.S.-I. journal, Elsevier, 2012.
[7] A. Aliane, S. Abboudi, C. Seladji, B.G.-R. Sustainable, An Illustrated Review on Solar Absorption Cooling Experimental Studies, Elsevier, 2016.
[8] Abdelhay, A.O.; Fath, H.E.S.; Nada, S.A.; Sharaf, M.A. Thermodynamic Analysis of a Poly-Generation System for Electrical Power, Cooling and Desalinated Water;.
[9] R. Leiva-Illanes, R. Escobar, J.C.-E. conversion, Comparison of the Levelized Cost and Thermoeconomic Methodologies–Cost Allocation in a Solar Polygeneration Plant to Produce Power, Desalted Water, Cooling and, Elsevier, 2018.
[10] C. Tzivanidis, E. Bellos, The use of parabolic trough collectors for solar cooling—a case study for Athens climate, Case Stud. Therm. Eng. 8 (2016) 403–413.
[11] K. Wang, Y. He, A. Kan, W. Yu, D. Wang, L. Zhang, G.Z.-A. Energy, Significant Photothermal Conversion Enhancement of Nanofluids Induced by Rayleigh-Bénard Convection for Direct Absorption Solar Collectors, Elsevier, 2019.
[12] O. Marc, F. Sinama, J.P. Praene, F. Lucas, J.-P. Praene, J. Castaing-Lasvignottes, Dynamic Modeling and Experimental Validation Elements of a 30 kW LiBr/H2O Single Effect Absorption Chiller for Solar Application Dynamic Modeling and Experimental Validation Elements of a 30 kW LiBr/H 2 O Single Effect Absorption Chiller for Solar Application, Elsevier, 2015.
[13] A. Al-Falahi, F. Alobaid, B. Epple, A new design of an integrated solar absorption cooling system driven by an evacuated tube collector: a case study for Baghdad, Iraq, Appl. Sci. 10 (2020) 3622.
[14] O. Rejeb, C. Ghenai, M. Bettayeb, Modeling and simulation analysis of solar absorption chiller driven by nanofluid-based parabolic trough collectors (PTC) under hot climatic conditions, Case Studies in Thermal Engineering (2020) 100624.
[15] M. Behi, S. Mirmohammadi, M. Ghanbarpour, H.B. Energy, Evaluation of a Novel Solar Driven Sorption Cooling/heating System Integrated with PCM Storage Compartment, Elsevier, 2018.
[16] S. Salehi, M. Yari, M.R.-A.T. Engineering, Exergoeconomic Comparison of Solar-Assisted Absorption Heat Pumps, Solar Heaters and Gas Boiler Systems for District Heating in Sarein Town, Iran, Elsevier, 2019.
[17] Marc, O.; Lucas, F.; Sinama, F.; Monceyron, E. Experimental Investigation of a Solar Cooling Absorption System Operating without Any Backup System under Tropical Climate. Elsevier.
[18] X. Zhai, Y. Li, X. Cheng, R. Wang, Experimental Investigation on a Solar-Powered Absorption Radiant Cooling System, 2015 cyberleninka.org.

[19] K. Gommed, Investigation of an Improved Solar-Powered Open Absorption System for Cooling, Dehumidification and Air Conditioning, refrigeration, G.G.-I. journal of, Elsevier, 2012.

[20] D. Zambrano, C. Bordons, W. Garcia-Gabin, E.F. Camacho, Model Development and Validation of a Solar Cooling Plant, Elsevier, 2007.

[21] J. Lopez-Villada, A. Montero-Izquierdo, L. Carlos Mendoza Toledo Bitzer, J. López-Villada, I. Andrés Montero, L. Carlos Mendoza, D.S. Ayou, J. Carles Bruno, A. Coronas, Modeling, Simulation and Analysis of Solar Absorption Power-Cooling Systems, 2012.

[22] https://webbook.nist.gov/chemistry/name-ser/.

[23] Author, C.; Ha, Q.; Author, F.; Vakiloroaya Order of Authors, V.; Vakiloroaya, V.; Skibniewski, M.; Skibniewski, M.; Clark, A. Elsevier Editorial System(tm) for Energy and Buildings Manuscript Draft Title: Modeling and Experimental Validation of a Solar-Assisted Direct Expansion Air Conditioning System Modeling and Experimental Validation of a Solar-Assisted Direct Expansion Air Conditioning System;.

[24] J. Carles Bruno, J. Ló pez-Villada, E. Letelier, S. Romera, A. Coronas, Modelling and Optimisation of Solar Organic Rankine Cycle Engines for Reverse Osmosis Desalination, Elsevier, 2008.

[25] A.S. Nafey, M.A. Sharaf, L. García-Rodríguez, A New Visual Library for Design and Simulation of Solar Desalination Systems (SDS), Elsevier, 2010.

[26] M.A. Sharaf Eldean, A.M. Soliman, A new visual library for modeling and simulation of renewable energy desalination systems (REDS), Desalination and Water Treatment 51 (2013) 6905–6920.

[27] J. Staff, Title and Subtitle THE DEEP SPACE NETWORK PROGRESS REPORT JANUARY AND FEBRUARY, 1976.

[28] M. Sharaf, Design and Simulation of Solar Desalination Systems, 2011.

[29] M.A. Sharaf, A.S. Nafey, L. García-Rodríguez, Author's Personal Copy Thermo-Economic Analysis of Solar Thermal Power Cycles Assisted MED-VC (Multi Effect Distillation-Vapor Compression) Desalination Processes, Elsevier, 2011.

[30] M. Sharaf, A. Nafey, L.G.-R.- Desalination, Exergy and Thermo-Economic Analyses of a Combined Solar Organic Cycle with Multi Effect Distillation (MED) Desalination Process, Elsevier, 2011.

[31] M.M. Castro, T.W. Song, J.M. Pinto, Minimization of operational costs IN cooling water systems, IChemE 78 (2000).

Paper C

Thermo-Economic Evaluation of Aqua-Ammonia Solar Absorption Air Conditioning System Integrated with Various Collector Types

Adil Al-Falahi * , Falah Alobaid and Bernd Epple

Institut Energiesysteme und Energietechnik, Technische Universität Darmstadt, Otto-Berndt-Straße 2,
64287 Darmstadt, Germany; falah.alobaid@est.tu-darmstadt.de (F.A.); bernd.epple@est.tu-darmstadt.de (B.E.)
* Correspondence: adil.al-falahi@est.tu-darmstadt.de; Tel.: +49-6151/16-20724; Fax: +49-(0)-6151/16-22690

Abstract: The main objective of this paper is to simulate solar absorption cooling systems that use ammonia mixture as a working fluid to produce cooling. In this study, we have considered different configurations based on the ammonia–water (NH_3–H_2O) cooling cycle depending on the solar thermal technology: Evacuated tube collectors (ETC) and parabolic trough (PTC) solar collectors. To compare the configurations we have performed the energy, exergy, and economic analysis. The effect of heat source temperature on the critical parameters such as coefficient of performance (COP) and exegetic efficiency has been investigated for each configuration. Furthermore, the required optimum area and associated cost for each collector type have been determined. The methodology is applied in a specific case study for a sports arena with a 700~800 kW total cooling load. Results reveal that (PTC/NH_3-H_2O)configuration gives lower design aspects and minimum rates of hourly costs (USD 11.3/h) while (ETC/NH_3-H_2O) configuration (USD 12.16/h). (ETC/NH_3-H_2O) gives lower thermo-economic product cost (USD 0.14/GJ). The cycle coefficient of performance (COP) (of 0.5).

Keywords: solar cooling; absorption cycles; solar thermal collector; parabolic trough collectors; solar energy; ammonia

1. Introduction

In recent years, the predominant technology in cooling systems worldwide is the conventional vapor compression cycle, which is known for its significant consumption of electricity due to the existence of a compressor and extremely high peak loads on the hottest summer days [1,2]. Solar energy is an attractive solution for operating air conditioning systems. It saves electricity and thus primary energy sources (natural gas or oil), and decreases the emission of air-polluting gases and greenhouse gases causing global warming. The air conditioning cooling loads and the available solar power match well with each other along the day and seasons. Therefore, solar air conditioning also leads to reducing the peak electric power demand, and thus reduces the initial cost used due to the expensive peak electricity [3]. According to the Internal Energy Agency (IEA), global energy demand will increase by 35% between 2010 and 2035 [4]. This increase is associated with world population and economic growth, especially in developing countries [5]. Heat-driven refrigeration cycles are a promising solution in this context. Absorption cycles are heat-driven cycles that can use solar energy directly without the need to transform it into electric energy. The other benefit of using the heat-driven cycle is the fact that the highest cooling demand is associated with the high solar energy in summer and that offers a good chance for the heat-driven cycle to match the cooling demand efficiently.

The temperature of the thermal energy source can affect the selection of the cooling technology as well as the performance of the cycle. The driving temperature depends on the solar energy capturing

technology that can be adopted and efficiently available. Most of the cooling technologies are working in the range of 80–100 °C, which can be easily achieved using different low-cost solar energy collectors. Two kinds of absorption cycles are commercially available; depending on the refrigerant–absorbent pair; these two cycles are water–lithium bromide (H_2O–LiBr) and ammonia–water (NH_3–H_2O) mixtures.

Kurem and Horuz [6] carried out a comprehensive study to investigate and analyze the absorption heat pump and using water–lithium bromide (H_2O–LiBr) and ammonia–water (NH_3–H_2O) mixtures. The authors highlighted and pinpointed the advantages and disadvantages of both solutions. They concluded that the absorption heat transformer systems using water–lithium bromide solution produce better COP than that of using an ammonia–water solution.

Said et al. [7] presented an experimental investigation of a solar thermal powered ammonia–water absorption refrigeration system. The focus of this study lies in the design of the components of the absorption chiller, the ice storages, and the solar collector field as well as the integration of the data acquisition and control unit. The results of the experiments indicated a chiller coefficient of performance (COP) of 0.69 and a cooling capacity of 10.1 kW at 114/23/−2 (°C) representing the temperatures of the generator inlet, the condenser/absorber inlet, and the evaporator outlet respectively.

One of the advantages of absorption air-conditioning (ACC) cycles is the possibility of using several heat sources as input to the generator. Calise et al. [8] presented design of a novel solar-assisted combined cycle power plant. The system includes a solar loop equipped with a double-stage absorption chiller driven by high-temperature high-vacuum non-concentrating flat-plate solar thermal collectors. The simulation also includes a detailed thermo-economic model that accurately evaluates system capital and operating costs as a function of design and operating parameters. The simulation results show that a very high thermal efficiency of solar collectors—on average equal to 34%—is achieved. Results from the economic point of view were also satisfactory. Neyer et al. [9] analyzed the influence of different heat rejection units to a solar- or combined heat and power systems(CHP)-driven single-/half-effect ammonia/water absorption chiller. The simulation results are used to analyze the annual impact on the technical and economic performance of the new single-/half-effect concept in various configurations and boundary conditions. They concluded that application for solar- and CHP-driven systems are reaching non-renewable primary energy savings of 30–70% at almost equal costs compared to conventional systems.

Different types of solar thermal energy collectors can be used with single-effect absorption cycles. Aman et al. [10] developed a thermodynamic based on a 10 kW air-cooled ammonia–water absorption chiller driven by flat plate collector (FPC) for domestic application. Both energy and exergy analyses have been conducted to enhance the thermal performance of the cooling system. The analyses uncovered that the absorber is where the most exergy loss occurs (63%) followed by the generator (13%) and the condenser (11%). Bellos et al. [11] tested four solar collectors (evacuated tube collectors ETC, flat plate collectors FPC, parabolic through collectors PTC, and compound parabolic collectors CPC) in an absorption cooling system. A financial comparison between the four optimized systems proves that evacuated tube collectors are the most beneficial technology. On the other hand, a system with parabolic trough collectors is the exergetic optimum one, but its high capital cost renders it an unprofitable solution. Fong et al. [12], investigated a comparative study of different types of solar cooling systems for buildings in a subtropical city, which is commonly featured with long hot, and humid summer. The results show that solar electric compression refrigeration and solar absorption refrigeration had the highest energy saving and it will provide a promising application potential of solar cooling for buildings in the subtropical region.

In a recent study, Al-Falahi Adil [13] investigated the energy performance of a solar absorption air-conditioning system integrated with ETC, in the climate of Baghdad, Iraq. It was concluded that the seasonal collector efficiency and solar fractions are 54% and 58% respectively and absorption chiller COP was 0.44. Another study was presented by Galindo et al. [14], where they report experimental results of an absorption cooling system with a nominal capacity of 5 kW based on a parabolic trough collector, which operates with the ammonia-lithium nitrate mixture. The results of the parametric

analysis revealed that the PTC field can provide up to 6.5 kW of useful heat to the absorption cooling system at temperatures up to 105 °C with thermal efficiencies up to 19.8% and exergy efficiency up to 14.93. The maximum value of the solar coefficient of performance reached 0.07. Cabrera et al. [15] presented a survey of the existing experiences and realizations on applications of PTC in solar cooling systems. as well as evaluated the use of the new collectors as an occasional alternative to other solar thermal collectors in air conditioning applications by dynamical simulation. The results for the case studies developed in this work show that PTC presents similar levelized costs of energy for cooling than flat plate collectors (FPC) and lower than evacuated tube collectors (ETC) and compound parabolic collectors (CPC).

Jakob et al. [16], presented a design of an air conditioning by diffusion absorption using the mixture NH_3-H_2O, with a cooling capacity of 2.5 kW. The unit was built and tested, achieving a maximum COP of 0.38. The collector used was an indirectly coupled flat plate collector (FPC).

Parabolic trough collectors are frequently employed for a solar steam generation because relatively high temperatures can be obtained without serious degradation in the collector efficiency. Qu et al. [17] developed a model of solar absorption cooling and heating system driven by PTC using transient system simulation software. The system incorporates 52 m^2 of parabolic trough solar collectors; a 16 kW absorption chiller capacity. The performances of the system have been analyzed and validated with experimental data under various solar radiations and wind velocity. They concluded that the absorption air conditioning (AAC) cycle may potentially provide 20% of the heating and 39% of the cooling demands of the building. Tzivanidis and Bellos [18] developed a numerical model is in order to simulate the dynamic performance of a solar cooling system. Many parameters have been investigated through sensitivity analyses and their optimum values are determined. The results proved that by using a PTC module with an aperture area of 14 m^2, a building area of about 25 m^2 can be cooled for 13 h daily during the summer period. The optimum specific mass flow rate was determined to 0.03 kg/s m^2 and the optimum storage tank volume to 0.3 m^3. Moreover, they presented a case study for a typical building of 100 m^2 with very satisfying results, where four PTC modules are used in parallel connection.

Molero-Villar et al. [19] developed a complete solar thermal cooling system using TRNSYS model to compare a configuration with just hot storage (of typical capacity 40 L/m^2 of solar collector surface) and a configuration with both, hot and cool storages. In their study, they analyzed the effect of other variables on the optimal configuration: collector efficiency curve, COP of the absorption chiller, storage size, and temperature set-points of the chillers. They concluded that the most suitable configuration is very sensible to the solar collector area. As the collector area increases, the advantages of cool storage vanish. Increasing the collector area tends to increase the temperature of the hot storage, leading to higher thermal losses in both the collector and the tank. When the storage volume is concentrated in one tank, these effects are mitigated.

Said [20] demonstrated and developed an alternate design for a 24 h operating solar-powered absorption refrigeration technology. The development includes an in-depth review of the design and operation of the conventional and solar-assisted absorption refrigeration systems coming-up with new alternative designs, detailed thermodynamic analysis of some of the new alternative designs, and selection of the most suitable alternative design. The analysis indicates that continuously operating a solar-powered ammonia–water absorption system with refrigerant storage is the most suitable alternative design for an uninterrupted supply of cooling effect.

Abdelhay et al. [21] carried out a parametric study to investigate the effects of the different design and operating parameters on the polygeneration plant energetic and exergetic parameters. Results reveal that the highest exergy loss was found to occur in PTC solar field with about 82.42% of the plant exergy destruction and for the cooling part to balance between the COP of the absorption refrigeration system and PTC area, the generator temperature should be 85–90 °C. Moreover, an economic evaluation of the proposed integrated system showed the unit cooling price (0.003 \$/kW h) and the highest exergetic efficiency is (23.95%). The absorption chiller capacity was

3.6TR (Ton of Refrigeration). In the same regard, Leiva et al. [22] performed a comparison between the levelized cost and thermo-economic methodologies of a solar polygeneration plant. They concluded that through the study they found differences between the two methods and this represent an increase of about 35.1% in the case of the electricity, and a reduction in the cost associated to the water, cooling, and heat production by around 34.4%, 78.1%, and 97.6%, respectively.

Related to thermo-economics, Al-Falahi [23] presented the design and thermo-economic evaluation of absorption air conditioning (AAC) to compare two various collectors (PTC, ETC). The results reveal that parabolic trough collectors combined with H_2O–LiBr (PTC/H_2O–LiBr)gives lower design aspects and minimum rates of hourly costs (USD 5.2/h), while ETC/H_2O–LiBr configuration give USD 5.6/h. The H_2O–LiBr thermo-economic product cost is USD 0.14/GJ. The cycle coefficient of performance COP was in the range of 0.5 to 0.9. Salehi [24] studied the feasibility of solar assisted absorption heat pumps for space heating; in this study, single-effect LiBr/H_2O and NH_3/H_2O absorption and absorption compression-assisted heat pumps are analyzed for heating loads of 50–2 MW(MegaWatt). Utilizing geothermal hot springs as heat sources for refrigerant evaporation. the results show that the maximum achievable exergy efficiency for the NH_3-H_2O and LiBr-H_2O absorption systems is 0.23 and 0.25, respectively. while, the solar heating system has the highest product unit cost, mainly due to its high capital costs. The minimum obtainable product unit costs for the $NH3$/H_2O and LiBr/H_2O absorption systems are about 22 \$/GJ and 55 \$/GJ, respectively.

Marc [25] studied an experimental solar absorption cooling. The solar field consists of 36 double-glazed flat-plate solar collectors of a total aperture area of 90 m^2 coupled to a single-effect absorption chiller with cooling capacity at 30 kW at 90/30/11 (°C) representing the temperatures of the generator, the condenser, and the evaporator respectively. The maximum electrical coefficient of performance was 1.65. Zhai [26] used the evacuated tube solar field for 8 kW cooling capacity. The system consumed and amount of 92 m^2 of solar area. Lopez et al. [27] performed energy and exergy analysis to compare several system cooling cycles configurations and different solar thermal technologies: evacuated tube, parabolic trough, and linear Fresnel solar collectors. The results show that NH_3-H_2O/(ETC or PTC) combinations offer the best efficiencies. In their work ammonia-based working fluid mixture is considered.

It is clear from the literature that solar energy has a great influence on refrigeration and/or air conditioning processes. Different types and configurations of solar collectors have been applied for such purposes. The most commonly used was the evacuated tube and parabolic through collectors especially for large capacities. Moreover, it has been noticed that H_2O-LiBr and NH_3-H_2O have been used for most of the research activities in this regard for air conditioning applications. The novelty of this work emerged from the connection type between the solar field and the absorption chiller. A flash evaporation tank has been used as an intermediate unit between both parts to generate steam; known as direct or in situ concept system, in which two-phase flow is allowed in the collector receiver so that steam is generated directly. The sub-cooled water is heated to boiling and steam forms directly in the receiver tube. The system use water, a superior heat transport fluid. The flash system uses a sensible heat change in the working fluid, which makes the temperature differential across the collector relatively high. The rapid increase in water vapor pressure with temperature requires a corresponding increase in system operating pressure to prevent boiling. The main objective of this work is to optimize and design NH_3-H_2O absorption air conditioning systems that are operated by different types of solar collectors (ETC and PTC), based on energy, exergy, design, and cost. Selecting the best operating condition is also been the focus. The following general outlines are proposed for this work:

✓　NH_3-H_2O absorption cycles have been studied under different operating conditions. The selection was made based on the best-operating conditions.

✓　Two different types of solar collectors (ETC and PTC) have been compared while combining them with absorption cycles.

✓　A detailed mathematical model has been performed.

✓ The comparison is performed based on the terms of energy, exergy, design, cost, and thermo-economic. The design technique of modeling has been adopted in this study.

✓ Based on the optimized selection, a case study for 700–800 kW (200–230 TR) cooling load has been performed.

2. Thermal Solar Cooling System Description

The working principle of the ammonia–water absorption refrigeration system is based on the simple vapor absorption refrigeration system. In this system ammonia is used as the refrigerant and water is used as the absorbent. The ammonia–water absorption system is used in the domestic as well the commercial applications where the requirement of the temperature is above 0 °C. The major advantage of the ammonia–water solution is that water has a strong affinity for ammonia and they are soluble with each other in wide operating conditions that occur in different refrigeration applications. Further, the ammonia–water solution is highly stable and works well with many materials except copper and its alloys that get corroded in the presence of ammonia. The proposed system, Figure 1a,b, consists of two subsystems, namely: (i) the solar field, and (ii) the absorption cycle. The solar field consists of the following:

➤ Evacuated tube collector (ETC) and/or parabolic trough collector (PTC) for thermal power generation. Water working fluid is the main fluid through the solar part.

➤ A Flash evaporation tank is used to separate steam at lower pressure. This is a vertical flash vessel, with the inlet of high-pressure high-temperature water located at about one-third of the way up to its height. The standard design of flash vessels requires that the diameter of the vessel is chosen so that the steam flows toward the top outlet connection at no more than about 3 m/s. This should ensure that any water droplets could fall through the steam in a contra-flow, to the bottom of the vessel. Adequate height above the inlet is necessary to ensure separation. The separation is also facilitated by having the inlet projecting downward into the vessel. The water connection is sized to minimize the pressure drop from the vessel to the pump inlet to avoid cavitation.

➤ The pumping unit has been used for flow circulation and pressure drop issues.
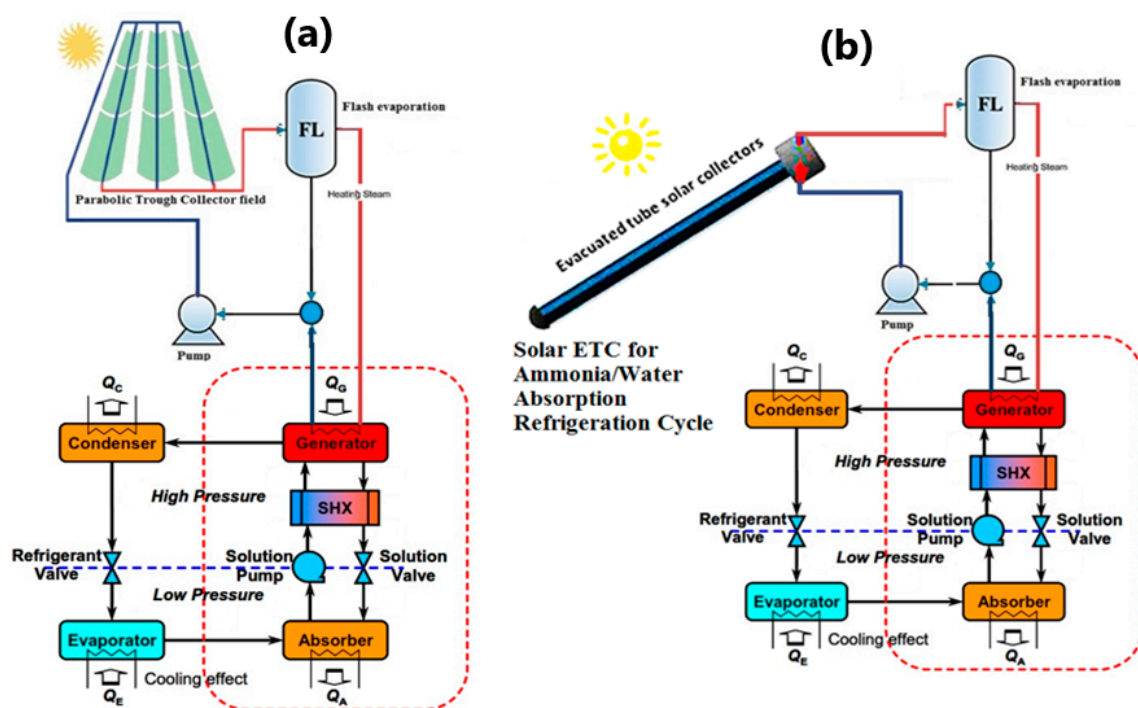

Figure 1. (**a**) Parabolic trough (**b**) evacuated tube solar collectors assisted NH_3-H_2O absorption air conditioning cycle.

The absorption refrigeration cycle (NH_3-H_2O) consists of an absorber, a generator, a condenser, an evaporator, expansion valves, a solution heat exchanger (SHX), and a solution pump as illustrated in Figure 1.

➢　In the evaporator, low-pressure liquid-vapor mixture refrigerant pure ammonia (NH_3), evaporates on the outer surface of the evaporator's tube bundle. Heat is supplied to the evaporator by water flowing inside the evaporator's tubes; this chilled water is subsequently used for refrigeration. The refrigerant vapor leaving the evaporator as saturated vapor enters the absorber at low-temperature and low-pressure conditions.

➢　In the absorber, The refrigerant vapor is then absorbed and dissolved by the weak ammonia–water (NH_3-H_2O) solution coming from the generator. It is worth mentioning that the weak solution is the solution with less amount of refrigerant, i.e., highly concentrated by water. The heat liberated during the absorption process is removed by using cooling water flowing inside the tubes.

➢　The solution pump receives a strong NH_3-H_2O solution and delivers it at high pressure to the generator via the solution heat exchanger. Note that the solution is a saturated liquid and hence the pump work is very small.

➢　In the generator, the high-pressure solution entering the generator is heated and the ammonia in the solution is vaporized. The heat for this process could be provided by solar energy or a gas burner. The remaining weak NH_3-H_2O solution exits via the heat exchanger to the absorber through a pressure-reducing solution valve.

➢　A solution heat exchanger (SHX) is included here; as the solution after the pump requires heating and the hot solution leaves the generator would increase the absorber temperature if it were not cooled before entry.

➢　In the condenser, the high-pressure, high-temperature refrigerant vapor leaving the generator is passed to the condenser where it is cooled by cooling water. The refrigerant saturated vapor is condensed to a liquid. This liquid is then flowed through an expansion refrigerant valve and to the evaporator.

The cycle is considered a closed cycle related to the working flowed through it.

3. Methodology, Assumptions and Mathematical Model

The proposed configurations in this work are required iterative programming in order to calculate the complicated streams (recycle and backward streams). Hence; to develop a specific model for this innovative kind of plan, the Simulink software, a product of a MATLAB work, has been chosen for its high versatility and capacity to handle unsteady situations. Two models were built according to the proposed configurations (ETC/NH_3-H_2O and PTC/NH_3-H_2O) and the design calculation method. The system border streams (outlet temperature, ambient temperature, inlet cooling water temperature, etc.) are assigned by the user than the entire design data (area, length, volume, mass flow rate, etc.) Will then be calculated. Therefore; a user would assign the amount of needed cooling load on the evaporator then all possible data for all the system units would be calculated in sequence. Specifying the system cooling load would calculate the required thermal load. Besides; the required design limits and performance calculations would be pass out instantly. The design operating conditions and assumptions that have been considered in this work are listed in Table 1.

Table 1. Data assumptions for the evacuated tube collector/parabolic trough collector (ETC/PTC)/NH_3-H_2O configuration.

Unit Process	Assigned Data	Calculated Data
		Solar Field:
		➢ Solar field top pressure, bar
		➢ Solar field pressure loss, bar
		➢ Total solar field area, m^2
		➢ Solar field thermal load, kW
		➢ Number of solar collectors, #
		➢ Solar field mass flow rate, kg/s
		➢ Solar field inlet temperature, °C
		➢ Efficiency, %
		➢ Exergy destruction, kW
	✓ Solar radiation: 500 W/m^2	**Flash Tank:**
	✓ Ambient temperature: 25 °C	➢ * Flash tank design data
	✓ Average relative humidity: 15%	➢ Total mass flow rate, kg/s
	✓ ETC top temperature: 100–200 °C	➢ Dryness fraction, %
	✓ PTC top temperature: 200–300 °C	➢ Flash tank water flow rate, kg/s
	✓ Absorber temperature: 30–35 °C	➢ Steam flow rate, kg/s
	✓ Generator temperature: 80–90 °C	➢ Exergy destruction, kW
	✓ Condenser temperature: 40–45 °C	**AAC Unit:**
	✓ Hot air temperature: 35 °C	➢ Weak and strong solutions, kg/s
Absorption	✓ Target cooled air temperature: 20 °C	➢ * Design data
air-conditioning cycle	✓ Evaporator temperature: 5–10 °C	➢ Thermal power, kW
(AAC):	✓ Cooling load: 14–57 kW (50–200 TR)	➢ Total cycle flow rate, kg/s
(ETC/PTC)/NH_3-H_2O	✓ Condenser effectiveness: 80%	➢ Generator power, kW
	✓ Fan system efficiency: 85%	➢ Cooling fan power, kW
	✓ Pumping system efficiency: 75%	➢ COP
	✓ Plant life time: 20 year	➢ COPmax
	✓ Interest rate: 5%	➢ Relative performance
	✓ Load factor: 90%	➢ Exergy destruction, kW
	✓ Specific electric power cost: 0.065 $/kWh	**Pump:**
	✓ Water steam is the solar field working fluid	➢ Power, kW
		➢ Outlet temperature, °C
		➢ Exergy destruction, kW
		Cost and Performance:
		➢ Units hourly costs, $/h
		➢ Total hourly costs, $/h
		➢ Total power, kW
		➢ LPC, $/kWh
		➢ Thermo-economic cost, $/GJ
		➢ Total exergy destruction rate, kW
Notes:	■ Data are run out based on steady-state operating conditions. ■ Ambient temperature is fixed as 25 °C for all process runs. ■ Solar radiation is fixed at 500 W/m^2. ■ * Design data means area, length, width, etc.	

Saturated liquid and vapor phases of pressure, temperature, enthalpy, specific volume, and specific entropy are recorded after the modeled blocks and lookup tables. The source of physical properties is obtained by the chemistry book on the National Institute of Standards and Technology NIST

website [28]. Generally, the optimization process has been done in order to bring down costs and techno-economic solutions.

3.1. Thermodynamic Model

A schematic diagram of the main component of the proposed is shown in Figure 1. The mathematical approaches used in the analysis for solar absorption air conditioning (AAC) plants are performed according to the 1st and 2nd laws of thermodynamics. The following assumptions are considered in the developed mathematical model of the system:

(1) The system runs in a steady-state condition.
(2) Heat losses to the surroundings are neglected.

The thermodynamic model of each component is explained in the following section.

3.1.1. ETC Model

For ETC, the solar collector instantaneous efficiency can be determined from its characteristic curve using solar irradiance, mean collector, and ambient temperatures. The curve used for FPC is expressed by Equation (1) [29,30]:

$$\eta_{etc} = \eta_o - a_1 \left(\frac{T_o - T_{amb}}{I_s} \right) - a_2 \left(\frac{T_o - T_{amb}}{I_s} \right)^2 . I_s \tag{1}$$

where η_{etc} is the ETC efficiency, $\eta_o = 0.665$, $a_1 = 2.9$ W/m². °C, $a_2 = 0.0019$ W/m². °C², I_s is the solar flux over the collector area (W/m²), T_o is the outlet collector top temperature (°C), and ambient temperature T_{amb} in (°C). The useful collector thermal load Q_{th} (kW), may exist according to the following relation;

$$Q_{th} = M_{col}^{\cdot} \times C_p \times (T_o - T_i) \tag{2}$$

where, $M_{col}^{\cdot}$ in kg/s, C_p in kJ/kg °C and the temperature difference is in °C.

The collector total area A_t (m²), is estimated based on the collector energy balance equation as a function of collector efficiencies using;

$$A_t = \frac{Q_{th}}{\eta_{etc} \times I_s} \tag{3}$$

As shown in Equation (3), if the value of the heat exiting the collector is fixed, the necessary collector area is inversely proportional to solar radiation. This is why the value of solar radiation is fundamental for the development of projects involving solar energy. The ETC module aperture area A_{etc}, m² can be calculated as;

$$A_{etc} = D_t \times L_t \times NOT \tag{4}$$

where, D_t is the tube diameter (m), L_t is the tube length (m), and *NOT* is the number of tubes per one module. The total number of evacuated tube collectors *NOC* can be calculated from the following equation.

$$NOC = \frac{A_t}{A_{etc}} \tag{5}$$

The number of loops *NOL*, loop area A_{loop}, and the loop length, L_{loop} can be calculated by assigning the hydraulic mass flow rate $M_{hyd}^{\cdot}$, kg/s. $M_{col}^{\cdot}$ will be calculated based on the load between the flash tank and the AAC unit:

$$NOL = \frac{M_{col}^{\cdot}}{M_{hyd}^{\cdot}} \tag{6}$$

$$A_{loop} = \frac{A_t}{NOL} \tag{7}$$

$$L_{loop} = \frac{A_{loop}}{L_t} \qquad (8)$$

3.1.2. PTC Model

The corresponding efficiency equation for the medium-high temperature parabolic trough collectors (PTC) is given in Equation (9) [30]:

$$\eta_{ptc} = \eta_o - a_{11}(T_o - T_{amb}) - a_{21}\left(\frac{T_o - T_{amb}}{I_s}\right) - a_{31}\left(\frac{T_o - T_{amb}}{I_s}\right)^2 \qquad (9)$$

where, $a_{11} = 4.5 \times 10^{-6}$ 1/°C, $a_{21} = 0.039$ W/m^2. °C, $a_{31} = 3 \times 10^{-4}$ W^2/m^2. °C^2, $\eta_o = 0.75$.

The thermal efficiency of a PTC is the captured or gained useful energy divided by the incident radiation on the aperture plane, as shown in Equation (10)

$$\eta_{PTC} = \frac{Q_u}{A_{PTC} \times I_s} \qquad (10)$$

where η_{PTC} is the thermal efficiency of the collector; Qu is the useful power (W); A_{PTC} is the aperture area of the collector (m^2); and I is the solar radiation absorbed in the aperture plane (W/m^2).

The modification of Equation (10) yields Equation (11):

$$A_{PTC} = \frac{Q_u}{\eta_{PTC} \times I_s} \qquad (11)$$

However, the required land area for the installation of solar collectors is higher than the aperture area of collectors. This value varies approximately between three to four times the aperture area of collectors. The land area is greater because there is a distance between collectors besides the required space for pipes and other accessories of the system. The collector useful energy equation may exist according to the following relation:

$$Q_u = M_{col}^{\cdot} \times \Delta h_{o-i} \qquad (12)$$

where Δh is the enthalpy difference across the collector in kJ/kg, and $M_{col}^{\cdot}$ is the total field mass flow rate in kg/s. The PTC total length L_{PTC} is then calculated based on collector width W_c (m) and glass envelope diameter D_{env} (m):

$$L_{PTC} = \frac{A_{PTC}}{W_c - D_{env}} \qquad (13)$$

By knowing the total mass flow rate, which is calculated from the boiler heat exchanger load, and by assigning the hydraulic mass flow rate as an input, the total number of loops N_{loop}, loop area A_{loop}, loop width W_{loop}, and the number of solar PTC's ($N_{PTC's}$) are then calculated as follows;

$$N_{loop} = \frac{M_{col}^{\cdot}}{M_{hyd}^{\cdot}} \qquad (14)$$

$$A_{loop} = \frac{A_{PTC}}{N_{loop}} \qquad (15)$$

$$W_{loop} = \frac{A_{loop}}{L_m} \qquad (16)$$

where L_m (m) is assigned as module length.

$$N_{PTC's} = \frac{A_{PTC}}{L_m(W_c - D_{env})} \qquad (17)$$

Total pressure losses P_{tloss} are calculated based on major and minor losses along the field length. The general loss equation is performed as following [31,32]:

$$P_{tloss} = N_{loop} \times \Delta P_{loop} \tag{18}$$

where

$$\Delta P_{loop} = \frac{32 \times f \times L_{loop} \times \dot{M}_{hyd}^2}{\rho \times \pi^2 \times D_t} \tag{19}$$

D_t is the inner tube diameter (m)

$$f = [(1.82 \times \log Re) - 1.64]^{-2} \tag{20}$$

$$Re = 4 \times \frac{\dot{M}_{hyd}}{\mu \times \pi \times D_t} \tag{21}$$

3.1.3. Flashing Tank

Flash Cyclone tank design data are calculated as follows:

Tube Inlet and outlet tank steam area A_{t_i} based on steam velocity V_{st}, m/s, and vapor density ρ_v, kg/m^3:

$$A_{t_i} = \frac{M_{st}}{\rho_v \times V_{st}} \tag{22}$$

Tube diameter D_t (m):

$$D_t = \left(\frac{A_{t_i} \times 4}{\pi} \right)^{0.5} \tag{23}$$

Flash tank height H_{fst} (m) [31]:

$$H_{fst} = 7.15 \times D_t \tag{24}$$

Flash tank width W_{fst} (m):

$$W_{fst} = 3.5 \times D_t \tag{25}$$

Flash tank total volume Vol_{fst} (m^3):

$$Vol_{fst} = \left(\frac{pi}{4} \right) \times W_{fst}^2 \times H_{fst} \tag{26}$$

Flashing enthalpy h_{fsh} is equal to the enthalpy coming from the solar collector h_{col}, kJ/kg:

$$h_{fsh} = h_{col} \tag{27}$$

The flashing dryness fraction X_{fsh} is calculated based on flashing enthalpy h_{fsh}, liquid enthalpy h_f, (kJ/kg) and dry vapor enthalpy h_g (kJ/kg):

$$X_{fsh} = \frac{h_{fsh} - h_f}{h_g - h_f} \tag{28}$$

The total mass flow rate M_{total} (kg/s), and unvaporized water M_w (kg/s) are given by Equations (29) and (60), respectively:

$$M_{total} = \frac{M_{st}}{X_{fsh}} \tag{29}$$

$$M_w = \left(1 - X_{fsh} \right) \times M_{total} \tag{30}$$

3.1.4. Pump

The pump work W_p, kW can be calculated using [33]:

$$W_p = M_{total} \times \frac{\Delta P}{\rho} \times \eta_p \tag{31}$$

where ΔP, bar is the total pressure difference and it is calculated as:

$$\Delta P = P_{high} + P_{loss} \tag{32}$$

Outlet pump enthalpy h_{po} (kJ/kg):

$$h_{po} = \left(\frac{W_p}{M_{total}}\right) + h_{pi} \tag{33}$$

3.1.5. Mathmatical Model of the Absorption Cycle

A schematic diagram of a single-effect NH_3-H_2O absorption system is shown in Figure 1. The following assumptions are considered in the developed mathematical model of the absorption cycle:

(1) Refrigerant leaving the evaporator is saturated ammonia vapor.
(2) Refrigerant leaving the condenser is saturated ammonia liquid.
(3) No liquid carry over from evaporator.
(4) Refrigerant vapor leaving the generator has the equilibrium temperatures of the weak solution of the generator's pressure and is salt free.
(5) The solutions leaving the generator and absorber are saturated.
(6) The pumping process is isentropic.

The thermodynamic model of each component is explained in the following section.

The mathematical model for determining the thermal powers to be transferred in the main components of the absorption cooling system, was a first-law thermodynamic model, which was based on the Equations (34) to (62).

Absorber

In the absorber, the saturated vapor refrigerant from evaporator is absorbed by the weak solution from generator and converted to low pressure strong solution. The generated heat is removed by the cooling water. For the absorber, the flow factor parameter is especially important in the calculation procedures of the thermal power through the model. The flow rate ratio factor f is calculated based on the absorber temperature as following [33]:

$$f = 0.4067 \times exp(0.05606 \times T_a) + 5.09e - 07 \times exp(0.3293 \times T_a) \tag{34}$$

The strong solution mass flow rate M_{str} (kg/s) is calculated based on the total refrigerant flow rate M_r (kg/s) and the flow factor f:

$$M_{str} = M_r \times f \tag{35}$$

The weak solution mass flow rate M_{wk} (kg/s):

$$M_{wk} = M_{str} - M_r \tag{36}$$

The Absorber thermal power Q_a, kW is calculated based on the energy balance across the absorber between inlet and outlet streams, where H denotes to enthalpy (kJ/kg):

$$Q_a = M_r \times (H_{e-abs} + (M_{wk} \times H_{hex-a}) - (M_{str} \times H_{a-hex})) \tag{37}$$

Overall heat loss U_a (kW/m^2 °C) [34]:

$$U_a = 1.6175 + 0.1537e - 3 \times T_a + 0.1825e - 3 \times T_a^2 - 8.026e - 8 \times T_a^3 \tag{38}$$

The absorber area A_a (m^2):

$$A_a = \frac{Q_a}{U_a \times \Delta T} \tag{39}$$

Solution Heat Exchanger SHX

A solution heat exchangeris (SHX) is included in the absorption cycle to exchange heat between the streams flowing in and out of the generator, the use of the SHX augments the coefficient of performance (COP) by reducing the heat released in the absorber and the heat supplied to the generator. For the heat exchanger unit, the mass flow ratio is obtained as follows f:

$$f = \frac{M_{str}}{M_{str} - M_{wk}} \tag{40}$$

The NH$_3$ concentration percentage $XNH3$ [33,35]:

$$XNH3 = \frac{\frac{M_{str}}{f}}{M_r + M_{wk}} \tag{41}$$

The outlet heat exchanger stream temperature towards the absorber unit T_{hex_a} (°C) is calculated based on the heat exchanger effectiveness ε_{hex}:

$$T_{hex\_a} = T_g - \left(\varepsilon_{hex} \times \left(T_g - T_a\right)\right) \tag{42}$$

Outlet heat exchanger temperature to the generator unit T_{hex_g} (°C):

$$T_{hex\_g} = T_a + \left(\varepsilon_{hex} \times \left(T_g - T_a\right)\right) \tag{43}$$

The enthalpy of NH$_3$-H$_2$O solution outlet to the absorber unit H_{hex_a} (kJ/kg) is calculated based on temperature T_{hex-a} (K) and specific heat capacity Cp_{NH3} (kJ/kg K):

$$H_{hex\_a} = Cp_{NH3}(T_{hex-a} + 273) \times (T_{hex-a} + 273) \tag{44}$$

where the specific heat capacity for NH$_3$, Cp_{NH3} (kJ/kg K):

$$Cp_{NH3} = \frac{27.31 + 0.02383 \times T + 1.707e - 5 \times \left(T^2\right) - 1.185e - 8 \times \left(T^3\right)}{17.0305} \tag{45}$$

The enthalpy of NH$_3$-H$_2$O solution outlet to the generator unit H_{hex_g} (kJ/kg):

$$H_{hex\_g} = Cp_{NH3}\left(T_{hex-g} + 273\right) \times \left(T_{hex-g} + 273\right) \tag{46}$$

The heat exchanger thermal power Q_{hex} (kW) is then calculated based on the thermal energy balance between inlet and outlet streams:

$$Q_{hex} = (M_{str} - M_{wk}) \times (f - 1) \times \left(H_{g-hex} - H_{hex-a}\right) \tag{47}$$

Enthalpy stream from the absorber towards the heat exchanger H_{a-hex} (kJ/kg):

$$H_{a-hex} = H_{hex-g} - \left(\left(\frac{f-1}{f}\right) \times \left(H_{g-hex} - H_{hex-a}\right)\right) \tag{48}$$

Mean temperature T_{hex_m} (°C):

$$T_{hex_m} = \frac{T_{hex-a} + T_{hex-g}}{2} \tag{49}$$

Overall heat loss U_{hex} (kW/m² °C):

$$U_{hex} = 1.6175 + 0.1537e - 3 \times T^1_{hex_m} + 0.1825e - 3 \times T^2_{hex_m} - 8.026e - 8 \times T^3_{hex_m} \tag{50}$$

Heat exchanger area A_{hex} (m²):

$$A_{hex} = \frac{Q_{hex}}{U_{hex} \times \Delta T} \tag{51}$$

Generator

The strong solution is introduced to the generator, where heat energy is supplied by hot water or steam. The heat energy separates the refrigerant vapor from the solution and a high water concentrated solution is exits to HEX. The outlet enthalpy to the HEX, H_{g_hex} (kJ/kg) is calculated based on the energy balance between both units and flow rate ratio [34–36]:

$$H_{g\_hex} = \frac{\left(\frac{Q_g}{M_r}\right) - H_{g-cond} + \left(f \times H_{hex-g}\right)}{f - 1} \tag{52}$$

Overall heat loss U_g (kW/m² °C) through the generator tubes is calculated as following [36]:

$$U_g = 1.6175 + 0.1537e - 3 \times T^1_g + 0.1825e - 3 \times T^2_g - 8.026e - 8 \times T^3_g \tag{53}$$

Generator area A_g (m²):

$$A_g = \frac{Q_g}{U_g \times \Delta T} \tag{54}$$

Inlet driving steam mass flow rate Ms, (kg/s) is calculated based on the latent heat h_{fg}, (kJ/kg) from the heat source:

$$Ms = \frac{Q_g}{0.95 \times h_{fg}} \tag{55}$$

where h_{fg} is the latent heat of distillate vapor evaporation (pure ammonia) [33–36]:

$$h_{fg} = -46.53 \times exp(0.02096 \times T) + 1305 \times exp(-0.001835 \times T) \tag{56}$$

Condenser

In the condenser, the ammonia vapor is liquefied by means of the cooling water supplied by the auxiliary cooling system. Once the ammonia has been condensed. The condenser thermal power Q_c (Kw) can be calculated using:

$$Q_c = M_r \times \left(H_{g-cond} - H_{cond-e}\right) \tag{57}$$

The overall heat loss U_c (kW/m² °C):

$$U_c = 1.6175 + 0.1537e - 3 \times T^1_c + 0.1825e - 3 \times T^2_c - 8.026e - 8 \times T^3_c \tag{58}$$

The condenser area A_c, (m²):

$$A_c = \frac{Q_c}{U_c \times \Delta T} \tag{59}$$

Inlet cooling water enthalpy $H_{c_{cwi}}$ (kJ/kg):

$$H_{c_{cwi}} = 421.2 \times exp(0.004008 \times T_{c_{cwi}}) - 435.9 \times exp(-0.007559 \times T_{c_{cwi}}) \tag{60}$$

Outlet cooling water enthalpy $H_{c_{cwo}}$ (kJ/kg):

$$H_{c_{cwo}} = \left(\frac{Q_c}{M_{cw}}\right) + H_{c_{cwi}} \tag{61}$$

Evaporator

In the evaporator, the low-pressure, low temperature refrigerant (after the refrigerant expansion valve) is sprayed over the evaporator tube, where the cold water circulates through the tubes and gets chilled. The refrigerant mass flow rate M_r (kg/s) can be calculated based on the energy balance across the evaporator [36]:

$$M_r = \frac{Q_e}{H_{e-abs} - H_{cond-e}} \tag{62}$$

where Q_e is a thermal load on evaporator unit, (kW).

3.1.6. Availability, Cost, and Performance

The availability, cost, and performance were calculated based on the formulas provided in the references [37–41]. The availability equation for any system goes under a steady-state, uniform flow process can be developed with the first and second law of thermodynamics. Neglecting the changes in kinetic and potential energy. The general form of the availability can be defined by the following equation [37]:

$$A_2 - A_1 = A_q + A_w + A_{fi} - A_{fo} - I \tag{63}$$

where $A_2 - A_1 = 0$ is the non-flow availability change in a steady-state condition, $A_q = \Sigma_J(1 - T_{amb}/T_J)Q_J$ is the availability transfer due to the heat transfer between the control volume and its surroundings, $A_w = -W_{cv} + P_o(V_2 - V_1)$ is equal to the negative value of the work produced by the control volume W_{cv} but in most cases, the control volume has a constant volume, therefore A_w can be further simplified, and $I = T_{amb}.S_{gen}$ is the availability of destruction in the process. The flow availability is expressed as $A_{fi,o} = \Sigma_{i,o}\dot{m}_{i,o}a_{fi,o}$. Thus, the general form in steady-state condition would become:

$$0 = A_q + A_w + A_{fi} - A_{fo} - I \tag{64}$$

In conventional economic analysis, a cost balance is usually formulated for the overall system operating at steady state as following:

$$\Sigma_{out}\dot{C} = \Sigma_{in}\dot{C} + Z^{IC\&OM} \tag{65}$$

where $\dot{C}$ the cost rate according to inlet and outlet streams, and $Z^{IC\&OM}$ is the capital investment and operating and maintenance costs. In exergy costing a cost is associated with each exergy stream. Thus, for inlet and outlet streams of matter with associated rates of exergy transfer $\dot{E}_{i,o}$, power $\dot{W}$, and the exergy transfer rate associated with heat transfer Equation $\dot{E}_q$, can write as follows:

$$\dot{C}_{i,o} = c_{i,o}\dot{E}_{i,o} \tag{66}$$

$$\dot{C}_w = c_w\dot{W} \tag{67}$$

$$\dot{C}_q = c_q\dot{E}_q \tag{68}$$

where $c_{i,o}, w, q$ denote average costs per unit of exergy in (USD/Kj) for inlet (i), outlet (o), power (w), and energy (q) respectively. For hourly costs estimation, the following correlations are considered:

For cost analysis, the amortization factor A_f is estimated based on the following relation:

$$A_f = \frac{i.(1+i)^{LTp}}{(1+i)^{LTp} - 1}$$

(69)

Collector investment cost IC_{col} (USD) is calculated based on the following area correlation:

$$IC_{col} = 150 \times A_{col}^{0.95}$$

(70)

operating and maintenance cost OMC_{col} is then calculated (USD):

$$OMC_{col} = 0.15 \times IC_{col}$$

(71)

Total annual cost TAC_{col} (USD/y) is then calculated based on operating and maintenance cost and investment cost parameters as following:

$$TAC_{col} = (IC_{col} + OMC_{col}) \times A_f$$

(72)

hourly costs are calculated Z_{col} (USD/h):

$$Z_{col} = \frac{TAC_{col}}{OH \times 365}$$

(73)

Flashing tank investment cost IC_{fsh} (USD) is calculated based on the following total tank volume Vol_{fst} correlation:

$$IC_{fsh} = \frac{Vol_{fst} \times 6.3e3}{3.8}$$

(74)

The total annual cost TAC_{fsh} USD/y is then calculated:

$$TAC_{fsh} = IC_{fsh} \times A_f$$

(75)

hourly costs are calculated Z_{fsh} (USD/h):

$$Z_{fsh} = \frac{TAC_{fsh}}{OH \times 365}$$

(76)

Absorption cycle investment cost IC_{aac} (USD), is calculated based on the following total area correlation:

$$IC_{aac} = 150 \times A_{aac}^{0.8}$$

(77)

Total annual cost TAC_{aac} (USD/y) is then calculated:

$$TAC_{aac} = IC_{aac} \times A_f,$$

(78)

hourly costs are calculated Z_{aac} (USD/h):

$$Z_{aac} = \frac{TAC_{aac}}{OH \times 365}$$

(79)

Pump investment cost IC_p (USD) is calculated based on the following pump power correlation:

$$IC_p = 3500 \times W_p^{0.47}$$

(80)

Total annual cost TAC_p (USD/y) is then calculated:

$$TAC_p = IC_p \times A_f \tag{81}$$

hourly costs are calculated Z_p (USD/h):

$$Z_p = \frac{TAC_p}{OH \times 365} \tag{82}$$

Total hourly costs Z_{tot} (USD/h) is then calculated based on all parameters as following:

$$Z_{tot} = Z_{col} + Z_{fsh} + Z_{aac} + Z_p \tag{83}$$

Total Plant Costs TPC (USD/y) is also calculated based on the total annual costs for all unit:

$$TPC = TAC_{col} + TAC_{fsh} + TAC_{aac} + TAC_p \tag{84}$$

The total thermo-economic equation is calculated based on the cost and exergy stream through the proposed cycles (USD/GJ):

$$c_p = 1000 \times \left(\frac{(W_{tot} \times c_w) + \left(\frac{Z_{tot}}{3600}\right)}{Ex_{fo}} \right) \tag{85}$$

where, c_p is the thermo-economic product cost (USD/GJ), c_w is the power cost in (USD/kWh) (~0.065), and W_{tot} is the total cycle power (kW), Ex_{fo} is the exergy stream outlet from the system to the user (kW).

For performance calculations, the COP is calculated based on evaporator Q_e and generator Q_g thermal powers:

$$COP = \frac{Q_e}{Q_g} \tag{86}$$

where the Max COP is found as:

$$COP_{max} = \frac{(T_e + 273.15) \times \left(T_g - T_a\right)}{\left(T_g + 273.15\right) \times (T_c - T_e)} \tag{87}$$

and the relative performance ratio RPR could be then estimated as:

$$RPR = \frac{COP}{COP_{max}} \tag{88}$$

The values of the design variables in Table 1 will be used in this work. The equations comprising the mathematical model of the combined system are utilized in MATLAB software, and the results are presented hereafter.

4. Results and Comments

As illustrated earlier, the proposed cycles for the current study are two cycles. Therefore, it is very important to optimize the absorption air conditioning AAC cycle before the attachment of solar collectors. Such optimization would reduce the design aspects, such as area. Meanwhile, lowering of the cost values and the thermo-economic product cost goes to the end-user. For such optimization purposes, different operating conditions have been examined in this section. The optimization processes addressed the effect of different operating conditions on COP, COP_{max}, Exergy destruction rate, mass flow rates, and design aspects such as areas and volume.

4.1. Optimization of NH₃-H₂O Cycle

4.1.1. Absorber Temperature Effect

The effect of changing absorber temperature on the system performance parameters is shown in Figure 2 such as COP_{max}, exergy destruction rate, mass flow rates, and design aspects. The data has been obtained at different cooling loads (50–150 TR), and different values of absorber operating temperature (30–35 °C). The effect of absorber temperature on the COP_{max} of the absorption cycle is illustrated in Figure 2a. Increasing the absorber temperature would cause a notable decrease in the COP_{max}. This was happened because of the following relation between the absorber temperature and COP_{max} ($COP_{max} = \frac{(T_e+273.15) \times (T_g-T_a)}{(T_g+273.15) \times (T_c-T_e)}$). In general, the COP_{max} was in the relatively higher range of 1.2–1.4. Figure 2b shows that there is no significant change in the exergy destruction rate. The same behavior was noticed on the total mass flow rate as shown in Figure 2c. The mass flow rate has not been changed vs. the increasing absorber temperature.
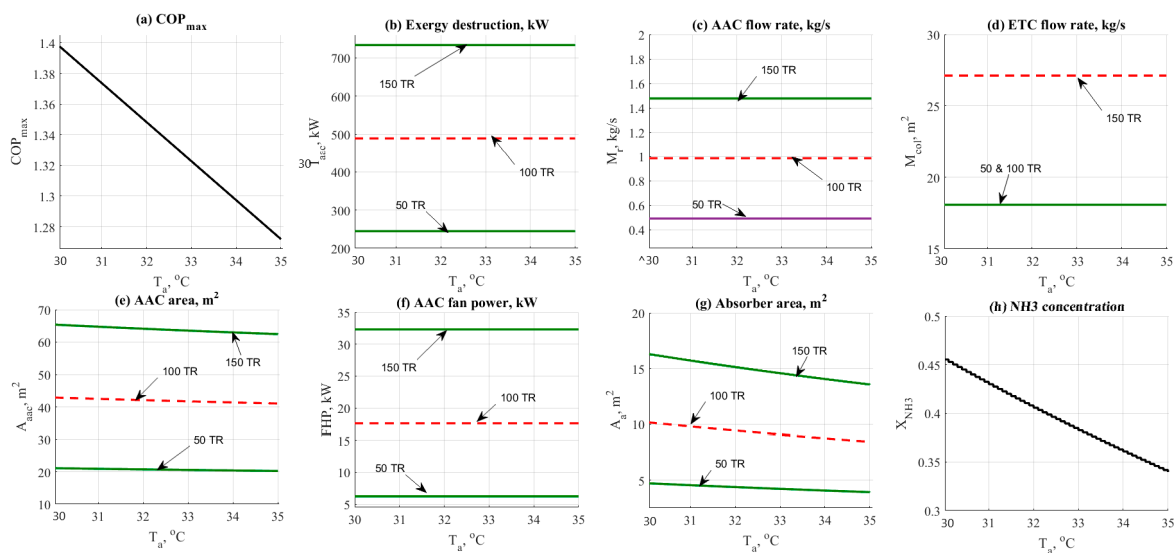
Figure 2. NH₃-H₂O data results based on the effect of absorber temperature parameter.

The effect of absorber temperature on the flow rate is not significantly high while comparing against the refrigerant load. The same behavior was noticed in Figure 2d. Absorber temperature has no effect on the ETC mass flow rate. A minor reduction in the AAC area has been noticed in Figure 2e. For instance, the total AAC area has been decreased from 65 down to 62 m² at 150 TR load. Figure 2f shows that there is no effect on the evaporator fan cooler unit. The effect would happen in case of the change in evaporator temperature. Figure 2g reflected the change in the absorber area by the cause of absorber temperature. The area has been decreased significantly. Figure 2h shows that by increasing the absorber temperature the NH₃ concentration has been decreased with no effect of the cooling load.

4.1.2. Condenser Temperature Effect

Figure 3 shows the data result based on the effect of condenser temperature on the other design parameters such as COP_{max}, exergy destruction rate, mass flow rates, and design aspects. Data has been obtained at different refrigerant loads (50–150 TR), and at different values of condenser operating temperature (40–45 °C). Figure 3a shows the effect of condenser temperature on the COP_{max}. Increasing the condenser temperature would cause a notable decrease in the COP_{max}. At the same time, increasing the load has no effect on the COP_{max} as noticed on the same figure. Figure 3b shows that there is no significant change in the exergy destruction rate. The same behavior was noticed on the total

mass flow rate as shown in Figure 3c; the mass flow rate has not been changed vs. the increase of condenser temperature.
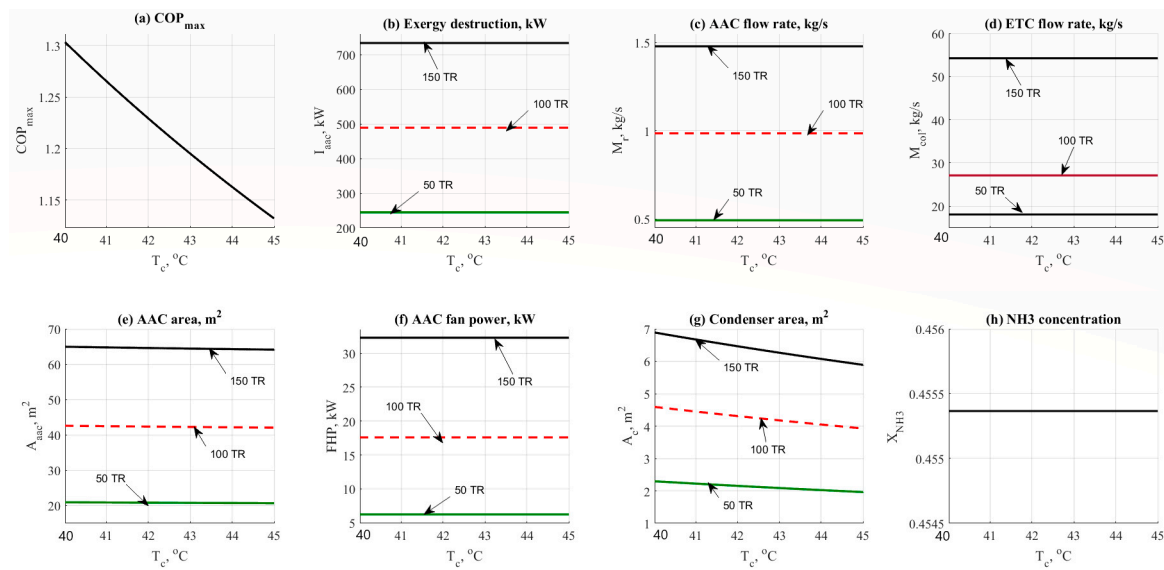

Figure 3. NH_3-H_2O data results based on the effect of condenser temperature parameter.

The effect of condenser temperature on the flow rate is not significantly high while comparing against the refrigerant load. The same behavior was noticed in Figure 3d. Condenser temperature has no effect on the ETC mass flow rate too. A minor reduction in the AAC area has been noticed in Figure 3e. For instance, the total AAC area has been decreased from 65 m^2 down to 64 m^2 at 150 TR load. Figure 3f shows that there is no effect on the evaporator fan cooler unit. The effect would be happened in case of the change in evaporator temperature or based on the temperature difference between the room temperature and the user target temperature. Figure 3g reflected the change in the condenser area by the cause of condenser temperature. The area has been decreased significantly causing a minor decrease in the total AAC area. The condenser area was ranged between 2 and 7 m^2 at 50 TR and 150 TR respectively. Figure 3h shows that by increasing the condenser temperature the NH_3 concentration has not been changed and it remained constant at 45% concentration.

4.1.3. Evaporator Temperature Effect

Figure 4 shows the data result based on the effect of evaporator temperature on the other design parameters such as COP_{max}, exergy destruction rate, mass flow rates, and design aspects. Data has been obtained at different refrigerant loads (50–150 TR) and at different values of evaporator operating temperature (-5 to 10 °C). Figure 4a shows the effect of the evaporator temperature on the COP_{max}. Increasing the evaporator temperature would cause a notable increase in the COP_{max}. At the same time, increasing the load has no effect on the COP_{max} as noticed on the same figure. Figure 4b shows that there is no significant change in the exergy destruction rate caused by the evaporator temperature. The same behavior was noticed on the total mass flow rate as shown in Figure 4c. The mass flow rate has not been changed vs. the increase of evaporator temperature. The effect of evaporator temperature on the flow rate is not significantly high while comparing against the refrigerant load. The same behavior was noticed in Figure 4d. Evaporator temperature has no effect on the ETC mass flow rate too. A minor reduction in the AAC area has been noticed in Figure 4e. For instance, the total AAC area has been decreased from 65 down to 64 m^2 at 150 TR load. Figure 4f shows that there is no effect on the evaporator fan cooler unit. The effect would be happened in case of the change in evaporator temperature or based on the temperature difference between the room temperature and the user target temperature. Figure 4g reflected the change in the evaporator area by the cause of the evaporator temperature. The area has been decreased significantly causing a minor decrease in the total AAC area.

The evaporator area was ranged between 10 and 35 m^2 at 50 and 150 TR respectively Figure 4h shows that by increasing the evaporator temperature the NH$_3$ concentration has not been changed and it remained constant at 45% concentration.
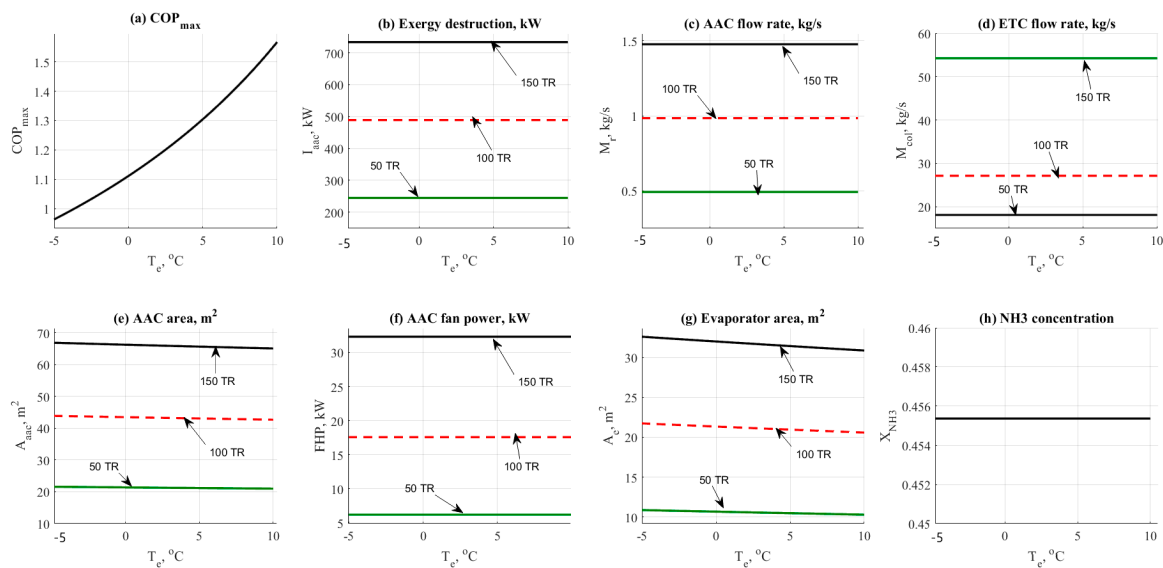

Figure 4. NH$_3$-H$_2$O data results based on the effect of evaporator temperature parameter.

4.1.4. Generator Temperature Effect

The generator operating temperature has a great influence on this cycle. Figure 5 shows the data result based on the effect of generator temperature on the other design parameters such as COP$_{max}$, exergy destruction rate, mass flow rates, and design aspects. Data has been obtained at different refrigerant loads (50–150 TR) and different values of the generator operating temperature (80 to 95 °C). Figure 5a shows the effect of the generator temperature on the COP$_{max}$. Increasing the generator temperature would cause a notable increase in the COP$_{max}$ from 1.45 to 1.8. The driving temperature depends on the solar energy capturing technology that can be adopted and efficiently available. At the same time as shown in Figure 5b that the exergy destruction has also increased as a normal reflection to the generator temperature changing. The same behavior was noticed on the total mass flow rate as shown in Figure 5c. The mass flow rate has been changed to be increasing vs. the increasing generator temperature.

The effect of generator temperature on the flow rate is significantly high. The same behavior was noticed in Figure 5d. Generator temperature has a remarkable effect on the ETC mass flow rate too. A minor reduction in the total AAC area has been noticed in Figure 5e. For instance, the total AAC area has been decreased from 65 down to 62 m^2 at 150 TR load. Figure 5f shows that there is no effect on the generator fan cooler unit. Figure 5g reflected the change in the generator area by the cause of the generator temperature. The area has been remarkably decreased causing a minor decrease in the total AAC area. The generator area was ranged between 1.5 and 5 m^2 at 50 and 150 TR respectively Figure 5h shows that by increasing the generator temperature the NH$_3$ concentration has not been changed and it remained constant at 45% concentration.
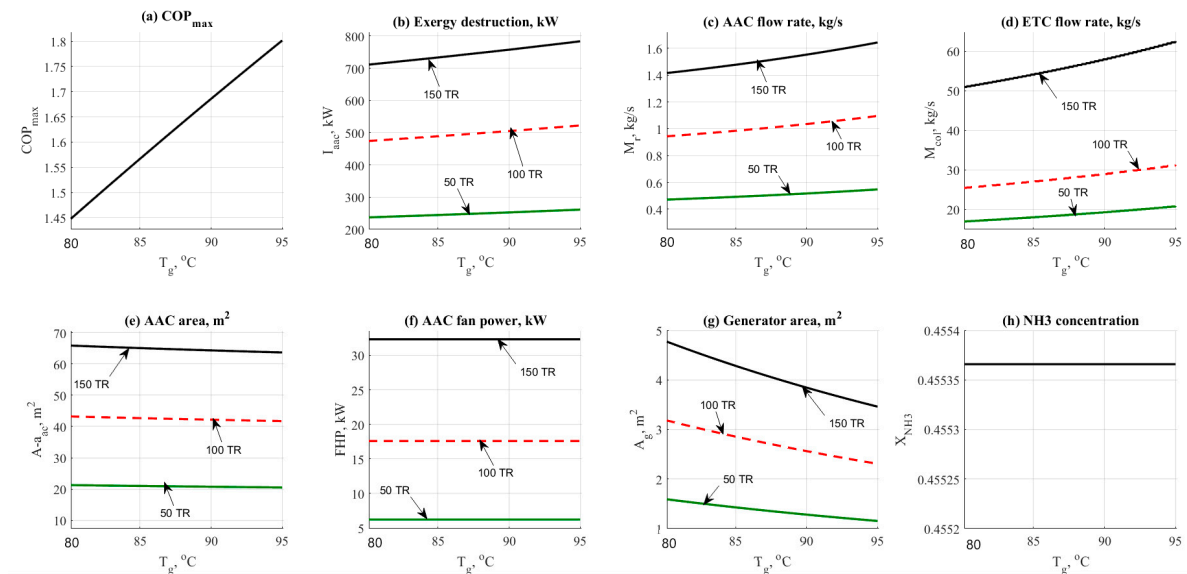
Figure 5. NH$_3$-H$_2$O data results based on the effect of generator temperature parameter.

4.1.5. Solar Field Top Temperature Effect

Solar field top temperature is considered a very important parameter in this cycle. Figures 6 and 7 show the variations on the performance and design parameters for both operational cases ETC and PTC. For ETC, the temperature range was 110 to 200 °C. The temperature range for PTC was 150 to 300 °C. Figure 6a shows the effect of ETC top temperature on the solar field mass flow rate.
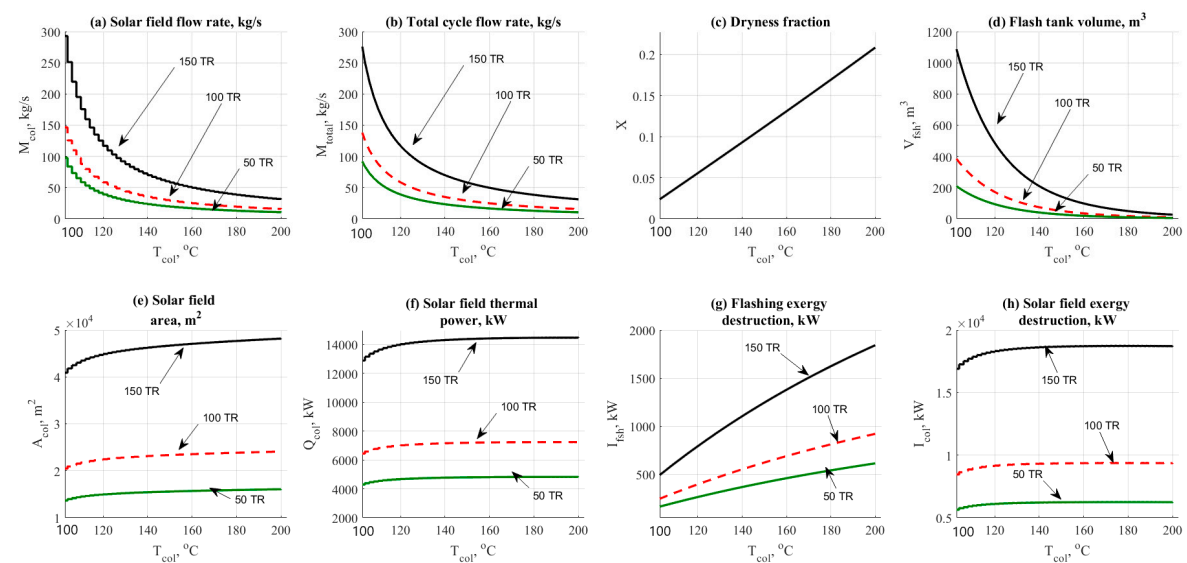
Figure 6. NH$_3$-H$_2$O data results based on the effect of ETC outlet top temperature.
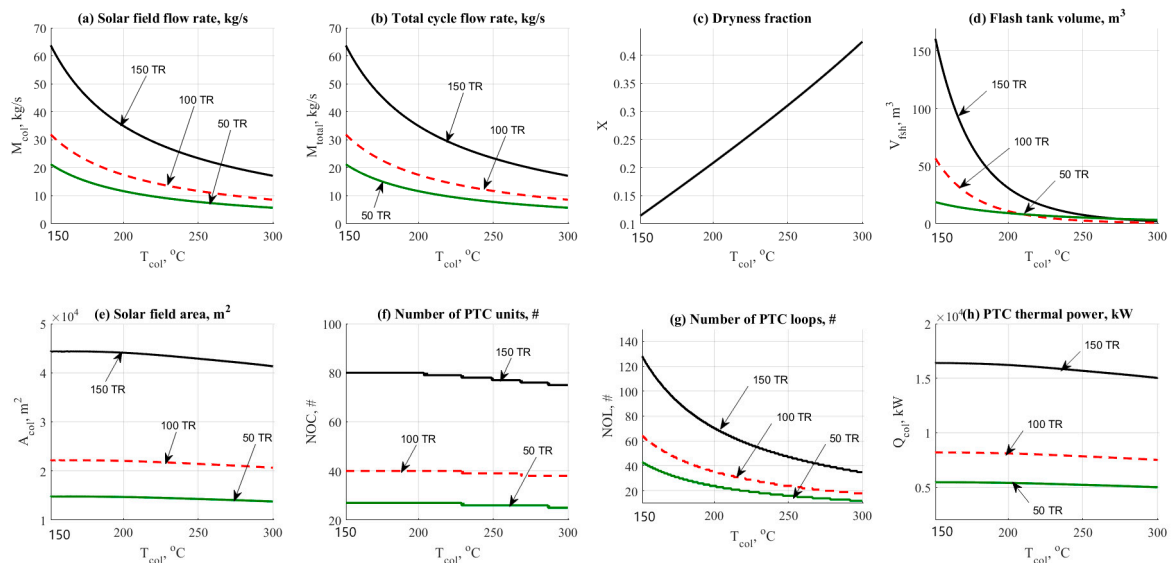
Figure 7. NH_3-H_2O data results based on the effect of PTC outlet top temperature.

The figure shows that increasing the top temperature would reduce the total mass flow rate as a normal result extracted from the energy balance across the solar field. The same behavior was also noticed in Figure 7a which represents the PTC operation. However, PTC conceded lower flow rates which means lower costs. The difference is considered huge if we compared between 50 to 300 kg/s @ 150 TR for the ETC and 15 to 65 kg/s @ 150 TR for the PTC. The same behavior was also noticed for both collector's type related to the total cycle flow rate as shown in Figures 6b and 7b.

Figures 6c and 7c also reflects the advantage of using PTC rather than ETC. The figure shows that the dryness fraction was in increasing mode by the increase of the solar filed operating temperature. ETC gives a range of 10% to 20% of generating steam while the PTC gave 20% to 40% which is considered attractive and reasonable. For both cases, flash tank volume has been presented in Figures 6d and 7d. The difference is quite clear with an advantage to the PTC.

Increasing the top solar field temperature would decrease the flashing tank volume. However, ECT will need larger tanks because of lower dryness fraction in comparison against the PTC operation. Figures 6e and 7e shows the effect of solar temperature on the solar field design area. The changes in Figures 6e and 7e were not massive; however, lower area, i.e., lower costs and control are recorded for the PTC as expected.

For instance, at 150 TR, ETC will consume about 45,000 to 50,000 m^2. However, the PTC will consume about 45,000 down to 40,000 m^2 under the same operating conditions. For ETC, Figure 6f–h represents the effect on the thermal power, kW, flashing, and solar field exergy destruction rates, kW. Increasing the operating temperature would increase thermal power and exergy destruction rates as well.

Figure 7f,g shows that increasing the PTC temperature would decrease the number of units and the number of loops as well. The number of loops parameter is affected by the total PTC area required for the load. Figure 7h shows the effect on PTC thermal power. The figure shows a decreasing behavior vs. the increasing of the top solar field temperature. Generally, increasing the load from the AAC unit would request more solar field areas leading to the increase of mass flow rate and exergy destruction rates.

A value of 150~200 °C and 250~300 °C would be recommended in this study for ETC and PTC solar collectors respectively. Based on the currently obtained results, it is quite interesting to assign the operating temperature as follows:

➢ $T_a = 35$ °C.
➢ $T_c = 43$ °C.

➢ T_e = 7~10 °C.
➢ T_g = 85~90 °C.
➢   ETC T_{high} = 150~200 °C.
➢   PTC T_{high} = 250~300 °C.

4.1.6. Cooling Load Effect

The cooling load effect on ETC/NH$_3$-H$_2$O and PTC/NH$_3$-H$_2$O cycles are shown in Figures 8 and 9. Both figures addressed the effect on hourly costs, Levelized power cost, and thermo-economic product cost. As expected, the behavior on the figure was in varying mode due to the load and energy demand for all units. Solar collectors recorded the highest values of hourly costs among the other units as shown in Figures 8a and 9a.
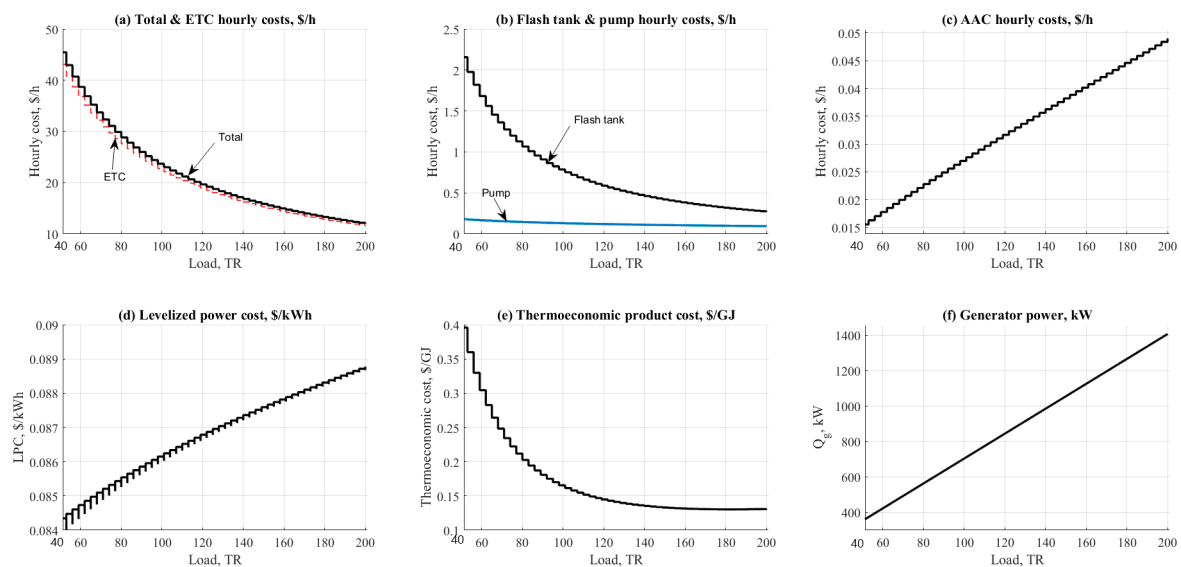

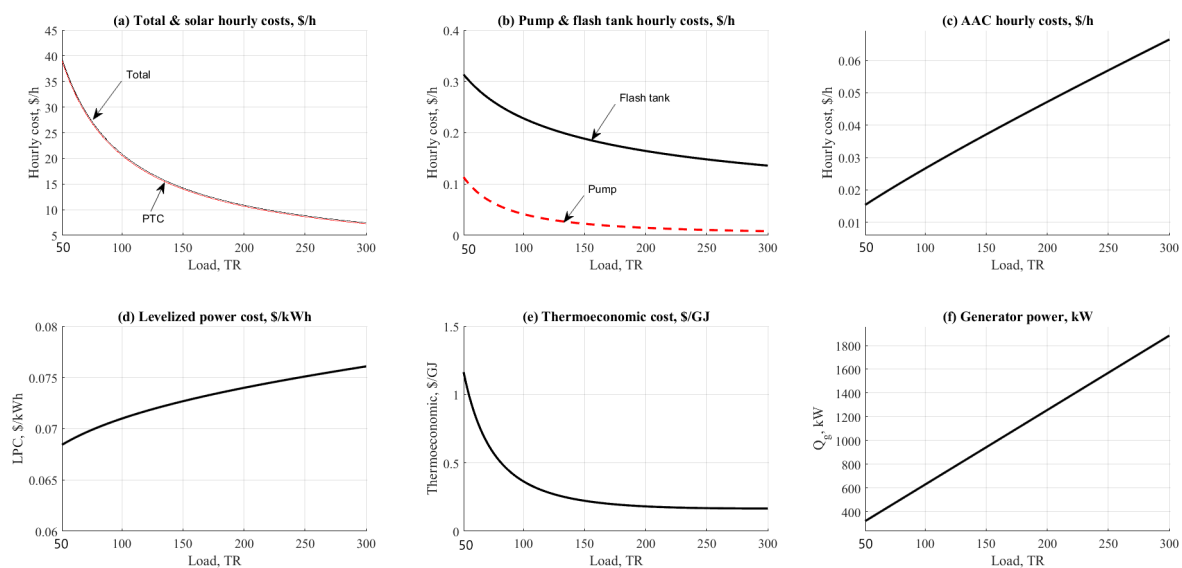**Figure 8.** ETC-NH$_3$-H$_2$O data results based on the effect of cooling load.

Figure 9. PTC-NH$_3$-H$_2$O data results based on the effect of cooling load.

However, PTC was recorded lower by 8% against the ETC related to the hourly costs parameter. The main reason for this was referring to the increasing in collector operating temperature (250 vs. 150 °C). Increasing the collector temperature will generate more steam for the AAC unit. AAC, pumps,

and flashing tanks are shown in Figure 8b,c and Figure 9b. It was clear on the figures that the flashing tank is recorded higher than the pump and the AAC unit based on the total tank volume. PTC operation was recorded lower in flashing tank hourly cost because it has lower tank volume 0.2–0.3 $/h vs. USD 0.5–2.2/h. Figures 8d and 9d show the effect of cooling load on the levelized power cost, USD /kWh.

The results are nearly the same based on the close results between the two configurations related to the pumping unit. The levelized power cost was ranged between USD 0.07/kWh to USD 0.08/kWh for PTC, ETC respectively. The same close behavior was noticed while comparing related to the thermo-economic product cost. Results were centralized 0.1 to USD 1/GJ for both configurations with a minor advantage to the ETC (Figures 8e and 9e). As anticipated, increasing the load would increase the cost of exergy. Solar PTC and/or ETC are considered the main cause of such an effect related to the large area needed to cover on the load. Figures 8f and 9f show the effect on the generator thermal power which is recorded increasing vs. the increase of cooling load.

4.2. Case Study Results

The case study presented in this section compares between two configurations at a specific load point. The case study was about a sports arena which is located in Baghdad, Iraq. The arena is a USD 14 million, 3000-seat indoor sports facility is focused around basketball, volleyball, and athletics. The whole project will be centrally air-conditioned by a 700–800 kW solar absorption cycle. The evaporator will be designed to work between 7 and 12 °C. Table 2 shows the data results for two configurations in case of using the solar absorption cycle. A 200 TR cooling load has been selected as an example of such a comparison. Environmental operating conditions are fixed at a specific value for simplicity. From solar field results, PTC/NH_3-H_2O resulted in the lowest in the area needed, and it is quite important to reduce the needed area. ETC/NH_3-H_2O comes next. For design aspects such as flashing tank design, it was clear the operation of PTC/NH_3-H_2O gives the lowest results which were the most favorable, at 3.8 m^3, followed by ETC/NH_3-H_2O with 7.8 m^3. The same behavior was also noticed related to the dryness fraction. The same behavior is also noticed related to the exergy destruction rate. The results reveal that PTC is considered an advantage to the cycle vs. the ETC operation. PTC/NH_3-H_2O recorded lower in the absorber area with 21 m^2. Minimum driving steam was recorded by PTC/NH_3-H_2O (1.8 kg/s) which lead to low flashing tank volume and lower solar field area. COP was found remarkable related to PTC/NH_3-H_2O cycle. For hourly costs, PTC/NH_3-H_2O is noticed as the lowest among the rest. By achieving USD11.3/h, PTC/NH_3-H_2O is considered the best option for this case study. Lower hourly costs for the solar field is considered the vital term to judge the system cost. Thermo-economic cost is nearly the same for two configurations within the range of USD 0.14–0.15/GJ with an advantage to PTC/NH_3-H_2O configurations.

Table 2. Data results based on 200 TR load case study.

Solar radiation, W/m^2	500	
T_{amb}, **°C**	25	
T_a, T_e, T_g, T_c, T_{col}, **°C**	30, 10, 90, 40, 175	30, 10, 90, 40, 250
Load, TR	200	
Target cooled air, °C	20	
Interest rate, %	5	
Load factor, %	95	
Plant life time, yr	20	
Electric cost, $/kWh	0.065	
Fans efficiency, %	80~85	
Pumps efficiency, %	75	

Table 2. *Cont.*

Configuration:	ETC/NH$_3$-H$_2$O	PTC/NH$_3$-H$_2$O
Solar field:		
Total solar field area, m^2	1.188e4	1.102e4
Solar thermal power, kW	3612	4051
Inlet temperature, °C	91.82	92.04
Mass flow rate, kg/s	10.17	8.727
Inlet exergy, kW	5646	4217
Exergy destruction, kW	4683	5143
Flash tank:		
Height/Width, m	3.381/1.655	2.743/1.343
Volume, m^3	7.276	3.883
Total flow rate, kg/s	10.17	8.727
Water content, kg/s	8.551	6.91
Dryness fraction	0.1595	0.208
Exergy destruction, kW	391.1	515.6
AAC unit:		
Q_a, *kW*	1251	1153
A_a, *m^2*	23.37	21.3
M_{str}, *kg/s*	1.428	1.428
M_{wk}, *kg/s*	0.778	0.778
$X_{hex\text{-}NH3}$	0.4554	0.4554
A_{hex}, *m^2*	7.837	6.73
Q_g, *kW*	1407	1256
A_g, *m^2*	5.123	4.574
Driving steam flow, kg/s	2.07	1.848
Q_c, *kW*	694.9	694.9
A_c, *m^2*	9.1	9.1
M_r, *kg/s*	0.6505	0.6505
Q_e, *kW*	703.4	703.4
A_e, *m^2*	41.15	41.15
FHP, kW	70.64	70.64
M_{air}, *kg/s*	119.5~120	119.5~120
COP/COP_{max}	0.5/1.559	0.5/1.559
RPR	0.3206	0.3591
Exergy destruction, kW	1010	977.3
Fan exergy destruction, kW	164	164
Pump unit:		
W_p, *kW*	12.63	18.97~19
Exergy destruction, kW	64.7	62.25

Table 2. *Cont.*

Cost and Thermo-economics:		
Z_{col}, USD/**h**	11.75	10.93
Z_{fsh}, USD/**h**	0.11	0.06
Z_{aac}, USD/**h**	0.0487	0.04716
Z_{p+f}, USD/**h**	0.256	0.2652
Z_{tot}, USD/**h**	12.16	11.3
LPC, USD/**h**	0.089	0.0744
cp, USD/*GJ*	0.144	0.1554

5. Conclusions

A two configurations of solar-assisted NH_3-H_2O absorption refrigeration system was proposed, modeled, and simulated in this paper. A Flash evaporation tank has been used as a steam generation unit between the solar part and absorption chiller. A parametric study on the effect of the temperature of the absorption cycle component on the performance of the system is carried out and the results are presented. In addition, energy, exergy and cost analyses are presented in this work. According to the analysis results, the following conclusions can be drawn:

■ Design aspects, such as solar area and flashing tank volume were found to have a great influence on the cycle cost.

■ Increasing the cooling load increases the required solar field area and the flow rate of the heat transfer fluid.

■ Optimization of the operating conditions, such as temperatures, has been performed for two configurations. The following values of operating conditions are considered the best, related to design aspects, COP, exergy destruction rate, and cost:

  ○ T_a = 35 °C.
  ○ T_c = 43 °C.
  ○ T_e = 7~10 °C.
  ○ T_g = 85~90 °C.
  ○ ETC T_{high} = 150~200 °C.
  ○ PTC T_{high} = 250~300 °C.

■ A case study is presented in a sports arena located in Baghdad, Iraq, for which the needed cooling load was in the range of 700 to 800 kW. PTC/NH_3-H_2O was recorded the best based on design and hourly costs. The required solar area was in the range of 2000–2500 m^2. While the total hourly costs were in the range of USD 11.3–12.6/h which is quite attractive.

■ PTC/NH_3-H_2O gives the lowest values related to exergy destruction rates for all units. As expected, the solar filed would harvest a larger amount of exergy destruction rates for two configurations due to the large area and mass flow rate effect. The PTC/NH_3-H_2O exergy destruction rate results are in the range of 4600–5000 kW.

■ PTC/NH_3-H_2O gives the lowest value of flashing tank design aspects such as width, 1.343 m, height, 2.743 m, and volume, 3.883 m^3. ETC/NH_3-H_2O comes next with a total flashing tank equal to ~7.276 m^3.

■ It is quite clear that PTC/NH_3-H_2O followed by ETC/NH_3-H_2O have a remarkable result according to the terms of energy, design, and cost. Generally, the PTC system is considered the best choice for the NH_3-H_2O solar cooling system.

Nomenclature

A	Availability, kW, Area, m^2
A_t	Tube cross-sectional area, m^2
A_f	Amortization factor, 1/y
AAC	Absorption Air Conditioning
C	Thermo-economic cost stream, USD/kJ
C_p	Specific heat capacity, kJ/kg °C @ constant pressure
COP	Coefficient of Performance
D	Diameter, m
D_{env}	Collector glass envelope diameter, m
E	Exergy stream, kW
ETC	Evacuated Tube Collector
f	Function
FHP	Fan power, kW
H, h	Height, m, Enthalpy, kJ/kg
H_{dish}	Dish parabola height, m
I_s	Solar intensity, W/m^2
i	Interest rate, %
L	Length, m
L_m	Module length, m
LMT	Logarithmic Mean Temperature, °C
LPC	Levelized Power Cost, USD/kWh
LTp	Plant life time, y
M	Mass flow rate, kg/s
NOT	Number of Tubes
NOC	Number of Collectors
NOL	Number of Loops
P	Power, or Pressure, bar
ΔP	Pressure, bar
Q	Thermal power, kW
RPR	Relative Performance Ratio
Re	Raynold's Number
S, s	Entropy, kJ/kg °C
SHX	Solution Heat Exchanger
T	Temperature, °C
U	Overall heat transfer coefficient, W/m^2 °C
V, Vol	Volume, cm^3
v	Velocity, m/s
W	Power, Work, kW
W_c	Collector width, m
X	Concentration percentage, %
Z	Hourly cost, USD/h

Subscripts

a, abs	Absorber
air	Air
amb	Ambient
a-hex	From absorber to heat exchanger stream
c	Condenser
c-evp	From condenser to evaporator stream
col	Collector
cw	Cooling water
e	Evaporator
etc	Evacuated tube collector
e-abs	From evaporator to absorber stream
f	Liquid phase
fan	Fan
fsh	Flashing tank
fst	Flashing steam
g	Generator, vapor phase
g-hex	From generator to heat exchanger stream
i	Inlet
loop	Loop
o	Out
p	Pump
ptc	Parabolic trough collector
$p_{i,o}$	Pump inlet and outlet
q	Heat
r	Refrigerant
s	Steam
st	Steam
str	Strong
t	Turbine, total
w	Water
wk	Weak solution

Greek

η	Efficiency, %
ρ	Density, kg/m^3
μ	Dynamic viscosity, Pa.s

References

1. Zeyghami, M.; Goswami, D.Y.; Stefanakos, E. A review of solar thermo-mechanical refrigeration and cooling methods. *Renew. Sustain. Energy Rev.* **2015**, *51*, 1428–1445. [CrossRef]
2. Hassan, H.; Mohamad, A. A review on solar-powered closed physisorption cooling systems. *Renew. Sustain. Energy Rev.* **2012**, *16*, 2516–2538. [CrossRef]
3. Baniyounes, A.M.; Ghadi, Y.Y.; Rasul, M.G.; Khan, M.M.K. An overview of solar assisted air conditioning in Queensland's sub-tropical regions, Australia. *Renew. Sustain. Energy Rev.* **2013**, *26*, 781–804. [CrossRef]
4. Al-Alili, A.; Hwang, Y.; Radermacher, R. Review of solar thermal air conditioning technologies. *Int. J. Refrig.* **2014**, *39*, 4–22. [CrossRef]
5. Baniyounes, A.M.; Liu, G.; Rasul, M.; Khan, M. Comparison study of solar cooling technologies for an institutional building in subtropical Queensland, Australia. *Renew. Sustain. Energy Rev.* **2013**, *23*, 421–430. [CrossRef]
6. Kurem, E.; Horuz, I. A comparison between ammonia-water and water-lithium bromide solutions in absorption heat transformers. *Int. Commun. Heat Mass Transf.* **2001**, *28*, 427–438. [CrossRef]

7. Said, S.; Spindler, K.; El-Shaarawi, M.; Siddiqui, M.; Schmid, F.; Bierling, B.; Khan, M. Design, construction and operation of a solar powered ammonia–water absorption refrigeration system in Saudi Arabia. *Int. J. Refrig.* **2016**, *62*, 222–231. [CrossRef]

8. Calise, F.; Libertini, L.; Vicidomini, M. Design and optimization of a novel solar cooling system for combined cycle power plants. *J. Clean. Prod.* **2017**, *161*, 1385–1403. [CrossRef]

9. Neyer, D.; Ostheimer, M.; Hauer, N.; Halmdienst, C.; Pink, W. Application of an adapted single-/half-effect NH_3/H_2O absorption chiller in tri-generation and solar cooling systems. *Sol. Energy* **2018**, *173*, 715–727. [CrossRef]

10. Aman, J.; Ting, D.-K.; Henshaw, P. Residential solar air conditioning: Energy and exergy analyses of an ammonia–water absorption cooling system. *Appl. Therm. Eng.* **2014**, *62*, 424–432. [CrossRef]

11. Bellos, E.; Tzivanidis, C.; Antonopoulos, K.A. Exergetic, energetic and financial evaluation of a solar driven absorption cooling system with various collector types. *Appl. Therm. Eng.* **2016**, *102*, 749–759. [CrossRef]

12. Fong, K.; Chow, T.; Lee, C.; Lin, Z.; Chan, L. Comparative study of different solar cooling systems for buildings in subtropical city. *Sol. Energy* **2010**, *84*, 227–244. [CrossRef]

13. Al-Falahi, A.; Alobaid, F.; Epple, B. A New Design of an Integrated Solar Absorption Cooling System Driven by an Evacuated Tube Collector: A Case Study for Baghdad, Iraq. *Appl. Sci.* **2020**, *10*, 3622. [CrossRef]

14. Galindo-Luna, Y.R.; Franco, W.R.G.; Carrasco, U.D.; Romero, R.; Jiménez-García, J.C. Integration of the Experimental Results of a Parabolic Trough Collector (PTC) Solar Plant to an Absorption Air-Conditioning System. *Appl. Sci.* **2018**, *8*, 2163. [CrossRef]

15. Cabrera, F.; Fernández-García, A.; Silva, R.; Pérez-García, M. Use of parabolic trough solar collectors for solar refrigeration and air-conditioning applications. *Renew. Sustain. Energy Rev.* **2013**, *20*, 103–118. [CrossRef]

16. Jakob, U.; Eicker, U.; Schneider, D.; Taki, A.; Cook, M. Simulation and experimental investigation into diffusion absorption cooling machines for air-conditioning applications. *Appl. Therm. Eng.* **2008**, *28*, 1138–1150. [CrossRef]

17. Qu, M.; Yin, H.; Archer, D.H. A solar thermal cooling and heating system for a building: Experimental and model based performance analysis and design. *Sol. Energy* **2010**, *84*, 166–182. [CrossRef]

18. Tzivanidis, C.; Bellos, E. The use of parabolic trough collectors for solar cooling–A case study for Athens climate. *Case Stud. Therm. Eng.* **2016**, *8*, 403–413. [CrossRef]

19. Molero-Villar, N.; Cejudo-López, J.; Domínguez-Muñoz, F.; Carrillo-Andrés, A. A comparison of solar absorption system configurations. *Sol. Energy* **2012**, *86*, 242–252. [CrossRef]

20. Said, S.A.; El-Shaarawi, M.A.; Siddiqui, M.U. Alternative designs for a 24-h operating solar-powered absorption refrigeration technology. *Int. J. Refrig.* **2012**, *35*, 1967–1977. [CrossRef]

21. Abdelhay, A.; Fath, H.; Nada, S. Solar driven polygeneration system for power, desalination and cooling. *Energy* **2020**, *198*, 117341. [CrossRef]

22. Leiva-Illanes, R.; Escobar, R.; Cardemil, J.M.; Alarcón-Padilla, D.-C. Comparison of the levelized cost and thermoeconomic methodologies–Cost allocation in a solar polygeneration plant to produce power, desalted water, cooling and process heat. *Energy Convers. Manag.* **2018**, *168*, 215–229. [CrossRef]

23. Al-Falahi, A.; Alobaid, F.; Epple, B. Design and Thermo-Economic Comparisons of an Absorption Air Conditioning System Based on Parabolic Trough and Evacuated Tube Solar Collectors. *Energies* **2020**, *13*, 3198. [CrossRef]

24. Salehi, S.; Yari, M.; Rosen, M. Exergoeconomic comparison of solar-assisted absorption heat pumps, solar heaters and gas boiler systems for district heating in Sarein Town, Iran. *Appl. Therm. Eng.* **2019**, *153*, 409–425. [CrossRef]

25. Marc, O.; Sinama, F.; Praene, J.-P.; Lucas, F.; Castaing-Lasvignottes, J. Dynamic modeling and experimental validation elements of a 30 kW $LiBr/H_2O$ single effect absorption chiller for solar application. *Appl. Therm. Eng.* **2015**, *90*, 980–993. [CrossRef]

26. Zhai, X.; Li, Y.; Cheng, X.; Wang, R. Experimental Investigation on a Solar-powered Absorption Radiant Cooling System. *Energy Procedia* **2015**, *70*, 552–559. [CrossRef]

27. López-Villada, J.; Ayoua, D.S.; Bruno, J.C.; Coronas, A. Modelling, simulation and analysis of solar absorption power-cooling systems. *Int. J. Refrig.* **2014**, *39*, 125–136. [CrossRef]

28. Available online: https://webbook.nist.gov/chemistry/name-ser/ (accessed on 3 February 2020).

29. Vakiloroaya, V.; Ha, Q.; Skibniewski, M.J. Modeling and experimental validation of a solar-assisted direct expansion air conditioning system. *Energy Build.* **2013**, *66*, 524–536. [CrossRef]

30. Carles Bruno, J.; Ló pez-Villada, J.; Letelier, E.; Romera, S.; Coronas, A. *Modelling and Optimisation of Solar Organic Rankine Cycle Engines for Reverse Osmosis Desalination*; Elsevier: Amsterdam, The Netherlands, 2008.

31. Nafey, A.S.; Sharaf, M.A.; García-Rodríguez, L. *A New Visual Library for Design and Simulation of Solar Desalination Systems (SDS)*; Elsevier: Amsterdam, The Netherlands, 2010.

32. Eldean, M.A.S.; Soliman, A.M. A new visual library for modeling and simulation of renewable energy desalination systems (REDS). *Desalin. Water Treat.* **2013**, *51*, 6905–6920. [CrossRef]

33. Singh, R.; Kumar, D.R. Theoritical Analysis of Nh_3-H_2o Refrigeration System Coupled with Diesel Engine: A Thermodynamic Study. *IOSR J. Mech. Civ. Eng.* **2014**, *11*, 29–36. [CrossRef]

34. Vanderzee, E.C.; King, D.L. The enthalpies of solution and formation of ammonia. *J. Chem. Thermodyn.* **1972**, *4*, 675–683. [CrossRef]

35. Ge, Y.; Tassou, S.; Chaer, I. Modelling and performance evaluation of a low-temperature ammonia-water absorption refrigeration system. *Int. J. Low-Carbon Technol.* **2009**, *4*, 68–77. [CrossRef]

36. Shankar Ganesh, N.; Srinivas, T. Evaluation of thermodynamic properties of ammonia/water mixture up to 100bar for power application systems. *J. Mech. Eng. Res.* **2011**, *3*, 25–39.

37. Li, K.W. *Applied Thermodynamics: Availability Method and Energy Conversion*; CRC Press: Boca Raton, FL, USA, 1995.

38. Sharaf, M.A. Design and Simulation of Solar Desalination Systems. Ph.D. Thesis, Suez Canal University, Ismailia Governorate, Egypt, 2011.

39. Sharaf, M.A.; Nafey, A.S.; García-Rodríguez, L. *Author's Personal Copy Thermo-Economic Analysis of Solar Thermal Power Cycles Assisted MED-VC (Multi Effect Distillation-Vapor Compression) Desalination Processes*; Elsevier: Amsterdam, The Netherlands, 2011.

40. Sharaf, M.; Nafey, A.; Desalination, L.G.-R. *Exergy and Thermo-Economic Analyses of A Combined Solar Organic Cycle with Multi Effect Distillation (MED) Desalination Process*; Elsevier: Amsterdam, The Netherlands, 2011.

41. Castro, M.M.; Song, T.W.; Pinto, J.M. Minimization of operational costs in cooling water systems. *Chem. Eng. Res. Des.* **2000**, *78*, 192–201. [CrossRef]

Publisher's Note: MDPI stays neutral with regard to jurisdictional claims in published maps and institutional affiliations.

Paper D

Article

Thermo-Economic Comparisons of Environmentally Friendly Solar Assisted Absorption Air Conditioning Systems

Adil Al-Falahi *, Falah Alobaid and Bernd Epple

Institute for Energy Systems and Technology, Technical University Darmstadt, Otto-Berndt-Straße 2,
64287 Darmstadt, Germany; falah.alobaid@est.tu-darmstadt.de (F.A.); bernd.epple@est.tu-darmstadt.de (B.E.)

* Correspondence: adil.al-falahi@est.tu-darmstadt.de; Tel.: +49-6151-16-20724; Fax: +49-0-6151-16-22690

Abstract: Absorption refrigeration cycle is considered a vital option for thermal cooling processes. Designing new systems is needed to meet the increasing communities' demands of space cooling. This should be given more attention especially with the increasing conventional fossil fuel energy costs and CO_2 emission. This work presents the thermo-economic analysis to compare between different solar absorption cooling system configurations. The proposed system combines a solar field, flashing tank and absorption chiller: two types of absorption cycle H_2O-LiBr and NH_3-H_2O have been compared to each other by parabolic trough collectors and evacuated tube collectors under the same operating conditions. A case study of 200 TR total cooling load is also presented. Results reveal that parabolic trough collector combined with H_2O-LiBr (PTC/H_2O-LiBr) gives lower design aspects and minimum rates of hourly costs (5.2 \$/h) followed by ETC/H_2O-LiBr configuration (5.6 \$/h). H_2O-LiBr gives lower thermo-economic product cost (0.14 \$/GJ) compared to the NH_3-H_2O (0.16 \$/GJ). The absorption refrigeration cycle coefficient of performance ranged between 0.5 and 0.9.

Keywords: thermo-economic; aqua-ammonia; lithium bromide-water; absorption systems; design; solar collectors

1. Introduction

Today, the substitution of traditional energy sources by renewable ones has becomes urgently needed for the clean and sustainable development of the energy sector worldwide. Climate change, the world's noticeable growth in population number, and the improvement in standard conditions of living make cooling demands to increase significantly. According to the International Institute of Refrigeration reports, approximately 15% of total electricity production in the world is used for refrigeration and air conditioning [1]. About 80% of the global electricity is produced from fossil fuels, which increases the emissions of greenhouse gases significantly [2]. Solar thermally activated cooling systems are more attractive than the other type because of the near concurrence of peak cooling loads with the available solar power. Taking into account the deficiency in electrical power in most developing countries, all these previous factors make solar cooling technology a suitable and clean alternative for a big problem. Current studies of solar thermal cooling technology should strive to realize modern, low-cost, energy-efficient, high-temperature collectors, and to develop a high-performance, low-temperature enabled air conditioning technology [3]. In particular, there has to be a determination to find the optimal operational capabilities that make the optimum total performance of the device to be reached despite the apparent specific use of high-efficiency technology. Today, absorption chillers are the most mature technology. Therefore, solar thermal absorption cooling units might be a great option to reduce the usage of electricity in cooling and obtain economic gains [4–6].

There are different technologies to produce cold (cooling of industrial processes, conservation of products, air conditioning, etc.) with solar energy (and with solar thermal energy in particular). Syed et al. [7] performed a simple economic analysis comparing eight different configurations of solar cooling systems. These configurations contemplated reasonable combinations of refrigeration (ejector, compression, and absorption) and solar electric drive (with photovoltaic collectors) or thermal drive (flat plate collectors FPC, evacuated tube collector ETC, and parabolic through collector PTC). They concluded that solar thermal systems using absorption refrigeration are the most economical; in particular those with low temperature (flat collectors coupled with single-effect absorption), solar collectors account for the highest life cycle costs in all the configurations analyzed.

In the solar thermal sector, the main technologies integrated with absorption cooling systems are FPC, ETC, and PTC [8]. Parabolic through collectors have been analyzed in many types of research through single impact absorption cycles. Li et al. [9] inspected experimentally the performance of this configuration for Kunming, China, and they concluded that 56 m² of PTCs can drive H2O-LiBr absorption cycle with 6 TR cooling capacity to serve the cooling requirements of a meeting room of 102 m². Besides this, they analyzed appropriate methods for improving cooling performance. In Iran, Mazloumi et al. [10] proved that 57.6 m² of PTC, storage tank of 1.26 m³ equipped with absorption system can satisfyingly meet building cooling load. The system operated from 6:00 to 19:00**.**

Shirazi et al. [11] compared three configurations of H2O-LiBr solar absorption cooling system with TRNSYS 17. The first one was a single effect absorption integrated with ETC. The second and third configurations were double and triple effect systems, respectively, with PTC. The results revealed that the use of multi-effect absorption solar cycles was not advantageous over single-effect solar systems when the fraction of direct normal irradiation is less than 60% of the total global solar irradiation. Furthermore, the analysis of cost results indicated that a fraction of minimum direct normal irradiation of about 70% was required for solar-powered multi-effect cooling systems in order to be cost-effective in comparison to single-effect solar cooling systems.

The use of ETC to provide refrigeration in Saudi Arabia has been examined by Khan et al. [12], and they demonstrated that the use of 116 m² of ETC can lead to satisfying results with 10 kW cooling capacity of NH3–H2O absorption refrigeration system.

Rajasekar et al. [13] examined a single effect NH3-H2O chiller of one KW, which was using an evacuated tube solar collector. They deduced that the optimum coefficient of performance (COP) was accomplished at the temperature of the generator of 83.2 °C and while the evaporator temperature was 23.59 °C. A comparison was achieved among their accomplished COP values with standard absorption solar cooling systems.

Flores et al. [14] compared the operation of the absorption cooling system with different working pairs and presented a computer program to study H2O-LiBr, NH3-H2O, and the other four pairs' performance. They found that due to crystallization problems, the H2O-LiBr pair operates at a small range of vapor temperature operation specifically at generator temperature of 75–95 °C. In the case of the NH3-H2O system, the range of generator temperature was 78–120 °C. The condenser, evaporator, and absorber temperatures were 40 °C, 10 °C, and 35 °C, respectively, for a cooling load of 1 kW for each working pair.

Many researchers have carried out exergetic analysis studies for different thermal solar absorption cooling systems. Gebreslassie et al. [15] studied an exergy analysis for all components in the absorption cycle. They found that the largest exergy destruction occurs at the absorbers and generators. In the same regard, Kilic et al. [16] utilized the first and second laws of thermodynamics to develop a mathematical model for single stage H2O-LiBr refrigeration cycle and they proved that the system COP increases with the increase of generator and evaporator temperature, while system COP decreases as condenser and absorber temperature increases. In the same regard, Ahmet Karkas et al. [17] carried out energy analysis for absorption cooling cycles and states that, above 0 °C, the cycles of H2O-LiBr cooling are more effective based on thermodynamics laws. Dincer et al. [18]

investigated procedures of calculating the total exergy, both chemical and physical exergy for the absorption cooling system, using the realization of a series of programming algorithms, with the help of the correlations supplied in the Engineering Equation Solver (EES).

Related to thermo-economics, Lu and Wang [19] analyzed economically three types of solar cooling systems. The first one was an adsorption system integrated with ETC solar collector the cycle employing water and silica gel as a working solution. The second system was a single-effect (H_2O-LiBr) absorption system connected by an efficient compound parabolic concentrating solar collector. Finally, the last system was a double-effect (H_2O-LiBr) absorption cycle equipped with PTC. They deduced that the third system had the highest solar coefficient of performance (COP). They also concluded that the cooling chiller can be driven at an ambient temperature of 35 °C from 14:30 to 17:00.

In recent years, the studies that have contributed to the improvement of the performance of absorption systems are related to hybrid absorption. Colorado and Rivera [20] have compared various refrigeration systems by vapor compression with a hybrid system(compression/absorption) based on the 1st and 2nd laws of thermodynamics; in the compression cycle, they utilized R134a and CO_2 as refrigerants, and for absorption cycle, they used H_2O-LiBr as an operating mixture. The hybrid system has a cascade heat exchanger, in this case, the condenser of the compression cycle is considered the evaporator of the absorption cycle. The study aims to enhance the efficiency and reduce the energy consumption in the compressor. The research results show that the hybrid system consumes 45% less electricity than the simple compression cycle. Likewise, the coefficient of performance (COP) achieved with the hybrid system was higher with R134a refrigerant.

A major benefit of the absorption cooling system is the opportunity to use different heat sources to drive the generator of absorption. Wang et al. [21] investigated the optimal heat sources for different absorption cooling system applications. The heat released from the exhaust gases of boilers, internal combustion engines, and gas turbines could be utilized as a heat source for an absorption system. Du et al. [22] constructed a prototype of a single-stage NH_3-H_2O cooling system that operated with a heat discarded from a diesel engine through an active open-pipe heating method, which was designed to provide a uniform amount of available heat. The authors designed the heat exchanger to recover energy discarded for a specific capacity, combining the processes of condensation and absorption in a refrigeration unit by circulating a solution that had been previously cooled.

Finally, two latest thermo-economic comparative studies by authors in this field need to be mentioned [23,24], which compared the use of ETC and PTC integrated with H_2O-LiBr and/or NH_3-H_2O absorption chiller energetically and financially. They found that, generally, PTC in both cases (PTC-H_2O-LiBr/NH_3-H_2O) is the best option with large capacities and the use of (ETC-H_2O-LiBr/NH_3-H_2O) as a next alternative.

The previous literature review states that there are a lot of investigations on thermal absorption cooling systems field and most of them deal with LiBr-H_2O or H_2O-NH_3 as working pairs, and that most of them used traditional absorption cycles. Numerous ideas on thermodynamic and economic studies are being examined. In general, for each comparative research, only one technique was investigated. In this direction, this work is a comparative analysis of four common solar thermal cooling systems. More specifically, it compares the use of two kinds of collectors (ETC and PTC) for the solar part and the absorption cycles H_2O-LiBr and NH_3-H_2O with each other under the same operating conditions.

The innovation of this work has arisen from the method of combination of solar field and absorption cycle by using flash tank as the investigated thermal enhancement method. To the authors' knowledge, no article available in literature has dealt with the proposed integration from that side, and in general, comparative researches are restricted. Therefore, this work is innovative because it systematically presents a comparison between four configurations. The solar cooling plant introduced in this work is suitable for

medium and high loads of cooling. This may be reasonable for coastal and tourist spots along with the solar beam areas like the Middle East, North Africa (MENA), and Gulf regions.

The main objective of this work is to improve and compare between the various configuration of absorption refrigeration cycles by various solar thermal collectors. In this sense, steady-state energetic, exergetic, cost, and design techniques of modeling are performed for an absorption cooling system powered by solar energy. The optimal operating condition of the system is reported as well. The following outlines were withdrawn in this work:

- Two different types of absorption cycles in different working conditions were studied. The selection process involved the optimum operating conditions.
- Comparison was made of two different types of solar thermal collectors when combined with an absorption chiller.
- The mathematical model has been carried out in detail.
- The comparison was performed based on the terms of energy, exergy, design, cost, and thermo-economic. Design technique of modeling has been adopted in this study.
- Based on the optimized selection, a detailed case study was performed for a cooling load of 700~800 kW.

2. System Description

As mentioned previously, the proposed system combines two systems: a solar power system and an absorption air conditioning (AAC) system. The solar power system includes a thermal solar collector and flash tank. Basically, the plant is driven by solar energy. The current proposed absorption cooling systems (H2O-LiBr/NH3-H2O) integrated with (PTC/ETC) are displayed in Figure 1.

Solar field loop combines a set of PTCs or ETCs. Water is employed as a working fluid. Solar radiation is collected and concentrated on the water by solar collectors. In simulation, solar intensity is assumed to be constant to accomplish the steady-state condition. Subsequently, the water with high temperature enters the flash tank to generate steam, and the condensed water is collected in the bottom of the flash tank and then back to the solar collector's field via the heat release. The AAC unit is a single-stage H2O-LiBr or NH3-H2O type. Flash tank steam condensation in the AAC generator results in the boiling of the solution and separation of the refrigerant (water or ammonia vapor). At the generator outlet, there is a two-phase flow. The steam phase involves the vapor of the refrigerant, which moves forward into a condenser unit; the liquid phase is a mixture (absorbent-refrigerant) with a low concentration of refrigerant (strong solution). Then, this solution is returned through a throttle valve to the absorber. In the AAC condenser, heat is removed from the refrigerant to the cooling water. The refrigerant is then throttled to fulfill the required temperature at the evaporator in which the chilled water acquires its low temperature needed for the cooling application. Besides this, the heat transfer results in a change in the thermodynamic state of the refrigerant from a saturated mixture of liquid and vapor to superheated vapor. The evaporated refrigerant is cooled, condensed, and mixed with the LiBr or water in the absorber forming a dilute solution. The refrigerant-absorber mixture causes an exothermic reaction, whereby the heat released in this process is discharged from the solution to the other stream via cooling water delivered from the secondary cooling system (air or cooling tower). The absorption process results in a mass flow of diluted solution leaving the absorber. Finally, the dilute solution is pumped back to the generator and so on. To enhance the AAC performance, strong and weak solutions exchange heat through a liquid-liquid heat exchanger. The utilization of the economizer increases the coefficient of performance (COP) by reducing heat released into the absorber and heat delivered to the generator. COP of a single effect system is defined as the relationship between the heat flow eliminated in the evaporator (cooling capacity) vs. the heat

flow into the generator and the energy consumption of the pump. The single effect is represented by the basic absorption cycle, half effect, double effect, triple, and multi-effect absorption cycles. The term "effect" refers to the times that the driving heat is used by the absorption system, and the number of generators refers to the number of effects.
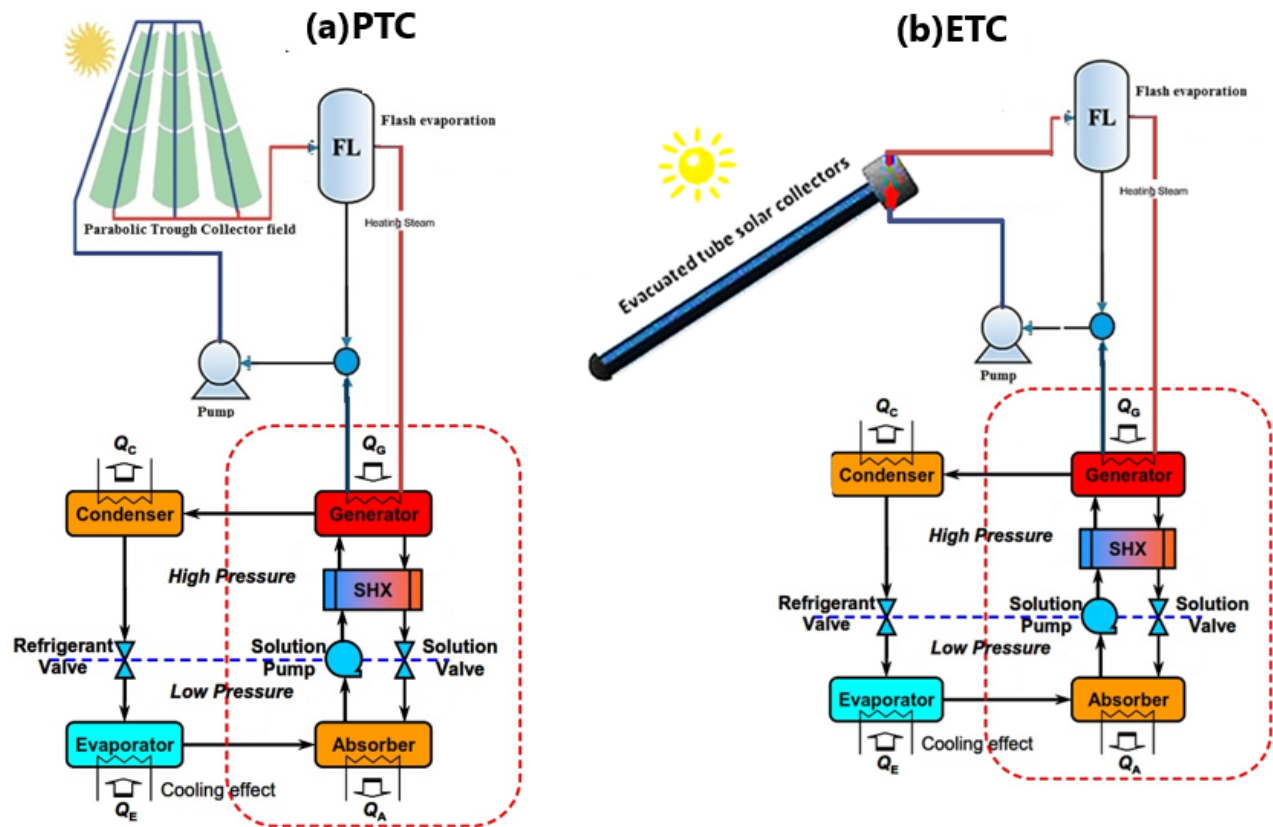

Figure 1. Absorption air-conditioning system integrated with solar thermal collector. (**a**) Parabolic trough collector PTC; (**b**) Evacuated tube collector ETC [24].

3. Methodology, Design Development Software, and Assumptions

The design of an absorption air conditioning cycle (AAC) requires a considerable amount of calculation. This makes it an extremely complex, cumbersome, and time-consuming process. That is why we chose to use software that facilitates it. MATLAB is a powerful software package for scientific computing, focusing on numerical calculations, matrix operations, and especially the applications of science and engineering. It can be used as a simple matrix calculator, but its main interest lies in the hundreds of functions—both general purpose and specialized—that it has, as well as its possibilities for graphic visualization.

In this work, the four configurations proposed model was coded in the MATLAB program, which allows you to establish a numerical method for solving the proposed model and makes it possible to solve the mathematical model of the simulator and provide the obtained results. Since it is a platform that allows making sequences of mathematical calculations, it is possible to model physical phenomena in the form of equations. In order to build the simulator, it is necessary to enter the equations with their respective nomenclatures and establish the criteria to be followed for the resolution of the sequence of steps. The origin of the physical characteristics is taken from the NIST chemistry book on their website [25]. More information about the optimization techniques considered in

this work is given in Refs. [23,24], to minimize techno-economic costs. Table 1 shows parameters considered for the simulation of the four different system proposed configurations. In simulation, solar intensity is assumed to be constant to accomplish the steady-state condition. In all the absorption cycles, the energy input was used in the form of steam. For the thermodynamic, exergetic, and cost analysis, the equations that were applied are described in the following sections.

Table 1. Design data for the solar absorption system configurations [24].

Unit Process	Assigned Data	Calculated Data
Absorption air-conditioning cycle (AAC)/(ETC/PTC)	✓ Solar radiation: 500 W/m² ✓ Ambient temperature:25 °C ✓ Average relative humidity: 15% ✓ ETC top temperature: 100–200 °C ✓ PTC top temperature: 200–300 °C ✓ Absorber temperature: 30–35 °C ✓ Generator temperature: 80–90 °C ✓ Condenser temperature: 40–45 °C ✓ Hot air temperature: 35 °C ✓ Target cooled air temperature: 20 °C ✓ Evaporator temperature: 5–10 °C ✓ Cooling load: 176–700 kW (50–200 TR) ✓ Condenser effectiveness: 80% ✓ Fan system efficiency: 85% ✓ Pumping system efficiency: 75% ✓ Plant life time: 20 years ✓ Interest rate: 5% ✓ Load factor: 90% ✓ Specific electric power cost: 0.065 $/kWh ✓ Water steam is the solar field working fluid	**Solar Field:** ➤ Solar field top pressure, bar ➤ Solar field pressure loss, bar ➤ Total solar field area, m² ➤ Solar field thermal load, kW ➤ Number of solar collectors, # ➤ Solar field mass flow rate, kg/s ➤ Solar field inlet temperature, °C ➤ Efficiency, % ➤ Exergy destruction, kW **Flash Tank:** ➤ * Flash tank design data ➤ Total mass flow rate, kg/s ➤ Dryness fraction, % ➤ Flash tank water flow rate, kg/s ➤ Steam flow rate, kg/s ➤ Exergy destruction, kW **AAC Unit:** ➤ Weak & strong solutions, kg/s ➤ * Design data ➤ Thermal power, kW ➤ Total cycle flow rate, kg/s ➤ Generator power, kW ➤ Cooling fan power, kW ➤ Coefficient of performance (COP) ➤ COPmax ➤ Relative performance ➤ Exergy destruction, kW **Pump:** ➤ Power, kW ➤ Outlet temperature, °C ➤ Exergy destruction, kW **Cost & Performance:** ➤ Units hourly costs, $/h ➤ Total hourly costs, $/h ➤ Total power, kW ➤ LPC, $/kWh ➤ Thermo-economic cost, $/GJ ➤ Total exergy destruction rate, kW

- Data are run out based on steady-state operating conditions.
- Ambient temperature is fixed as 25 °C for all process runs.
- Solar radiation is fixed at 500 W/m².
- * Design data means area, length, width, etc.

4. Mathematical Model

The studied system components are modeled and simulated depending on both first and second laws of thermodynamics. As a first step in modeling this system, the study is implemented depending on steady state basis at a constant value of solar radiation intensity. An explanation of the mathematical model of each part is clarified in the following sub-sections.

4.1. ETC Modeling

An immediate efficiency of the ETC solar collector can be calculated by the solar irradiance, average collector temperature, and environmental temperature based on its characteristic curve. For ETC, the curve adopted is specified by Equation (1) [26,27].

$$\eta_{etc} = \eta_o - a_1 \left(\frac{T_o - T_{amb}}{I_s} \right) - a_2 \left(\frac{T_o - T_{amb}}{I_s} \right)^2 . I_s \tag{1}$$

where, η_{etc} is the ETC efficiency, $\eta_o = 0.665$, $a_1 = 2.9$ W/m². °C, $a_2 = 0.0019$ W/m². °C², I_s is the solar flux (W/m²), T_o is the exit top temperature of the collector (°C), and T_{amb} (°C) is the ambient temperature. The thermal load of the collector Q_{th} (kW) is calculated according to Equation (2).

$$Q_{th} = M_{col}^{\cdot} \times C_p \times (T_o - T_i) \tag{2}$$

where, $M_{col}^{\cdot}$ is the mass flow rate in kg/s.

The total surface area of the collector A_t(m²), is calculated from the equation of the energy balance of the collector as a dependency of the efficiency using:

$$A_t = \frac{Q_{th}}{\eta_{etc} \times I_s} \tag{3}$$

The aperture area of the ETC module A_{etc}, m², can be calculated as:

$$A_{etc} = D_t \times L_t \times NOT \tag{4}$$

where, D_t and L_t is the diameter and length of the tube in (m), respectively, and NOT is the tube numbers of each module. The total number of ETCs, NOC could be estimated from the following relation:

$$NOC = \frac{A_t}{A_{etc}} \tag{5}$$

The loops number NOL, area of the loop A_{loop}, and the length of each loop, L_{loop} could be computed by allocating the hydraulic mass flow rate M_{hyd}, kg/s.

$$NOL = \frac{M_{col}^{\cdot}}{M_{hyd}} \tag{6}$$

$$A_{loop} = \frac{A_t}{NOL} \tag{7}$$

$$L_{loop} = \frac{A_{loop}}{L_t} \tag{8}$$

4.2. PTC Modeling

For the medium-high temperature of PTCs, the relevant efficiency can be found in Equation (9) [27]:

$$\eta_{ptc} = \eta_o - a_{11}(T_o - T_{amb}) - a_{21}\left(\frac{T_o - T_{amb}}{I_s}\right) - a_{31}\left(\frac{T_o - T_{amb}}{I_s}\right)^2 \tag{9}$$

where, a_{11} = 4.5 × 10⁻⁶ 1/ °C, a_{21} = 0.039 W/m². °C, a_{31} = 3 × 10⁻⁴ W²/m². °C², η_o = 0.75.

The thermodynamic performance of a PTC is expressed as:

$$\eta_{PTC} = \frac{Q_u}{A_{PTC} \times I_s} \tag{10}$$

where, η_{PTC} is the collector thermal efficiency; Qu is the useful thermal power (W); A_{PTC} is the aperture area of the collector (m²); and Is is the solar radiation (W/m²). Modifying Equation (10) results in Equation (11):

$$A_{PTC} = \frac{Q_u}{\eta_{PTC} \times I_s} \tag{11}$$

The ground area necessary for solar collector implementation, however, is larger than the collector's aperture area. This value ranges from about three to four times the collector's aperture area, due to the space between the collectors in addition to the space needed for the pipes and other system accessories. The useful thermal energy of the collectors can exist according to the following relationship:

$$Q_u = \dot{M}_{col} \times \Delta h_{o-i} \tag{12}$$

Here, Δh is the enthalpy difference of through collector in kJ/kg, and $\dot{M}_{col}$ is the mass flow rate in kg/s. The total length of PTC, L_{PTC} is then calculated depending on the width of the collector W_c (m) and the diameter of the glass envelope D_{env} (m):

$$L_{PTC} = \frac{A_{PTC}}{W_c - D_{env}} \tag{13}$$

By identifying the total mass flow rate, which is estimated based on the load of the boiler heat exchanger, and assigning a hydraulic mass flow rate to be the input, the entire number of loops N_{loop}, area of the loop A_{loop}, the width of the loop W_{loop}, and the solar PTC's number ($N_{PTC's}$) are calculated as follows:

$$N_{loop} = \frac{\dot{M}_{col}}{M_{hyd}} \tag{14}$$

$$A_{loop} = \frac{A_{PTC}}{N_{loop}} \tag{15}$$

$$W_{loop} = \frac{A_{loop}}{L_m} \tag{16}$$

where, L_m (m) is assigned as the length of the module.

$$N_{PTC's} = \frac{A_{PTC}}{L_m(W_c - D_{env})} \tag{17}$$

Overall pressure drops P_{tloss} are determined based on the major and minor drops over the length of the field. The general loss-equation is carried out as follows [28,29]:

$$P_{tloss} = N_{loop} \times \Delta P_{loop} \tag{18}$$

where,

$$\Delta P_{loop} = \frac{32 \times f \times L_{loop} \times M_{hyd}^2}{\rho \times \pi^2 \times D_t} \tag{19}$$

D_t is the inner tube diameter(m).

$$f = [(1.82 \times \log Re) - 1.64]^{-2} \tag{20}$$

$$Re = 4 \times \frac{M_{hyd}}{\mu \times \pi \times D_t} \tag{21}$$

4.3. Flash Tank Modeling

The design parameters of the cyclone flash tank have been derived in the following manner:

Tank inlet and outlet tube steam area A_{t_i} is determined according to the velocity of steam V_{st}, m/s, and the density of vapor ρ_v, kg/m³:

$$A_{t_i} = \frac{M_{st}}{\rho_v \times V_{st}} \tag{22}$$

Tube diameter D_t (m):

$$D_t = \left(\frac{A_{t_i} \times 4}{\pi}\right)^{0.5} \tag{23}$$

Height of flash tank H_{fst} (m) [29]:

$$H_{fst} = 7.15 \times D_t \tag{24}$$

Flash tank width W_{fst} (m):

$$W_{fst} = 3.5 \times D_t \tag{25}$$

Flash tank total volume Vol_{fst} (m³):

$$Vol_{fst} = \left(\frac{Pi}{4}\right) \times W_{fst}^2 \times H_{fst} \tag{26}$$

The flashing enthalpy h_{fsh} equals the fluid enthalpy that comes from the solar collector h_{col}, kJ/kg:

$$h_{fsh} = h_{col} \tag{27}$$

The flashing dryness fraction X_{fsh} is used to quantify the amount of water within steam and it is estimated depending on the enthalpy of flashing h_{fsh}, liquid enthalpy h_f, (kJ/kg), and dry vapor enthalpy h_g (kJ/kg):

$$X_{fsh} = \frac{h_{fsh} - h_f}{h_g - h_f} \tag{28}$$

The total mass flow rate M_{total} (kg/s) and non-vaporized water M_w (kg/s) were calculated using Equations (29) and (30), respectively:

$$M_{total} = \frac{M_{st}}{X_{fsh}} \tag{29}$$

$$M_w = \left(1 - X_{fsh}\right) \times M_{total} \tag{30}$$

4.4. Pump Modeling

The work of the pump W_p, kW may be determined using the following relation [30]:

$$W_p = M_{total} \times \frac{\Delta P}{\rho} \times \eta_p \tag{31}$$

where, ΔP (kPa) represents the difference in total pressure and it is computed as:

$$\Delta P = P_{high} + P_{loss} \tag{32}$$

Outlet pump enthalpy h_{po} (kJ/kg):

$$h_{po} = \left(\frac{W_p}{M_{total}}\right) + h_{pi} \tag{33}$$

4.5. Absorption Chiller Modeling

The absorption cycle was developed for a capacity of cooling and specific temperature ranges. Table 1 shows the input parameters considered for the simulation of the absorption chiller. The mathematical model that was developed for the study of single-effect absorption cycles is based on the theory reported by the authors [23,24]. The following assumptions are considered for analyzing absorption systems:

- Analysis is carried out in steady-state conditions.
- The refrigerant leaving the condenser is in a saturated liquid state.
- The refrigerant when leaving the evaporator is in the saturated vapor state.
- Temperature at the outlet of the absorber and the generator belong to mixing equilibrium and the conditions of separation, respectively.
- The pressure drops through the pipes and heat exchangers are negligible.
- The heat exchange among the system and the environment are negligible.

The thermodynamic analysis model of the absorption cycle components is done with the help of basic balances, mass balance, energy balance, and solution phase equilibrium, and the general formulation are listed as follows:

$$\sum m_i - \sum m_o = 0 \tag{34}$$

$$\sum m_i x_i - \sum m_o x_o = 0 \tag{35}$$

$$\sum m_i h_i - \sum m_o h_o = 0 \tag{36}$$

where, m, x, and h denote mass, concentration, and enthalpy for inlet (i) and outlet (o) of the component, respectively. The total energy balance for the absorption cycle is specified as follows:

$$Q_e + Q_g = Q_c + Q_a + W_p \tag{37}$$

where, Q_e is the thermal load on the evaporator, kW; Q_g is the heat added to the Generator, kW; Q_c is the heat expelled from the condenser, kW; Q_a is the absorber thermal power, kW; and W_p represents the pump work, kW. For performance calculations, the COP is defined as follows:

$$COP = \frac{Q_e}{Q_g} \tag{38}$$

The max COP of the ideal cycle is given by:

$$COP_{max} = \frac{(T_e + 273.15) \times (T_g - T_a)}{(T_g + 273.15) \times (T_c - T_e)} \tag{39}$$

The relative performance ratio RPR can be estimated as:

$$RPR = \frac{COP}{COP_{max}} \tag{40}$$

From the analysis thermodynamic, data are obtained to obtain thermo-physical properties and to dimension the system components.

4.6. Thermo-Economic Model

In this part, the proposed system is mathematically analyzed to be evaluated it using thermo-economic approach (exergy and cost). Thermo-economic is the branch of engineering that combines exergy analysis and cost principles to provide the system designer or operator with information not available through conventional energy analysis and economic evaluation. Thermo-economic balance for any unit is performed based on exergy and cost balances.

The availability (exergy) and cost have been estimated based on the formulas reported in Ref. [31–35]. The equation of availability for any system is a fixed point; a stable flow process with first and second thermodynamic laws can be applied. By ignorance of kinetic and potential energy alterations, the following equation can be used to describe the form of availability [31]:

$$A_2 - A_1 = A_q + A_w + A_{fi} - A_{fo} - I \tag{41}$$

where, $A_2 - A_1 = 0$ is the change of availability without flow in a steady-state condition; $A_q = \sum_J (1 - T_{amb}/T_J) Q_J$ is the transfer of availability due to heat exchange among the control volume and its surroundings; $A_w = -W_{cv} + P_o(V_2 - V_1)$ is equivalent to negative work value generated by the control volume W_{cv}. In certain instances, though, the control volume has a fixed volume; therefore, A_w can be simplified, and $I = T_{amb}.S_{gen}$ is the destruction availability of the process. Flow availability is specified as $A_{fi,o} = \sum_{i,o} m_{i,o} a_{fi,o}$. Hence, the general form in steady-state condition would become:

$$0 = A_q + A_w + A_{fi} - A_{fo} - I \tag{42}$$

In a conventional economic evaluation, a balance of costs for the total system running in a steady state is established as following [32]:

$$\sum_{out} C^{\cdot} = \sum_{in} C^{\cdot} + Z^{IC\&OM} \tag{43}$$

where, $C^{\cdot}$ is the rating of cost based on in and out streams, and $Z^{IC\&OM}$ are related to capital expenditure and operational and maintenance costs. In the calculation of exergy costs, a cost is identified for every exergy stream. Hence, for the incoming and outgoing matter streams that have attached exergy exchange rates $E_{i,o}$, power $W^{\cdot}$, and the exergy exchange rate assigned to the heat release $E_q^{\cdot}$, Equation (43) can be written as follows:

$$C_{i,o} = c_{i,o} E_{i,o} \tag{44}$$

$$C_w = c_w W^{\cdot} \tag{45}$$

$$C_{\dot{q}} = c_q E_{\dot{q}} \tag{46}$$

where, $c_{i,o}, w, q$ represent the average cost for each unit of exergy in (USD/kJ) for inlet (i), outlet (o), power (w), and energy (q) respectively. The following relationships are used to estimate the costs per hour:

For cost analysis, the amortization factor A_f is computed depend on:

$$A_f = \frac{i.(1+i)^{LTp}}{(1+i)^{LTp} - 1} \tag{47}$$

The collector's estimated cost of investment IC_{col} (USD) is determined according to the area correlation given below:

$$IC_{col} = 150 \times A_{col}^{0.95} \tag{48}$$

The cost of operation and maintenance OMC_{col} is then calculated (USD):

$$OMC_{col} = 0.15 \times IC_{col} \tag{49}$$

Total annual cost TAC_{col} (USD/y) is considered to depend on the parameters of operation and maintenance costs and investment costs, as indicated below:

$$TAC_{col} = (IC_{col} + OMC_{col}) \times A_f \tag{50}$$

Hourly costs are calculated Z_{col} (USD/:

$$Z_{col} = \frac{TAC_{col}}{OH \times 365} \tag{51}$$

where, OH is operating hours (h)

Flashing tank investment cost IC_{fsh} (USD) is calculated according to the total volume of the tank Vol_{fst} correlation:

$$IC_{fsh} = \frac{Vol_{fst} \times 6300}{3.8} \tag{52}$$

The total annual cost TAC_{fsh} USD/y is measured by:

$$TAC_{fsh} = IC_{fsh} \times A_f \tag{53}$$

Hourly costs are calculated Z_{fsh} (USD/h):

$$Z_{fsh} = \frac{TAC_{fsh}}{OH \times 365} \tag{54}$$

Absorption cycle investment cost IC_{aac} (USD), is estimated on the base of the correlation of total area as:

$$IC_{aac} = 150 \times A_{aac}^{0.8} \tag{55}$$

Total annual cost TAC_{aac} (USD/y) is then estimated:

$$TAC_{aac} = IC_{aac} \times A_f, \tag{56}$$

Hourly costs are calculated Z_{aac} (USD/h):

$$Z_{aac} = \frac{TAC_{aac}}{OH \times 365} \tag{57}$$

Pump investment cost IC_p (USD) It is estimated on pump power correlation:

$$IC_p = 3500 \times W_p^{0.47} \tag{58}$$

Total annual cost TAC_p (USD/y) It is estimated on:

$$TAC_p = IC_p \times A_f \tag{59}$$

Hourly costs are calculated Z_p (USD/h):

$$Z_p = \frac{TAC_p}{OH \times 365} \tag{60}$$

Total hourly costs Z_{tot} (USD/hr) It is estimated on all parameters:

$$Z_{tot} = Z_{col} + Z_{fsh} + Z_{aac} + Z_p \tag{61}$$

Total Plant Costs TPC (USD/y) is also identified based on the total annual costs for all units:

$$TPC = TAC_{col} + TAC_{fsh} + TAC_{aac} + TAC_p \tag{62}$$

The cumulative thermo-economic equation is determined based on the expense and exergy flow of the cycles (USD/GJ):

$$c_p = 1000 \times \left(\frac{(W_{tot} \times c_w) + \left(\frac{Z_{tot}}{3600}\right)}{Ex_{fo}} \right) \tag{63}$$

where, c_p is the thermo-economic product cost (USD/GJ), c_w is the energy price in (USD/kWh) (~0.065), and W_{tot} is the cycle power(kW), while Ex_{fo} is the exergy stream outlet from the system to the user (kW).

5. Results and Analysis

The purpose of the simulation study was to indicate which combination of the absorption cycle model and solar thermal collector provides the most accurate information in order to bring the cost down. The investigated unit has never been studied before. Therefore, no experimental data is available, but the complete design can be used for this study. The application of design data promises reliable results. A common problem for numerical studies of a large-scale system capacity is the lack of validation data. One approach to resolve this problem is the usage of very detailed models and special simulation tools. In this study, the detailed design data values from Table 1 were used for the simulation of the solar absorption cooling system.

5.1. Water-Lithium Bromide (H2O-LiBr) Cycle Results

5.1.1. Effect of Top Solar Field Temperature

The simulation data delivers temperature data of solar field at various cooling loads (50–150TR), and at different solar collector working temperature values (100–200 °C for ETC and 200–300 °C for PTC). Figures 2 and 3 depict the obtained results based on the influence of the temperature of the solar collector on the other design parameters, such as mass flow rates, and design aspects. Figures 2a and 3a show the impact of the solar collector temperature on solar field mass flow rate. The mass flow rate shows a strong temperature dependency. Higher temperature of the solar collector also causes a large decline in the mass flow rate of the solar field. The primary cause for this effect was referring to the energy balance throughout the solar field as provided in this partnership. $Q_{th} = \dot{M}_{col} \times C_p \times (T_o - T_i)$.

Even so, in contrast with the ETC, the PTC yielded a lower average mass flow rate dependent on an increase in top temperature. The solar field area also has an increasing influence depending on the temperature rise. This effect is shown in Figures 2b and 3b. The increase in the outlet temperature is quite certain to increase the area of the solar field. However, the PTC is registered less in the total area vs. the ETC. Figures 2c and 3c represent a significant impact on flash tank volume by the increase in solar collector temperature. Even so, in comparison with the ETC, PTC showed low tank volume results.

The total solar thermal energy variations due to the change in the upper temperature of the solar field have been depicted in Figures 2d and 3d. Raising the upper solar field temperature increases solar thermal power in the entire solar field in both cases. The exit temperature is an important value for designing the solar field. For ETC collectors and PTC solar collectors, a temperature level of 150~200 °C and 250~300 °C are suggested in this study. Based on the current obtained results, it is quite interesting to assign the operating temperature as follows:

- $T_a = 35$ °C.
- $T_c = 43$ °C.
- $T_e = 7$~10 °C.
- $T_g = 85$~90 °C.
- ETC $T_{high} = 150$~200 °C.
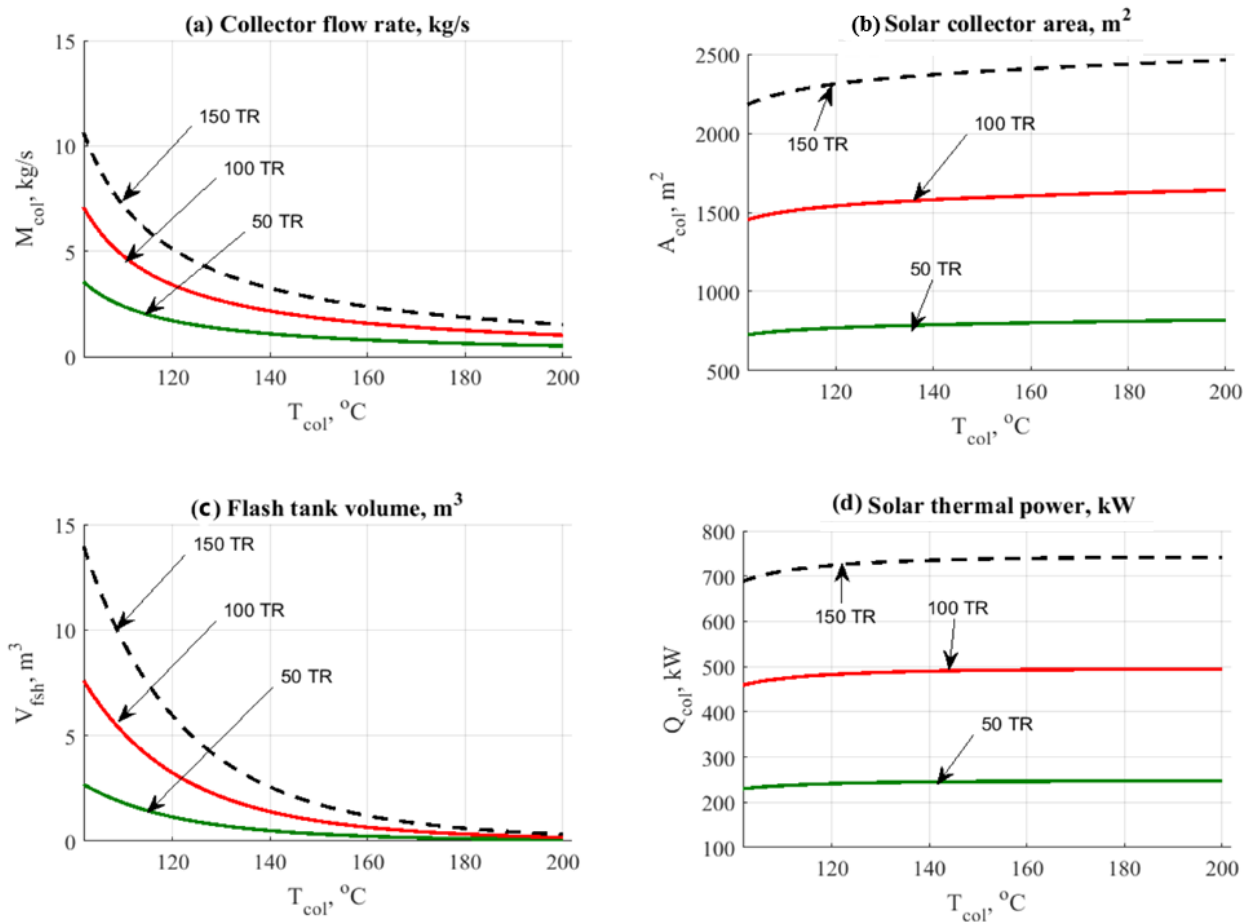- PTC $T_{high} = 250$~300 °C.

Figure 2. Data results for ETC/H2O-LiBr cycle vs. variation in exit upper temperature of the solar field. (a)Collector flow rate. (b)Solar collector area. (c)Flash tank volume. (d)Solar thermal power.
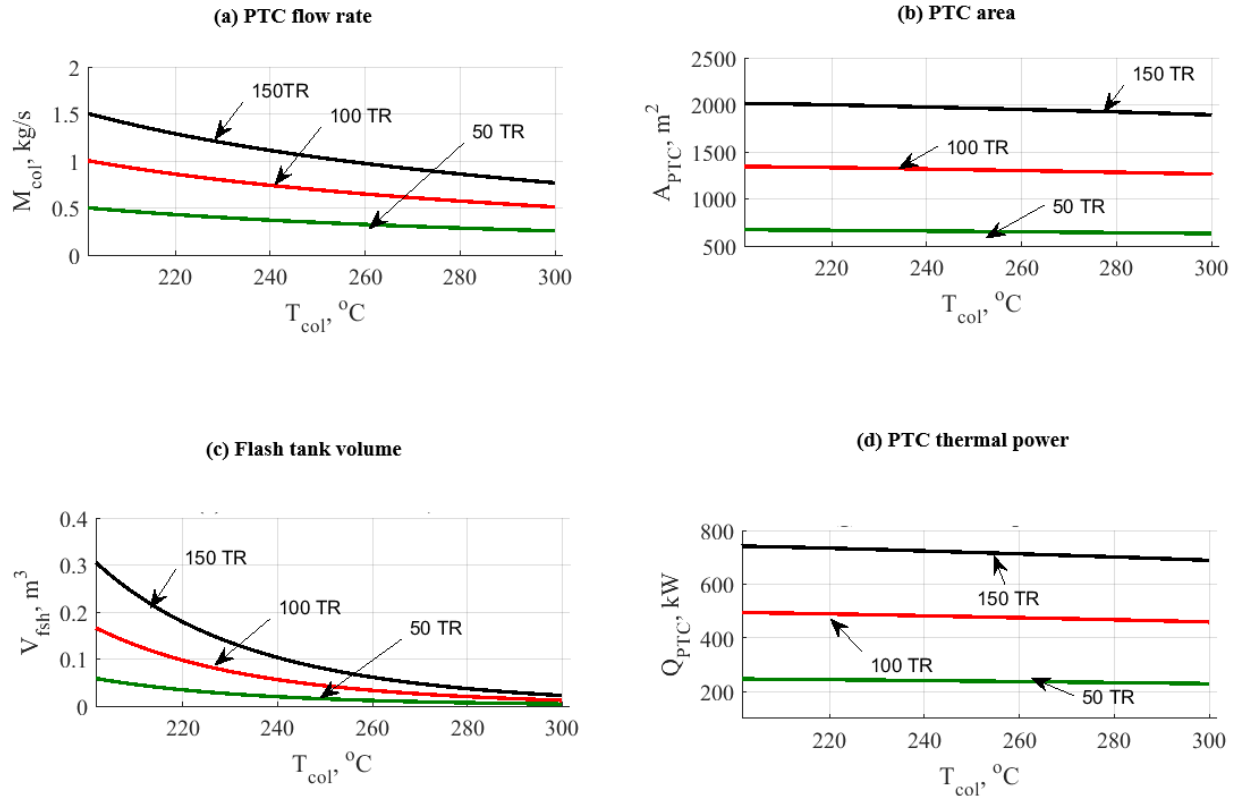
Figure 3. Data results for PTC/H2O-LiBr cycle vs. variation in exit upper temperature of the solar field. (a)Collector flow rate. (b)Solar collector area. (c)Flash tank volume. (d)Solar thermal power.

5.1.2. Effect of Cooling Load

Figures 4 and 5 demonstrate the influence of cooling load on cycles ETC/H2O-LiBr and PTC/H2O-LiBr. The two figures addressed the influence on the costs per hour, the cost of the levelized power, and the cost of the thermo-economic product. The thermo-economic parameter is very important because it reflect the combination between cost and exergy. At the same time, the exergy is also reflecting the maximum available work (gain) that be extracted from any system putting in consideration the entropy generation minimization. As expected, the trend in the figure has been increasing due to the load and energy consumption of all units. The solar collectors showed the largest hourly cost values compared to the corresponding other units, as illustrated in Figures 4a and 5a.

Even so, the PTC is reported to be 12% lower than the ETC associated with the hourly cost variable. The key factor was the rise in the working temperature of the collector (250 °C vs. 150 °C). More steam is produced for the AAC cycle by raising the collector temperature. The influence of increasing cooling load on pumps and flashing tanks is illustrated in Figures 4b and 5b. The figures clearly show that the pumps register slightly higher than the flash tank by the total work required.

Figures 4c and 5c demonstrate the impact of cooling on the cost of levelized power, $/kWh. The outcomes are almost the same depending on the approximate results of the related pumping unit in both configurations. The leveled power cost varied from 0.15 $/kWh to 0.35 $/kWh. A similar close was observed when comparing the cost of the thermo-economic product. For both configurations, the outcomes have been centralized at 0.08 to 0.14~0.16 $/GJ with a minor advantage to the ETC (Figures 4d and 5d). As expected, a higher load will increase the exergy cost. Both PTC and ETC have been identified

as the main reason for such an effect due to the large area that is required for covering the load.
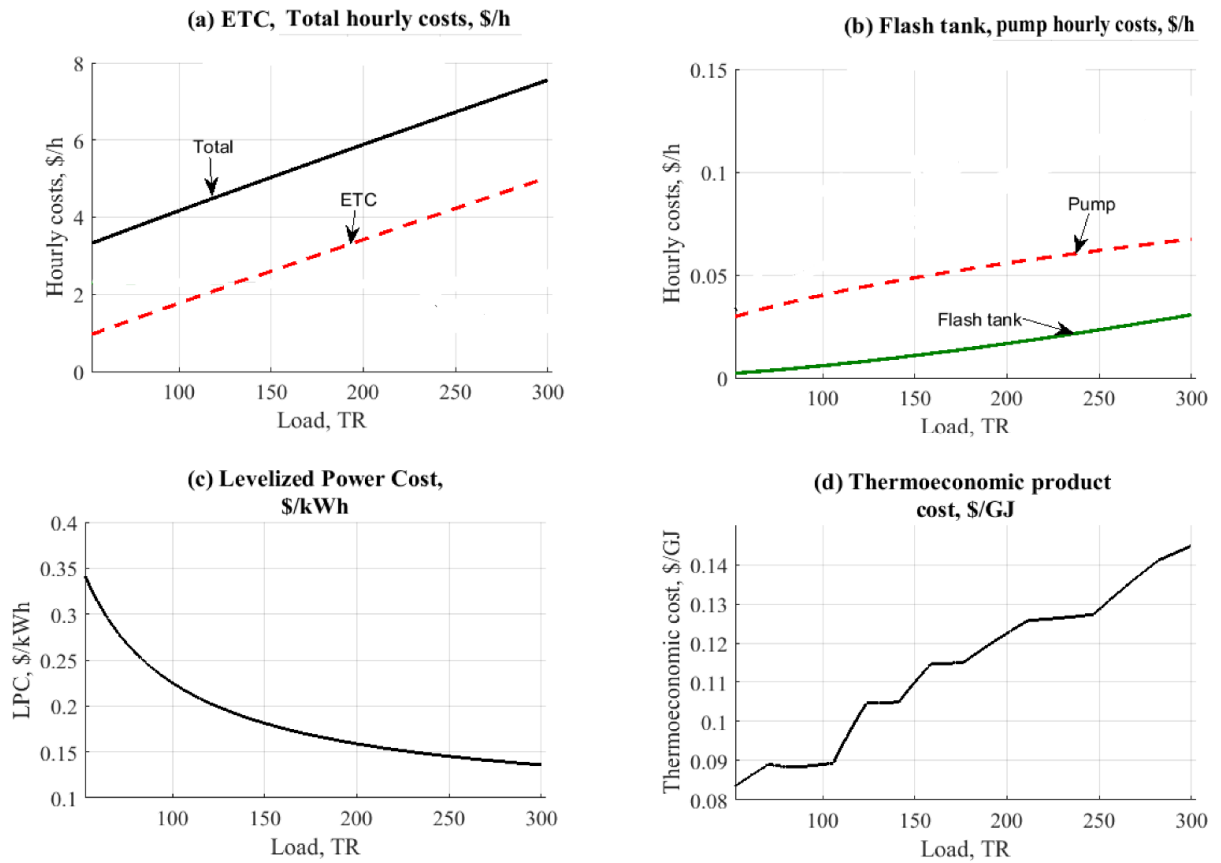

Figure 4. Data results for ETC-H2O-LiBr cycle vs. change in cooling load. (a)ETC total hourly cost. (b)Flash tank and pump hourly cost. (c)Levelized power cost. (d)Thermo-economic product.
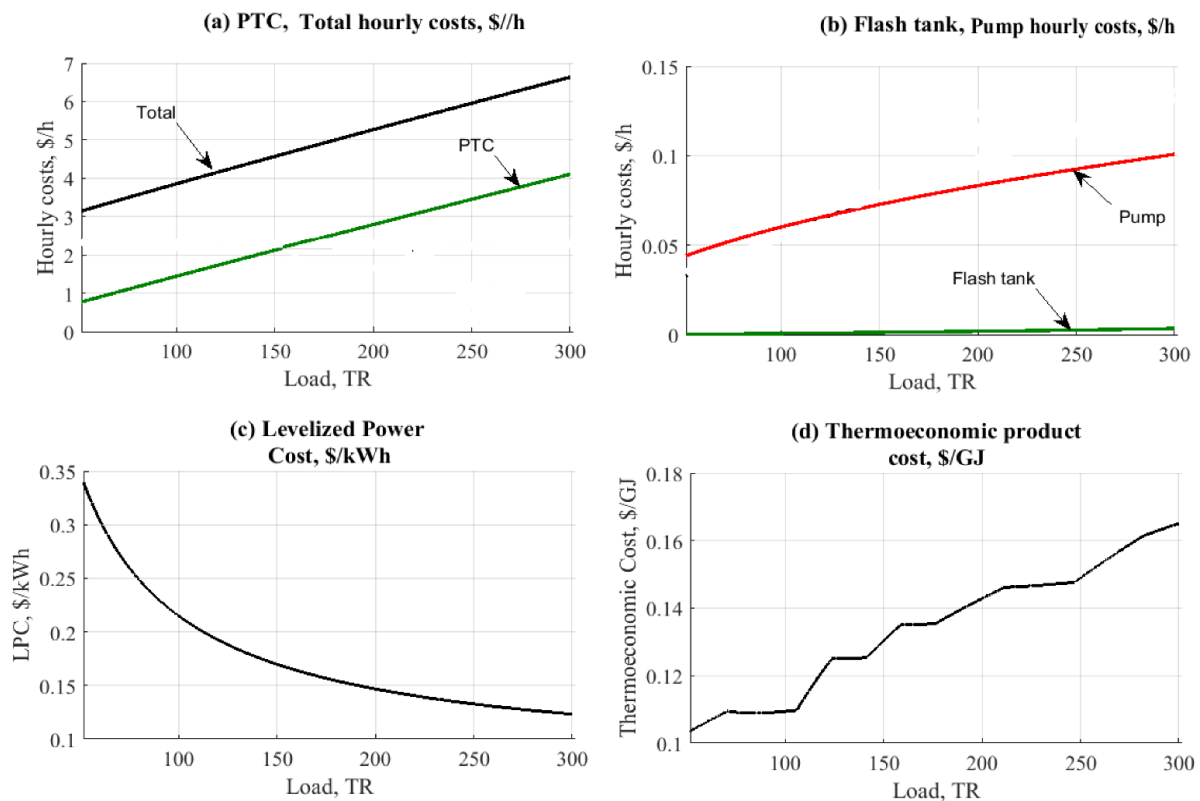
Figure 5. Data results for PTC-H2O-LiBr cycle vs. change in cooling load. (**a**)PTC total hourly cost. (**b**)Flash tank and pump hourly cost. (**c**)Levelized power cost. (**d**)Thermo-economic product.

5.2. Ammonia-Water (NH3-H2O) Cycle Results

5.2.1. Effect of Top Solar Field Temperature (NH3-H2O)

The upper temperature of the solar field is considered a very significant factor within this cycle. Figures 6 and 7 demonstrate the changes in the performance and design variables for both ETC and PTC installations. The temperature range for ETC was 110 °C up to 200 °C. For PTC, the temperature range was 150 °C up to 300 °C.

Figure 6a indicates the influence of the top ETC temperature on the mass flow rate of the solar field. The figure also shows that a rise in the upper temperature reduces the overall mass flow rate in the solar field as a common result of the energy balance. An identical trend was also observed in Figure 7a that depicts the PTC operation. Even so, the PTC granted smaller flow rates, leading to a lower cost. The difference is considerable when comparing 50 kg/s to 300 kg/s @150TR for the ETC and 15 kg/s to 65 kg/s @150TR for the PTC.

Figures 6b and 7b display the influence of solar field temperature on the design area of the solar collectors. The variations on the two figures were not massive, even though the lowest area, i.e., the lowest cost and control is reported for the PTC as anticipated. Raising the temperature of PTC will reduce both the loops and unit numbers as well. The number of loop variables is influenced by the total area of the PTC needed for the load. For instance, the ETC at 150TR would consume around 45,000 m² to 50,000 m². However, the PTC in the same operating conditions will require approximately 45,000 m² down to 40,000 m².

For both situations, the volume of the flash tank has been depicted in Figures 6c and 7c. The distinction is very obvious with the PTC advantage. Increasing the upper-temperature level of the solar field will reduce the volume of the flashing tank., However, the

ETC would require bigger tanks due to a massively lower dryness fraction relative to the PTC process.

For ETC, Figure 6d represents the effect on the thermal power, kW; the rise in working temperature also enhances the solar thermal energy. Figure 7d demonstrates the influence on the thermal power of the PTC. The figure exhibits a descending behavior concerning the upper solar field temperature increase. In general, the increase in AAC unit load would require a larger solar field area, resulting in the mass flow rate increase.

Ranges of 150~200 °C and 250~300 °C are advocated for ETC and PTC solar thermal collectors in this paper. Depending on the latest data achieved, it is quite important to assign the working temperature as follows:

- T_a = 35 °C.
- T_c = 43 °C.
- T_e = 7~10 °C.
- T_g = 85~90 °C.
- ETC T_{high} = 150~200 °C.
- PTC T_{high} = 250~300 °C.

Figure 6. Data results for ETC/NH3- H2O cycle vs. variation in upper temperature of the solar field. (**a**)Collector flow rate. (**b**)Solar collector area. (**c**)Flash tank volume. (**d**)Solar thermal power.
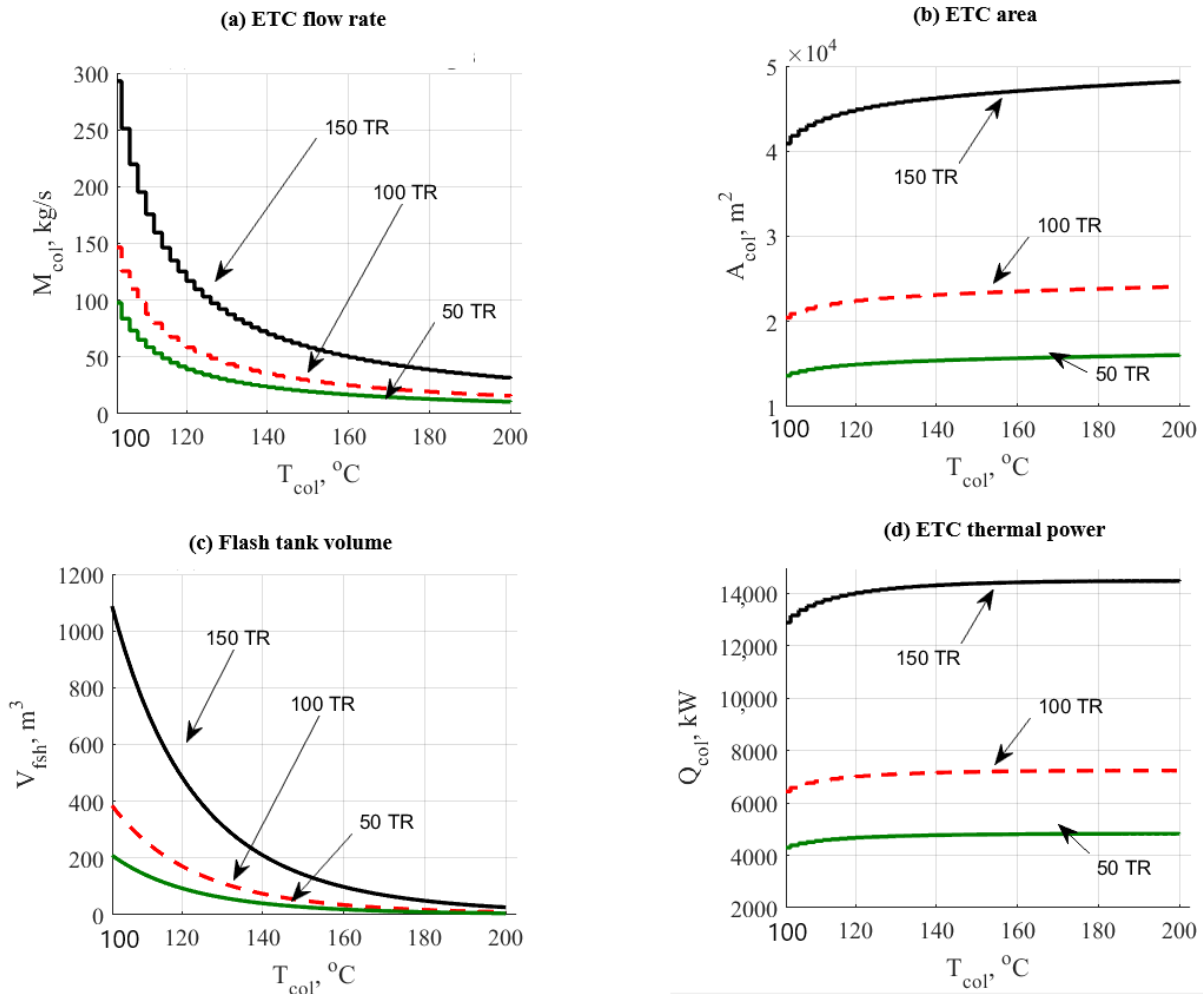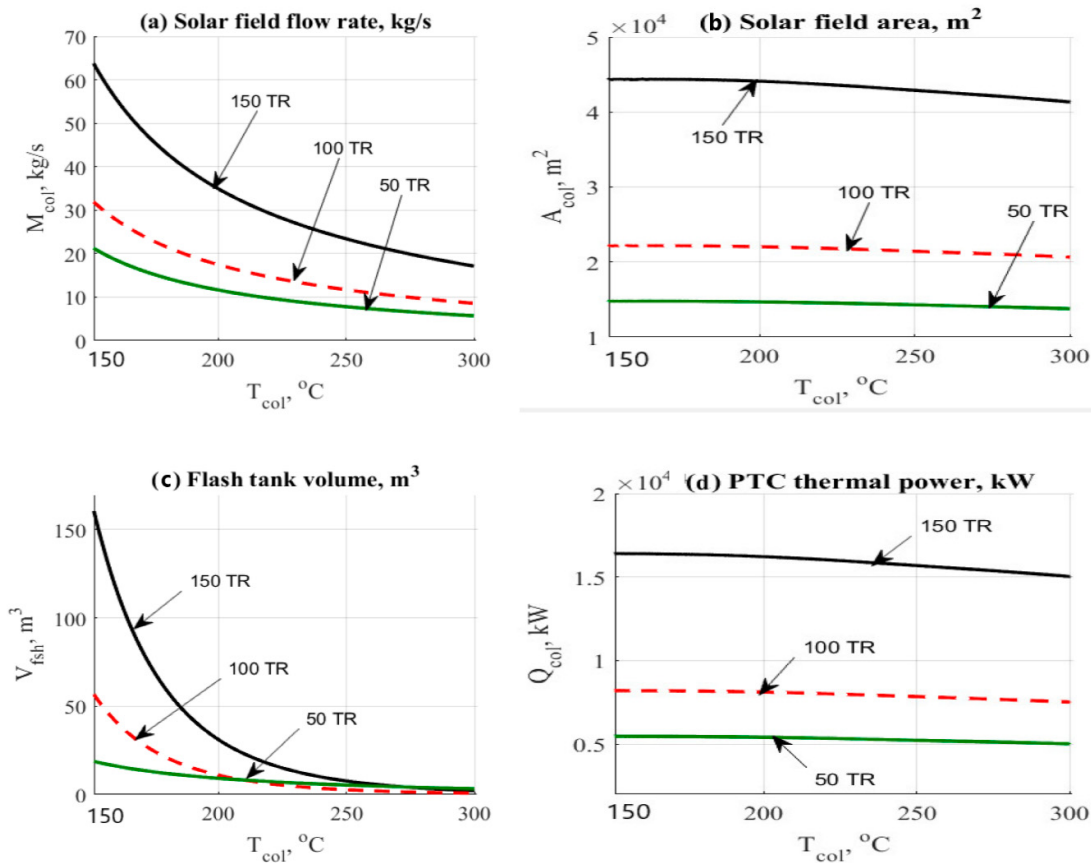
Figure 7. Data results for PTC/NH3- H2O cycle vs. variation in upper temperature of the solar field. (**a**)Collector flow rate. (**b**)Solar collector area. (**c**)Flash tank volume. (**d**)Solar thermal power.

5.2.2. Effect of Cooling Load Effect (NH3-H2O)

The effect of cooling capacity on the ETC-NH3-H2O and PTC-NH3-H2O configurations is illustrated in Figures 8 and 9. The two figures cover the impact on the costs per hour, the cost of the leveled energy, and the cost of the thermo-economic product. The trend in the figure was, as predicted, in a variable mode owing to the energy load and required by all units. The solar collectors showed the largest hourly cost values among the other units as illustrated in Figures 8a and 9a.

However, the PTC was lower by 8% against the ETC, associated with the variable cost of hour metric. This was mainly due to the increase in the collector's working temperature (250 °C vs. 150 °C). The increase in the temperature of the collector would produce further steam for the AAC unit. Pumps and flashing tanks are seen in Figures 8b and 9b. It is clear from the figures that the flashing tank is recorded higher than the pump unit based on the total tank volume. PTC operation was recorded lower in flashing tank hourly cost because it has lower tank volume 0.2–0.3 $/h vs. 0.5–2.2 $/h. Figures 8c and 9c display the impact of cooling capacity on the cost of levelized power rate, $/kWh. The outcomes are almost the same depending on the approximate results of the related pumping unit in both configurations. The leveled power cost varied from 0.07 $/kWh to 0.08 $/kWh for PTC and ETC, respectively. Identical close behavior was observed when compared related to the cost of the thermo-economic product. The results ranged from $0.1 to $1/GJ in both configurations with a smaller advantage for the ETC (Figures 8d and 9d).
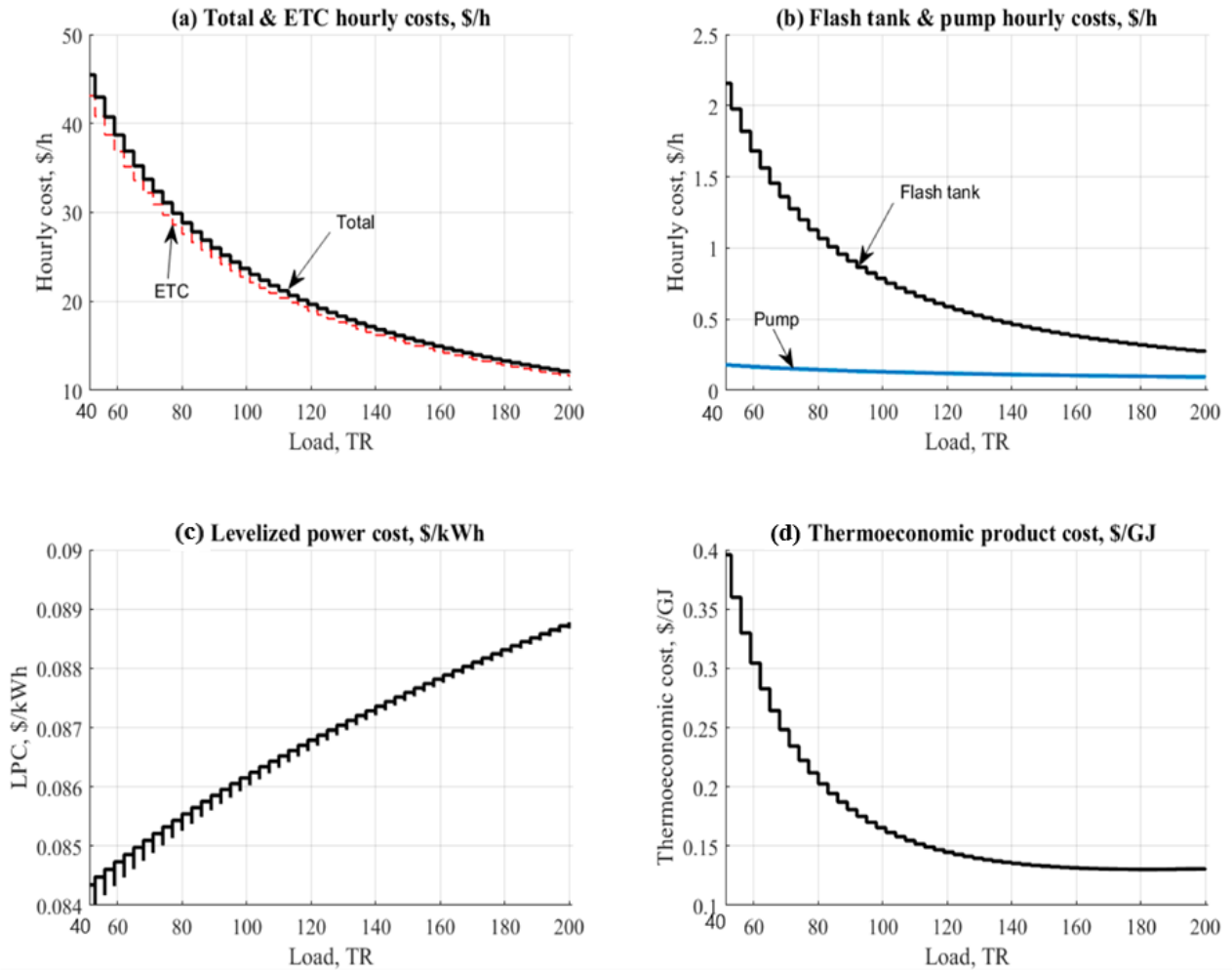
Figure 8. Data results for ETC/NH3-H2Ocycle vs. cooling load. (a)ETC total hourly cost. (b)Flash tank and pump hourly cost. (c)Levelized power cost. (d)Thermo-economic product.

Figure 9. Data results for PTC/NH3-H2O cycle vs. cooling load. (a)PTC total hourly cost. (b)Flash tank and pump hourly cost. (c)Levelized power cost. (d)Thermo-economic product.

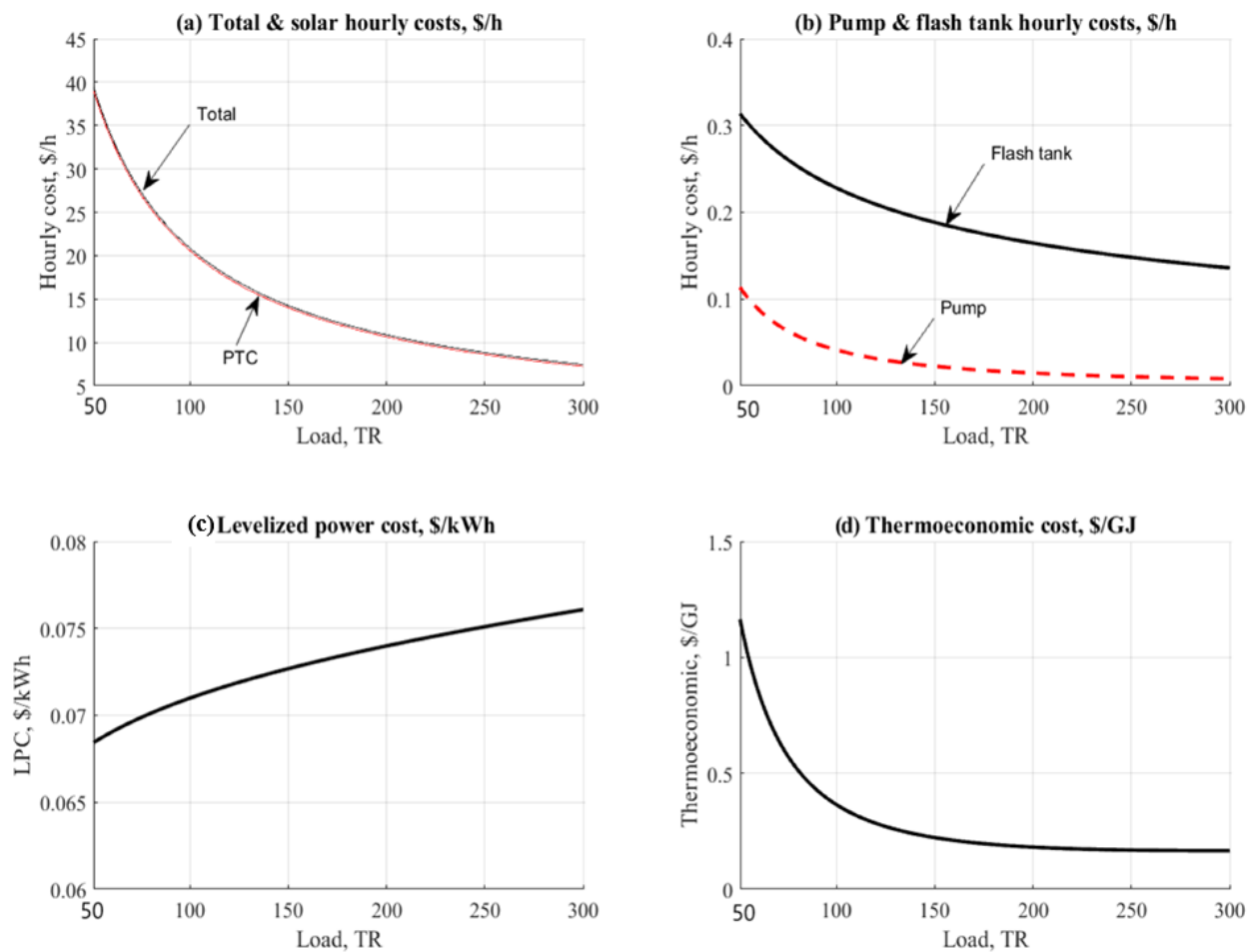*5.3. Case Study Results*

The case study introduced in this section compares all the configurations at a specified load point. This case study was conducted in a sports hall situated in Baghdad, Iraq. The stadium costs $14 million, and the 3000-seat capacity indoor sports facilities are focused on basketball, volleyball, and athletics. The entire project employs central air conditioning for an air-cooled absorption chiller of 700~800 kW. Its evaporator would be designed to operate in the range of 7~12 °C. Table 2 reports the results data in the case of using the solar absorption cooling cycle for all installations. A cooling load of 200TR was chosen for comparison. The ambient working conditions are set to a specified amount for simplicity. Regarding the results of the solar field, the PTC/H2O-LiBr configuration proved to be the lowest in the required area, which is quite significant for decreasing the required area. The ETC/H2O-LiBr was the next one. The same behavior was observed in PTC/NH3-H2O vs. ETC/NH3-H2O configurations. With respect to design features that include the design of the flash tank, the operation of the PTC/H2O-LiBr configuration provided the lowest results, and this was very advantageous by 0.11m³, while the ETC/H2O-LiBr has 1m³ and the PTC/NH3-H2O had 3.8 m³. We also observed the same trend concerning the exergy destruction and dryness fraction. Exergy destruction analysis showed that the most critical part in the system that causes the highest percent of the exergy destruction is the solar collectors due to the big difference between the highest exergy input, as it depends on the sun temperature, and the exergy output due to the heat transfer to

the heat carrier fluid (water). Consequently, in order to decrease the solar collector's exergy loss, the heat transfer between the solar radiation and the heat carried fluid has to be enhanced through new designs and investigations. For the entire AAC, the highest exergy loss was experienced in the absorber and generator. Therefore, special attention must be considered in the design of these components. The AAC was found to be lower in design results based on the H2O-LiBr operation. The results expose that PTC is regarded as a cycling advantage for ETC operation. The idle driving steam has been reported by PTC/H2O-LiBr with 0.4 kg/s, which led to a reduced volume of the flashing tank and solar field area. The COP value was substantial relative to the H2O-LiBr cycle. For cost per hour, PTC/H2O-LiBr was noticed to be the lowest among the others. By reaching 5.2 $/hr, PTC/H2O-LiBr was identified as the best alternative for this case study. The lowest hourly costs for the solar array were regarded as the vital term to judge the cost of the system. The thermo-economic cost was almost the same for all configurations in the range of 0.14–0.16 $/GJ with an advantage for H2O-LiBr configuration.

Table 2. Case study results @ 200 TR cooling load.

Solar Radiation, W/m²	500			
T_{amb}, °C	25			
T_a, T_e, T_g, T_c, T_{col}, °C	=30, 10, 90, 40, 175	=30, 10, 90, 40, 175	=30, 10, 90, 40, 250	=30, 10, 90, 40, 250
Load, TR	200			
Target cooled air, °C	20			
Interest rate, %	5			
Load factor, %	95			
Plant life time, yr	20			
Electric cost, $/kWh	0.065			
Pumps efficiency, %	75			
Configuration:	ETC-H2O/LiBr	ETC-NH3/H2O	PTC-LiBr/H2O	PTC-NH3/H2O
Solar field:				
Total solar field area, m²	3022	11,880	2433	11,020
Solar thermal power, kW	918.6	3612	890	4051
Inlet temperature, °C	91.64	91.82	92.66	92.04
Mass flow rate, kg/s	2.582	10.17	1.327	8.727
Inlet exergy, kW	1436	5646	1136	4217
Exergy destruction, kW	1191	4683	930	5143
Flash tank:				
Height/Width, m	1.742/0.852	3.381/1.655	0.837/0.41	2.743/1.343
Volume, m³	0.9942~1	7.276	0.1106	3.883
Total flow rate, kg/s	2.582	10.17	1.327	8.727
Water content, kg/s	2.1	8.551	0.897	6.91
Dryness fraction	0.1667	0.1595	0.324	0.208
Exergy destruction, kW	134.3	391.1	180.8	515.6
AAC unit:				
Q_a, kW	743.3	1251	743.3	1153
A_a, m²	190.5	23.37	190.5	21.3
M_{str}, kg/s	1.391	1.428	1.391	1.428
M_{wk}, kg/s	1.092	0.778	1.092	0.778
X_{a-hex}	0.4893	--	0.4893	--
$X_{hex-NH3}$	--	0.4554	--	0.4554
A_{hex}, m²	1.313	7.837	1.313	6.73
Q_g, kW	787.8	1407	787.8	1256

A_g, m^2	4.299	5.123	4.299	4.574
Driving steam flow, kg/s	0.4034	2.07	0.4034	1.848
X_{g-hex}	0.6233	--	0.6233	--
Q_c, kW	747.8	694.9	747.8	694.9
A_c, m^2	37.45	9.1	37.45	9.1
M_r, kg/s	0.299	0.6505	0.299	0.6505
Q_e, kW	703.4	703.4	703.4	703.4
A_e, m^2	36.35	41.15	36.35	41.15
FHP, kW	29.33~30	70.64	29.33~30	70.64
M_{air}, kg/s	68	119.5~120	68	119.5~120
COP/COP_{max}	0.89/1.56	0.5/1.559	0.89/1.56	0.5/1.559
RPR	0.573	0.3206	0.573	0.3591
Exergy destruction, kW	729.9	1010	729.9	977.3
Pump unit:				
W_p, kW	3.204	12.63	7.338	18.97~19
Exergy destruction, kW	14.8	64.7	12.33	62.25
Cost & Thermo-economics:				
Z_{col}, $/h$	3.918	11.75	2.604	10.93
Z_{fsh}, $/h$	0.02	0.11	0.001	0.06
Z_{aac}, $/h$	0.121	0.0487	0.121	0.04716
Z_{p+f}, $/h$	0.055	0.256	0.1743	0.2652
Z_{tot}, $/h$	4.114	12.16	2.9	11.3
LPC, $/kWh$	0.165	0.089	0.1557	0.0744
c_p, $/GJ$	0.1474	0.144	0.1602	0.1554

6. Conclusions

This study introduced different configurations of solar-assisted absorption air conditions (AAC) cycles. The proposed system is powered by solar energy. The system configuration combines solar field (PTC/ETC), flashing tank, and absorption chiller (H_2O-LiBr/NH_3-H_2O). A case study of 200 TR cooling is applied to the simulation program. Energetic and exegetic results are presented and have revealed that:

- Design aspects such as solar area and flashing tank volume were found have a great influence on the cycle cost.
- Among all configurations, PTC-H_2O-LiBr gives a remarkable result comparing against the ETC.
- For case study, PTC-H_2O-LiBr was recorded the best based on design and hourly costs. The required solar area was in the range of 2000~2500 m^2. Meanwhile, the total hourly cost was in the range of 4~5 $/h, which is quite attractive.
- Absorption chiller coefficient of performance was in the range of 0.5 to 0.9.
- The total rate of exergy destruction of the AAC was in the range of 55 kW.
- Solar field harvests a larger amount of exergy destruction rates for all configurations due to the large area and mass flow rate effect. PTC-H_2O-LiBr resulted in a 930~1000 kW of exergy destruction rate comparing against PTC-NH_3-H_2O, which resulted a value of 4600~5000 kW.
- PTC-H_2O-LiBr gives the lowest values related to exergy destruction rates for all units.
- PTC-H_2O-LiBr gives the lowest value of flashing tank design aspects such as width 0.4~0.5m, height 0.8 m, and volume 0.11 m^3. ETC-H_2O-LiBr comes next with a total flashing tank equal to ~1 m^3.
- The thermo-economic cost is almost the same for all configurations in the range of 0.14–0.16 $/GJ with an advantage for H_2O-LiBr configuration.

- It is quite clear that PTC-H2O-LiBr followed by ETC-H2O-LiBr have remarkable results according to the terms of energy, design, and cost. Generally, PTC system is considered the best choice for H2O-LiBr or NH3-H2O.

Nomenclature

A	Availability: kW, Area:m²
A_t	Tube cross sectional area, m²
A_f	Amortization factor, 1/y
AAC	Absorption Air Conditioning
C	Thermo-economic cost stream, $/kJ
C_p	Specific heat capacity, kJ/kg °C @ constant pressure
COP	Coefficient of Performance
D	Diameter, m
D_{env}	Collector glass envelope diameter, m
E	Exergy stream, kW
ETC	Evacuated Tube Collector
FPT	Flat Plate Collector
f	Function
FHP	Fan power, kW
H, h	Height, m, Enthalpy, kJ/kg
I_s	Solar intensity, W/m²
i	Interest rate, %
L	Length, m
L_m	Module length, m
LPC	Levelized Power Cost, $/kWh
LTp	Plant life time, y
M	Mass flow rate, kg/s
NOT	Number of Tubes
NOC	Number of Collectors
NOL	Number of Loops
OH	Operating hours
PTC	Parabolic Through Collector
P	Power (Kw), or Pressure, kPa
ΔP	Pressure, kPa
Q	Thermal power, kW
RPR	Relative Performance Ratio
Re	Raynold's Number
S, s	Entropy, kJ/kg °C
T	Temperature, °C
V, Vol	Volume, cm³
v	Velocity, m/s

W	Power, Work, kW
W_c	Collector width, m
X	Concentration percentage, %
Z	Hourly cost, $/h
Subscripts	
a, abs	Absorber
air	Air
amb	Ambient
c	Condenser
col	Collector
e	Evaporator
etc	Evacuated tube collector
f	Liquid phase
fan	Fan
fsh	Flashing tank
fst	Flashing steam
g	Generator, vapor phase
i	Inlet
$loop$	Loop
o	Out
p	Pump
ptc	Parabolic trough collector
$p_{i,o}$	Pump inlet and outlet
q	Heat
r	Refrigerant
s	Steam
st	Steam
w	Water
Greek	
η	Efficiency, %
ρ	Density, kg/m³
μ	Dynamic viscosity, Pa.s

References

1. Wang, R.Z.; Wu, J.Y.; Dai, Y.J.; Wang, W.; Jiangzhou, S. *Adsorption Refrigeration*; China Mechanical Industry Press: Beijing, China, 2002.
2. IEA (2020), Global CO2 emissions in 2019, IEA, Paris https://www.iea.org/articles/global-co2-emissions-in-2019. (accessed on 10.09.2020)
3. Al-Alili, A.; Hwang, Y.; Radermacher, R. Review of solar thermal air conditioning technologies. *Int. J. Refrig.* **2014**, *39*, 4–22.
4. Mone, C.D.; Chau, D.S.; Phelan, P.E. Economic feasibility of combined heat and power and absorption refrigeration with commercially available gas turbines. *Energy Convers. Manag.* **2001**, *42*, 1559–1573.
5. Rodríguez-Muñoz, J.L.; Belman-Flores, J.M. Review of diffusion–absorption refrigeration technologies. *Renew. Sustain. Energy Rev.* **2014**, *30*, 145–153.
6. Bataineh, K.; Taamneh, Y. Review and recent improvements of solar sorption cooling systems. *Energy Build.* **2016**, *128*, 22–37.
7. Syed, A., G. G. Maidment, R. M. Tozer and J. F. Missenden (2002) A Study of the Economic Perspectives of Solar Cooling Schemes, CIBSE National Conference, Part 2, London, October .
8. Balaras, C.A.; Hans-Martin, H.; Wiemken, E.; Grossman, G. Solar cooling: An overview of European applications design guidelines. *ASHRAE J.* **2006**, *48*, 14.
9. Li, M.; Xu, C.; Hassanien, R.H.E.; Xu, Y.; Zhuang, B. Experimental investigation on the performance of a solar powered lithium bromide–water absorption cooling system. *Int. J. Refrig.* **2016**, *71*, 46–59.
10. Mazloumi, M.; Naghashzadegan, M.; Javaherdeh, K.J.E.C. Simulation of solar lithium bromide–water absorption cooling system with parabolic trough collector. *Energy Convers. Manag.* **2008**, *49*, 2820–2832.
11. Shirazi, A.; Taylor, R.A.; White, S.D.; Morrison, G.L. Multi-effect absorption chillers powered by the sun: Reality or reverie. *Energy Procedia* **2016**, *91*, 844–856.

12. Zacarías, A.; Venegas, M.; Lecuona, A.; Ventas, R.; Carvajal, I. Experimental assessment of vapour adiabatic absorption into solution droplets using a full cone nozzle. *Exp. Therm. Fluid Sci.* **2015**, *68*, 228–238.

13. Rajasekar, D.; Ponshanmugakumar, A.; Rajavel, R. Design and Performance Validation of Vapour Absorption Solar Air Conditioning System. *Int. J. Future Revolut. Comput. Sci. Commun. Eng.* **2017**, *3*, 115–119.

14. Flores, V.H.F.; Román, J.C.; Alpírez, G.M. Performance analysis of different working fluids for an absorption refrigeration cycle. *Am. J. Environ. Eng.* **2014**, *4*, 1–10.

15. Gebreslassie, B.H.; Medrano, M.; Boer, D. Exergy analysis of multi-effect water–LiBr absorption systems: From half to triple effect. *Renew. Energy* **2010**, *35*, 1773–1782.

16. Kilic, M.; Kaynakli, O. Second law-based thermodynamic analysis of water-lithium bromide absorption refrigeration system. *Energy* **2007**, *32*, 1505–1512.

17. Karakas, A.; Egrican, N.; Uygur, S. Second-law analysis of solar absorption-cooling cycles using lithium bromide/water and ammonia/water as working fluids. *Appl. Energy* **1990**, *37*, 169–187.

18. Dincer, I.; Ratlamwala, T.A.H. Fundamentals of Absorption Refrigeration Systems. In *Integrated Absorption Refrigeration Systems*; Springer: Cham, Switzerland, 2016; pp. 1–25.

19. Lu, Z.S.; Wang, R.Z. Experimental performance investigation of small solar air-conditioning systems with different kinds of collectors and chillers. *Solar Energy* **2014**, *110*, 7–14.

20. Colorado, D.; Rivera, W. Performance comparison between a conventional vapor compression and compression-absorption single-stage and double-stage systems used for refrigeration. *Appl. Therm. Eng.* **2015**, *87*, 273–285.

21. Wang, Y.; Wang, C.; Feng, X. Optimal match between heat source and absorption refrigeration. *Comput. Chem. Eng.* **2017**, *102*, 268–277.

22. Du, S.; Wang, R.Z.; Chen, X. Development and experimental study of an ammonia water absorption refrigeration prototype driven by diesel engine exhaust heat. *Energy* **2017**, *130*, 420–432.

23. Al-Falahi, A.; Alobaid, F.; Epple, B. Design and Thermo-economic Comparisons of Large Scale Solar Absorption Air Conditioning Cycles. *Case Stud. Therm. Eng.* **2020**, *22*, 100763.

24. Al-Falahi, A.; Alobaid, F.; Epple, B. Thermo-Economic Evaluation of Aqua-Ammonia Solar Absorption Air Conditioning System Integrated with Various Collector Types. *Entropy* **2020**, *22*, 1165.

25. NIST Chemistry WebBook, SRD 69. Available online: https://webbook.nist.gov/chemistry/name-ser/ (accessed on 03.10.2020).

26. Vakiloroaya, V.; Ha, Q.; Skibniewski, M.J. Modeling and experimental validation of a solar-assisted direct expansion air conditioning system. *Energy Build.* **2013**, *66*, 524–536, doi:10.1016/j.enbuild.2013.07.073.

27. Carles Bruno, J.; López-Villada, J.; Letelier, E.; Romera, S.; Coronas, A. Modelling and Optimisation of Solar Organic Rankine Cycle Engines for Reverse Osmosis Desalination. *Appl. Therm. Eng.* **2008**, *28*, 2212–2226.

28. Nafey, A.S.; Sharaf, M.A.; García-Rodríguez, L. A New Visual Library for Design and Simulation of Solar Desalination Systems (SDS). *Desalination* **2010**, *259*, 197–207.

29. Eldean, M.A.S.; Soliman, A.M. A new visual library for modeling and simulation of renewable energy desalination systems (REDS). *Desalin. Water Treat.* **2013**, *51*, 6905–6920, doi:10.1080/19443994.2013.777369.

30. Singh, R.; Kumar, D.R. Theoritical Analysis of Nh3-H2o Refrigeration System Coupled with Diesel Engine: A Thermodynamic Study. *IOSR J. Mech. Civ. Eng.* **2014**, *11*, 29–36.

31. Li, K.W. *Applied Thermodynamics: Availability Method and Energy Conversion*; CRC Press: Boca Raton, FL, USA, 1995.

32. Adrian Bejan, George Tsatsaronis and Michael Moran. *Thermal Design and Optimization*; Wiley: New York, NY, USA, 1996; Chapter 8.

33. Sharaf, M.A.; Nafey, A.S.; García-Rodríguez, L. Author's Personal Copy Thermo-Economic Analysis of Solar Thermal Power Cycles Assisted MED-VC (Multi Effect Distillation-Vapor Compression) Desalination Processes. *Energy* **2011**, *36*, 2753–2764.

34. Sharaf, M.; Nafey, A.; Desalination, L.G.-R. Exergy and Thermo-Economic Analyses of a Combined Solar Organic Cycle with Multi Effect Distillation (MED) Desalination Process. *Desalination* **2011**, *272*, 135–147.

35. Castro, M.M.; Song, T.W.; Pinto, J.M. Minimization of operational costs in cooling water systems. *Chem. Eng. Res. Des.* **2000**, *78*, 192–201.